ABSTRACT

ADVANCED CLASSIFICATION OF OFDM AND MIMO SIGNALS WITH ENHANCED SECOND ORDER CYCLOSTATIONARITY DETECTION

by
Miao Shi

With the emergence of cognitive radio and the introduction of new modulation techniques such as OFDM and MIMO, the problem of Modulation Classification (MC) becomes more challenging and complicated. In the first part of the thesis, we explore the automatic modulation classification to blindly distinguish OFDM from single carrier signals. We use the fourth order cumulants; an approach which in the past has been also applied to classify single carrier signals. A blind OFDM parameter estimation scheme was then followed, which includes the estimation of number of subcarriers, CP length, timing and frequency offset and the oversampling factor for the OFDM signal. For the second part of the thesis, we improve the statistical signal processing techniques that were used in the first part. Particularly, the second order cyclostationarity based methods have been examined and improved. Based on the fact that most of the cyclostationary communication signals has a real cyclostationary part and a complex non-cyclostaionary part, we suggest an approach that enhance the second order cyclostationarity and hence increase its probability of detection. Using such improved second-order cyclostationarity, we present an improved synchronization method based on second order cyclostationarity. With the proposed approach, it is shown that the timing estimator, is independent of the frequency offset estimator, and therefore performs better than the previously proposed class of blind synchronization methods. To negate the dependence of the blind synchronization scheme on the prior knowledge of the raised cosine pulse shaping filters, we proposed a blind roll-off factor estimator based on the second order cyclostationarity. Last, we address the MIMO classification problem, wherein we estimate the number of transmitting antennas. Here the second order cyclostationarity test has been applied in distinguishing STC from BLAST modulation.

ADVANCED CLASSIFICATION OF OFDM AND MIMO SIGNALS WITH ENHANCED SECOND ORDER CYCLOSTATIONARITY DETECTION

by
Miao Shi

A Dissertation
Submitted to the Faculty of
New Jersey Institute of Technology
in Partial Fulfillment of the Requirements for the Degree of
Doctor of Philosophy in Electrical Engineering

Department of Electrical and Computer Engineering

January 2010

APPROVAL PAGE

ADVANCED CLASSIFICATION OF OFDM AND MIMO SIGNALS WITH ENHANCED SECOND ORDER CYCLOSTATIONARITY DETECTION

Miao Shi

6/8/09

Dr. Yeheskel Bar-Ness, Dissertation Advisor — Date
Distinguished Professor, Department of Electrical and Computer Engineering, NJIT

06/08/09

Dr. Alexander M. Haimovich, Committee Member — Date
Professor, Department of Electrical and Computer Engineering, NJIT

6/8/09

Dr. Ali Abdi, Committee Member — Date
Associate Professor, Department of Electrical and Computer Engineering, NJIT

07/01/09

Dr. Georgios B. Giannakis, Committee Member — Date
Professor, Department of Electrical and Computer Engineering, University of Minnesota

6/11/09

Dr. Wei Su, Committee Member — Date
US Army Communication-Electronics RD&E Center

BIOGRAPHICAL SKETCH

Author: Miao Shi

Degree: Doctor of Philosophy

Date: January 2010

Undergraduate and Graduate Education:

- Doctor of Philosophy in Electrical Engineering,
  New Jersey Institute of Technology, Newark, NJ, 2009
- Master of Science in Electrical Engineering,
  National University of Singapore, Singapore, 2003
- Bachelor of Science in Electrical Engineering,
  Xidian University, Xi'an, China, 1997

Major: Electrical Engineering

Presentations and Publications:

Miao Shi, Yeheskel Bar-Ness, and Seokhyun Yoon, "A novel frame synchronization method using correlation between permuted sequences," *IEEE 2007 WCNC* , March 2007, Page(s): 2446-2451.

Miao Shi, Yeheskel Bar-Ness, and Wei Su, "Blind OFDM Systems Parameters Estimation for Software Defined Radio," *IEEE DySpan 2007* , April, 2007, Page(s): 119-122.

Miao Shi, Yeheskel Bar-Ness, and Wei Su, "Adaptive estimation of the number of transmit antennas," *IEEE Milcom 2007* , Oct. 2007, Page(s): 1-5.

Miao Shi, Yeheskel Bar-Ness, and Wei Su, "STC and BLAST MIMO modulation recognition," *IEEE GlobeCom 2007* , Nov. 2007, Page(s): 3034-3039.

Miao Shi, Yeheskel Bar-Ness, and Wei Su, "Fourth order cumulants in Distinguishing Single Carrier from OFDM signals," *IEEE Milcom 2008* , Nov. 2008, Page(s): 1-6.

Miao Shi, Yeheskel Bar-Ness, and Wei Su, "A simple method to enhance the detection of the second order cyclostationarity," *IEEE GlobeCom 2008* , Dec. 2008, Page(s): 1-6.

Miao Shi, Yeheskel Bar-Ness, "A simple method to enhance the detection of the second order cyclostationarity," *submitted to IEEE Trans. Signal Processing*.

Miao Shi, Yeheskel Bar-Ness, "Revisiting the Timing and Frequency Offset Estimation Based on Cyclostationarity with new improved methods," *IEEE Communication letter* , Vol. 13, Issue 7, July, 2009, Page(s): 537 - 539.

To Bin and Liran.

ACKNOWLEDGMENT

It is difficult to overstate my gratitude to my Ph.D. supervisor, Prof. Yeheskel Bar-Ness. With his enthusiasm, his inspiration, and his great efforts to help me to write things clearly and simply. He helped to check every single equations in my papers and reports. Also, his great support for my family.

My deepest gratitude goes to my dissertation committee members, Professor Georgios B. Giannakis, Professor Alex Haimovich, Professor Ali Abdi, and Dr. Wei Su. Many thanks for reviewing my dissertation and sharing their time and expertise.

I would like to thank all my labmates for providing a stimulating and fun environment in which to learn and grow. I am especially grateful to Shuangquan Wang, who helped me with the start of research. Shengshan Cui helped me so many times in latex writing and also provide good discussion on research problems. Amir Laufer's help with presentation and paper writing during my pregnancy. And also so many labmates, Xiaoli, Vlad, Ciprian, Mingzheng, Huaihai, Da Xie for helping me in personal life and research. I wish to thank my dear husband, Bin Zhou, for helping me get through the difficult times, and for all the emotional support, entertainment, and caring. I am grateful to Marlene Toeroek, who is the number one help in my school life for all the troubles. I also wish to thank Dr. Misra Durgamadhab for wonderful suggestions and help in my teaching courses. Lastly, and most importantly, I wish to thank my parents, Yimin Shi and Caiyun Wang. They bore me, raised me, supported me, taught me, and loved me. To them I dedicate this dissertation.

TABLE OF CONTENTS

TABLE OF CONTENTS
(Continued)

Chapter **Page**

TABLE OF CONTENTS
(Continued)

Chapter **Page**

TABLE OF CONTENTS
(Continued)

Chapter **Page**

LIST OF TABLES

LIST OF FIGURES

LIST OF FIGURES
(Continued)

Figure **Page**

LIST OF FIGURES
(Continued)

Figure **Page**

Part I

OFDM MODULATION CLASSIFICATION AND BLIND ESTIMATION

CHAPTER 1

INTRODUCTION

Through years, automatic modulation classification (AMC) has been applied in many military applications. A lot of work has been done on AMC in literatures and in practice. With the introduction of cognitive radio concept, software defined radios, AMC became not only limited to military applications, as more civilian applications demanded blind modulation identification as a first step. Furthermore, with the need of high spectral efficiency and better performance in dispersive environment, Orthogonal Frequency Division Multiplexing (OFDM) systems and Multiple Input Multiple Output (MIMO) space systems were introduced and applied in various areas. Thus the task of AMC has become more complicated with the emergence of these new modulation techniques. New scenario introduce many new challenges for the design of AMC algorithms.

In our research, we concentrate on OFDM modulation classification and blind OFDM system parameters estimation methods. The goal of the OFDM classification and estimation includes distinguishing OFDM modulation from single carrier modulation and OFDM system parameters extraction, such as the number of subcarriers, the CP length as well as the timing and frequency offset in OFDM systems.

Several methods have been proposed for the OFDM signal modulation classification. *One class of methods* are based on the feature of the cyclic prefix (CP) of OFDM signal. Due to the introduction of CP, OFDM signal becomes cyclostationary [1]. A simple correlation test can find a correlation peak by which one can distinguish OFDM signal from single carrier signal [2]- [3]. Punchihewa, et al. [2] distinguished OFDM from the single carrier modulation signals by considering CP as a feature of the OFDM signal, which can introduce cyclostationarity. However, this method will fail when the single carrier is block coded (SC-BC) since the later also contains a CP and will depict cyclostationarity the same as the OFDM signal. Yücek and el. [3] proposed a likelihood based methods that also

uses CP as a feature of the OFDM signal. This will also fail in case of SC-BC signal. Furthermore, since most of the commercial signals has inherent cyclostationarity due to the training sequence, then in case of noisy environments, this cyclostationarity may be mistaken for the CP-induced cyclostationarity in OFDM signal.

Another class of methods are based on the asymptotic Gaussianity of the OFDM signal. In [4], [5] , Li H., et al. suggest to compare the EDF (Empirical Distribution Function) of the received signal to Gaussian distribution. The received signal is declared to be OFDM signal if its EDF is close enough to the Gaussian distribution within a given threshold. Due to the weakly convergence of EDF of OFDM signal to Gaussian distribution, this method proved to have poor performance in high SNR scenarios. Akmouche [6] proposed to use the fourth order cumulants to recognize OFDM signal. However, in approximating the OFDM signal as Gaussian, the method also face the same problem as Li H.'s method in high SNR scenarios. Furthermore, this method is very complicated compared other methods (require $O(M^6)$ computation, where M is the observed number of data sample).

We also had explored the CP feature based method using a simple correlation test. Then, a fourth order cumulants method was proposed. Although we use the same feature as Akmouche's paper, our work is inspired by Swami's approach [7] for single carrier classification, is more simple than [6] (with only $O(M)$ computation). Instead of setting threshold based on the asymptotic Gaussian property of the OFDM signal, we set the threshold simply as the center of the cumulants average of the OFDM and single carrier signals. It is also proved that the difference between OFDM signal and Gaussian signal is not large enough to deteriorate the performance in high SNR scenarios.

Standard notation is used throughout the thesis. $E[\cdot]$ denotes expectation. $\mathrm{Re}(\cdot)$ and $\mathrm{Im}(\cdot)$ are the real and imaginary operator. Superscripts $(*)$, (T), and (H) represents the complex conjugate of a scalar, the transpose and the Hermitian of a matrix, respectively. $\lfloor \cdot \rceil$ denotes the nearest integer function. arg denotes the unwrapped phase. arg denotes the unwrapped phase. Column vectors are denoted using bold characters. Matrices are

denoted using upper case bold characters. I, and Z represents the set of integers and complex numbers respectively. 0 represents the zero matrix.

The organization of the thesis is as follows:

The first part "OFDM modulation classification and blind estimation" includes four chapters.

Chapter 1 briefly introduces the OFDM modulation classification problem.

Chapter 2 presents the OFDM modulation classification method by using the CP feature.

Chapter 3 introduces the OFDM modulation classification method based on the fourth order cumulants.

Chapter 4 proposes the first version of the blind estimation scheme for OFDM system parameters.

The second part "Second order Cyclostationarity analysis and applications" has three chapters.

Chapter 5 presents the simple method to enhance the detection of the second order cyclostationarity.

In Chapter 6, after revisiting the previous proposed joint timing and frequency offset estimation based on the second order cyclostationarity, we propose a new scheme where the timing estimator is independent of the frequency estimator.

Chapter 7 presents a new method to estimate the raised cosine pulse shaping by using the second order cyclostationarity. Specifically, the roll-off factor of the raised cosine pulse shaping filter is estimated using the delay "0" second order cyclostationarity.

Last part "MIMO classification" has one chapter.

Chapter 8 presents a scheme for distinguishing the STC signal from BLAST signal.

CHAPTER 2

CP BASED OFDM SIGNAL CLASSIFICATION METHODS

2.1 Frame structure (preamble based and CP based)

Conventionally in practice, there are two kinds of frame structure. One frame structure is called preamble based frame structure, wherein a known preambles are appended at the front of each unknown data block (or in the middle, termed, midamble). These preambles are usually correlated with each other (or most likely (in practice), they are the same.). Such preambles, that use repeated patterns can generate multiple periodic correlation peaks.

Another frame structure uses CP as in OFDM or in single carrier block coded (SC-BC) system. The correlation introduced here is only over the CP length. It is limited to one OFDM symbol or single carrier block coded signal. Therefore, in this case, the correlation test will give rise to one peak whose index corresponds to the number of sub-carriers (in OFDM) or the length of the data part (in SC-BC), multiplied by the over-sampling factor.

Frequently in commercial systems, both frame structure are used. For example, in IEEE 802.11a [8], 802.16g [9], and ETSI system [10], there are preambles for each large OFDM frame, and, a CP for each OFDM symbol.

2.2 Conventional single carrier system and CP based block modulation

In the second and third generation wireless systems, GSM and CDMA systems have been used. Both are single carrier systems. The frame is that of preamble based structure. For example, in GSM systems, a TDMA frame of 4.615 ms contains 8 time slots, each includes around 16% training bits. For TD-CDMA system, each frame of 10ms contains 10 time slots and each slot includes around 17% training bits in the middle.

In the OFDM systems and the SC-BC systems, both CP and preambles have been applied. For example, in IEEE 802.16, each OFDM frame (burst) has two OFDM symbols at the front of the frame (burst) used as preambles. Besides, each OFDM symbol has a CP

appended at the front to combat ISI. The length of CP can be from 1/32 to 1/4 of the data part of the OFDM symbol. In the single carrier block systems (3GPP LTE uplink) [11], the similar frame structure as OFDM is used.

2.3 Scheme for using CP to distinguish between CP based block modulation from regular single carrier system

We propose to use CP as a feature to distinguish CP based block modulation, which includes both OFDM and SC-BC system from the regular single carrier system. According to a paper by the authors [12] on OFDM blind estimation, the correlation test can serve well for the detection [12].

A flowchart of the scheme is shown as in Fig. 2.1.

2.4 Threshold set up

As shown in the flowchart of the scheme, we need to set up the threshold to decide whether correlation peaks indicate that the signal contains CP. When the threshold is sufficiently low and the preambles are in a large percent of the data block, then a regular single carrier signal will also generate multiple peaks above the threshold. That is why we need another step to check whether the peaks we got is in multiples. For the CP based modulation schemes, there is only one CP generated peak in the correlation test.

Consider the correlation test as given by

$$\mathcal{R}(\tau) = \mathrm{Re}\left\{ \frac{1}{M} \sum_{n=0}^{M-1} \left[s\left(n\right) + w\left(n\right) \right] \ \left[s(n-\tau) + w\left(n-\tau\right) \right]^{*} \right\} \tag{2.1}$$

$s(n)$ is the transmitted signal with variance σ_s^2 and $w(n)$ is the noise at the receiver with variance σ_w^2. M is the length of the observed data samples. Re[.] represents the real part operator. The above equation becomes power of the signal when $\tau = 0$.

When $\tau \neq 0$, when there are no correlation peaks, the correlation $\mathcal{R}(\tau)$ is a Gaussian distributed random signal with zero mean, because in such case, $s(n)$ and $s(n-\tau)$ is not

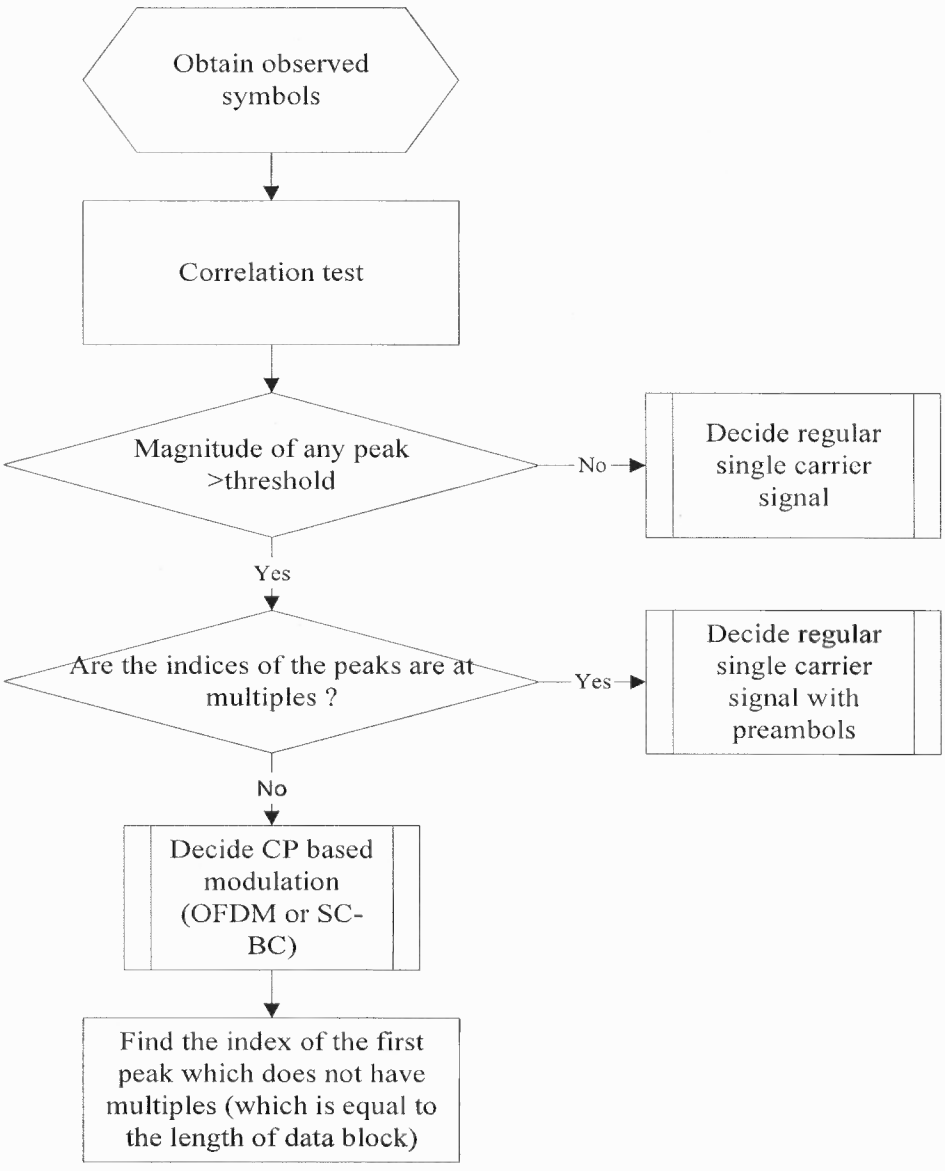

Figure 2.1 Flowchart of the scheme.

correlated with each other.($E[s(n)s^*(n-\tau)] = 0$, while the expectation of the cross term of signal and noise,

$$E[s(n)w^*(n-\tau)] = E[w(n)s^*(n-\tau)] = 0$$

The expectation of the noise correlation term,

$$E[w(n)w^*(n-\tau)] = 0 \text{ when} \tau \neq 0.)$$

On the other hand, at the correlation peaks, when τ equals to the length of the data part of the OFDM or SC-BC modulated signal, $s(n)$ and $s(n-\tau)$ is the copy of each other due to the adding of the CP.

For another case, when τ is equal to the length of the time slot, when n corresponds to the times where the training symbols located, $s(n)$ and $s(n-\tau)$ is equal to each other. Hence, $E[s(n)s^*(n-\tau)] \neq 0$. The correlation $\mathcal{R}(\tau)$ is a Gaussian distributed signal with nonzero mean.

This is a simple detection problem. Denote Hypothesis 1 as $\mathcal{R}(\tau)$ has a peak generated by the CP; Hypothesis 0 as $\mathcal{R}(\tau)$ does not have a correlation peak. To set up the threshold, we need to find out the mean value of the magnitude of $\mathcal{R}(\tau)$ when τ corresponds to the length of the data part (of the OFDM or SC-BC signal). Also, we need to find out the variance of different hypotheses.

2.4.1 Mean value

The following equations give the mean values of $R(\tau) = E[\mathcal{R}(\tau)]$ with different delay τ. Let T_N represents the length of the data part of the OFDM or SC-BC signal (which equals Nq, where N is the number of subcarriers, q is the oversampling factor). G is the length of CP. T_p represents the length of the time slot [1] (which equals Lq). L is the length of

[1] A frame contains many time slots. Generally, each time slot contains data part, training symbols part, and the synchronization part.

the burst or time slot. Denote α as a fractional number which depends on the portion of the preambles in the data time slot. For example, in IEEE 802.16 [9], there are 2 OFDM symbols appended as preambles in front of each OFDM burst [2]. Hence, α depends on the number of OFDM data symbols in each burst. For the regular single carrier signal, α depends on the portion of the training bits in each time slot. Note that we do not have the prior knowledge of N, G, and α.

$$R(\tau) = E\left[\mathcal{R}(0)\right] = \left(\sigma_s^2 + \sigma_w^2\right) \tag{2.2}$$

$$R(T_N) = E\left[\mathcal{R}(T_N)\right] = E[\frac{1}{M} \sum_{\{n \bmod [(N+G)q]\}=0}^{\{n \bmod [(N+G)q]\}=G-1} |s(n)|^2] \approx \frac{G}{N+G}\sigma_s^2 \tag{2.3}$$

$$R(T_p) = E\left[\mathcal{R}(T_p))\right] = E\left[\frac{1}{M} \sum_{\{n \bmod L\}=0}^{\{n \bmod Lq\}=\alpha Lq-1} |s(n)|^2\right] \approx \alpha\sigma_s^2 \tag{2.4}$$

As shown above the mean value depends on many parameters. To eliminate the effect of the signal power σ_s^2, we normalize the mean value by the correlation at delay 0, $\mathcal{R}(0)$. Thus the mean value of the normalized correlation peak $\mathcal{R}(T_N)$ will become

$$E\left[\mathcal{R}_{nor}(T_N)\right] = \frac{G}{N+G}\frac{\sigma_s^2}{\sigma_s^2 + \sigma_w^2} = \frac{G}{N+G}\frac{SNR}{1+SNR} \tag{2.5}$$

where $E\left[\mathcal{R}_{nor}(T_N)\right]$ is the normalized mean value of $\mathcal{R}(T_N)$. SNR is the signal to noise ratio.

It can be seen from equation (2.5), that the normalized mean value $E\left[\mathcal{R}_{nor}(T_N)\right]$ depends on SNR, the length of CP and the number of subcarriers. At high SNR scenarios, the second term at the RHS of equation (2.5) can be approximated by 1. Here, to simplify the detection process, we can instead take $\frac{G}{N+G}$ as 1/33 due to the fact that in most of the current OFDM systems, the CP length is 1/32 to 1/4 of the length of data part [8]- [10].

[2]Each OFDM frame may contain one or a few OFDM bursts, while each burst contains one or many OFDM symbols.

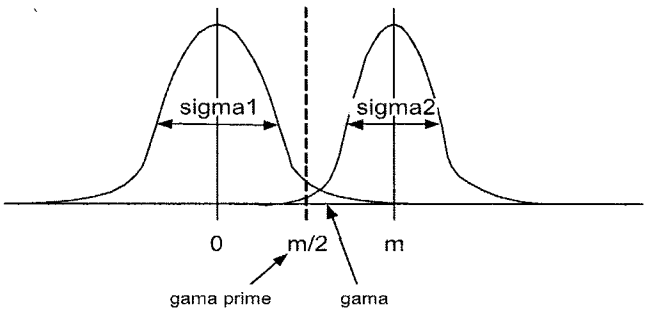

Figure 2.2 Pdfs for the detection problem.

2.4.2 Variance

The variance of $\mathcal{R}(\tau)$ under the two hypotheses are given by

$$Var\left[\mathcal{R}(T_N)\right] \approx \frac{1}{2M}\left(\frac{N}{N+G}\sigma_s^4 + 2\sigma_s^2\sigma_w^2 + \sigma_w^4\right) \tag{2.6}$$

$$Var\left[R(\tau \neq T_N)\right] = \frac{1}{2M}\left(\sigma_s^4 + 2\sigma_s^2\sigma_w^2 + \sigma_w^4\right) \tag{2.7}$$

According to the above equations, the variances of $\mathcal{R}(\tau)$ under the two hypotheses are different from each other. (Note that we ignore the case when $\tau = T_p$ for simplicity.) The variance of $\mathcal{R}(T_N)$ is less than that of $\mathcal{R}(\tau \neq T_N)$. The difference is very little when the CP length is small which result in $\frac{N}{N+G}$ close to 1.

2.4.3 Threshold

Based on the above derivation, we set up the threshold γ at the intersection of the two pdf for the Gaussian distribution of the two hypothesis according to their means value and variances. Using $\sigma_1^2 = Var\left[\mathcal{R}(\tau \neq T_N)\right]$, $\sigma_2^2 = Var\left[\mathcal{R}(T_N)\right]$ and $m = E\left[\mathcal{R}(T_N)\right]$ (The mean value $E\left[\mathcal{R}(\tau \neq T_N)\right] = 0$). We have (see Fig. 2.2)

$$\frac{1}{\sigma_1}\exp\left(-\frac{\gamma^2}{2\sigma_1^2}\right) = \frac{1}{\sigma_2}\exp\left(-\frac{\gamma^2}{2\sigma_2^2}\right)$$

which leads to:

$$\left(\sigma_1^2 - \sigma_2^2\right)\gamma^2 - 2\sigma_1^2 m\gamma + \left(\sigma_1^2 m^2 + \sigma_1^2\sigma_2^2 \ln\frac{\sigma_2}{\sigma_1}\right) = 0$$

From the above equation, one can find that the threshold according to the above mean value and variances is given by

$$\gamma = \frac{\sigma_1^2 m + \sqrt{\sigma_1^4 m^2 - \left(\sigma_1^2 - \sigma_2^2\right)\left(\sigma_1^2 m^2 - \sigma_1^2\sigma_2^2 \ln\frac{\sigma_1}{\sigma_2}\right)}}{\sigma_1^2 - \sigma_2^2} \tag{2.8}$$

Apparently, the above threshold is complicated and contains a lot of parameters which is hard to get for our detection problem. Therefore, in practice, we may set the threshold as $\gamma' = \frac{m}{2}$. As shown from Fig. 2.2, the less the CP length, the closer the two variances, and the two pdf will be alike to each other and the threshold γ' is approaching the true threshold γ.

Alternatively, we can also set the threshold according to a given false alarm probability of the pdf of hypothesis 0 using the cdf table of the Gaussian distributed pdf.

2.5 Example of possible correlation from different systems

In this section, we list some examples of the possible correlation pattern from different systems. The observed time duration is 0.12 ms. [3]

According to IEEE 802.11a, we set the OFDM symbol duration as 4us. The CP is 1/4 of the length of the data part of the OFDM symbol. Each frame contains 10 bursts and each burst contains a preamble of 2 OFDM symbols. SNR=0dB. We average 100 runs to get the correlation pattern. The normalized timing correlation is given below.

[3]Note here, different from Hong Li's simulation set up [5], we use the same observed time duration instead of the same number of symbols for the detection. This is more reasonable because in practical detection process, we collect certain time duration of the sampled data. That means, for the regular single carrier signals, which tend to have larger time frame than the OFDM signals, we actually collect less data symbols than for OFDM signal. While on the other hand, for the OFDM signal, for example in IEEE 802.11 [8], its symbol time duration is only $4\mu s$, we may collect much more OFDM symbols. Therefore, it is not appropriate to use the same number of symbols for the detection problem.

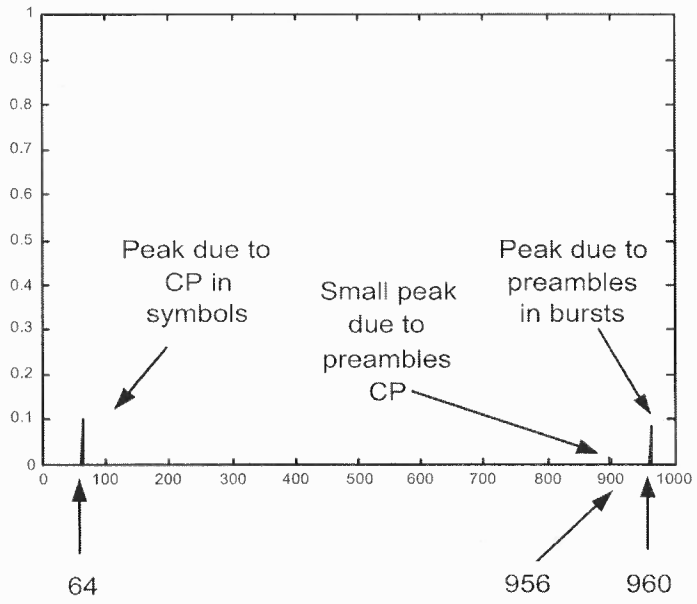

Figure 2.3 Correlation peaks of the OFDM signal.

As shown in Fig. 2.3, there are several peaks with delay less than 1000. The first peak is the correlation peak due to the CP. The magnitude is 0.0997, which is quite near the theoretical value we derive $\frac{G}{N+G}\frac{SNR}{1+SNR} = 1/5/2$ (equation (2.5) for SNR=0dB). The second obvious peak is due to the preambles. Its magnitude is 0.0836, which is also very near to the theoretical value $\alpha\frac{SNR}{1+SNR} = 1/6/2 = 0.0833$ (equation (2.2) and (2.4)). Note that $1/6$ comes from that there are 2 preambols in a burst of 12 OFDM symbols. There is also a very small peak which is due to the CP of the preambles (Each preamble are 2 OFDM symbols which contains CP and thus introduce correlation).

For the regular single carrier system, we set the time slot (TS) duration as 0.1ms (In GSM system, it is larger than 0.1ms. We set it smaller than the TS duration in GSM system to ensure that there are correlation peaks in the range of $\tau < 1000$.) The number of symbols (we use QPSK) in each TS is 200. The length of the training symbols is 39 (which can generate an approximate 16% training symbols). The normalized timing correlation is as the following.

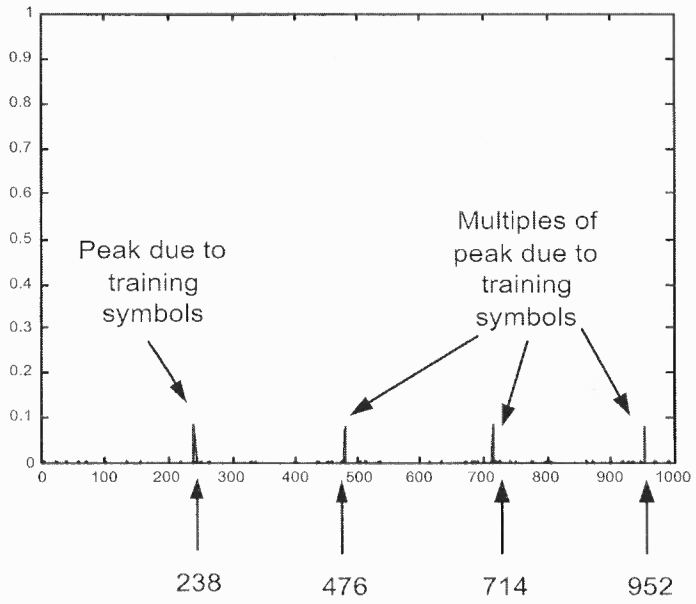

Figure 2.4 Correlation peaks of the regular carrier signal with training symbols.

As shown in Fig. 2.4, there are several peaks with delay τ less than 1000. The peaks behind the first peak are all located at multiples of the first peak's index. This is due to the repeated preambles (or training symbols). The magnitude is 0.0796, which is very near to the theoretical value we derive $\alpha \frac{\sigma_s^2}{\sigma_s^2+\sigma_w^2} = 0.16/2$ (formulated by equation (2.2) and (2.4)).

2.6 Effect of pulse shaping

In practice, raised cosine pulse shaping filters are used. This will result in side-lobes around the correlation peaks. As shown in Fig. 2.5, a raised cosine pulse filter of upsampling rate [4] 3 and delay 10 symbols (result in a filter of 30 taps) is used in the OFDM systems.

As shown in Fig. 2.5, there are many side-lobes around the peak at delay 0 and delay $192 = 64 \times 3$ (where the number of subcarriers $N = 64$). The 3 is due to the upsampling factor of the raised cosine filter. Note also the magnitude is lower than that of figure 1 (0.0497). In simulation, the raised cosine pulse shaping allocated the signal power to more

[4]Oversampling with extra points deleted.

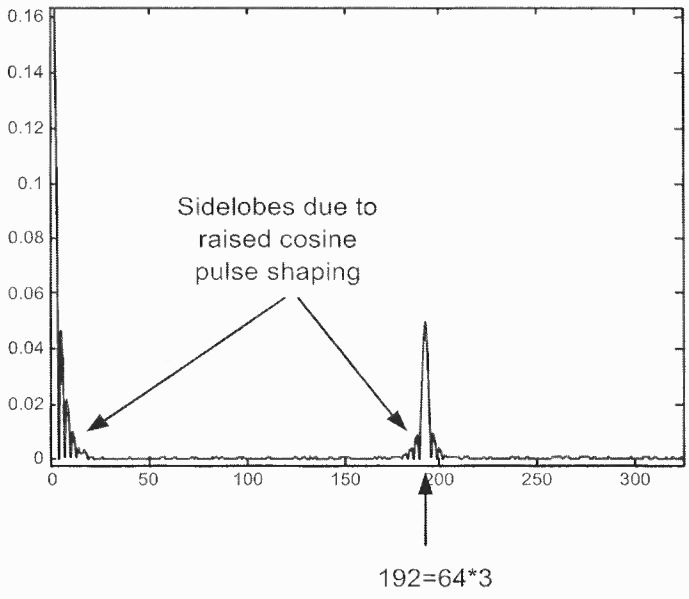

Figure 2.5 Correlation peaks of the OFDM signal with raised cosine pulse shaping.

samples while the noise term maintains the same for each data sample. Therefore, the overall SNR is lower. The correlation at delay 0 given by $E\left[\mathcal{R}\left(0\right)\right] = (\sigma_s^2 + \sigma_w^2)$ from (2.2) changes to $E\left[\mathcal{R}\left(0\right)\right] = (\sigma_s^2 + 3\sigma_w^2)$, while the correlation at delay corresponding to the CP length is given by equation (2.5) $E\left[\mathcal{R}(T_N)\right] = \frac{G}{N+G}\sigma_s^2$. When SNR=0dB, this will result in another 1/2 loss compared to the previous normalized mean value $\frac{G}{N+G}\frac{SNR}{1+SNR} = 1/5/2$ [5].

Since with pulse shaping, the correlation peak becomes broader, to locate the peak at index 192, we should modify our detection method. First, all possible peaks are found by setting a threshold according to the equations (2.2)-(2.5). Second, find the local maximum if there are a group of peaks. These peaks correspond to the main lobe and side-lobes.

[5] According to (2.5), the term $SNR/(1 + SNR) = 1/2$.

2.7 Effect of timing offset and frequency offset

The timing offset does not affect our correlation test because we are summing over all the samples in the observed window.

The frequency offset will affect the previous method due to the fact that the mean of $\mathcal{R}(T_N)$ becomes complex instead of real number. The previous correlation test in (2.1) only takes the real part and thus frequency offset will result in performance loss. Therefore, we suggest to change the correlation test as follows:

$$\check{\mathcal{R}}(\tau) = \left| \left\{ \frac{1}{M} \sum_{n=0}^{M-1} [s(n) + w(n)] \ [s(n-\tau) + w(n-\tau)]^* \right\} \right|^2 \tag{2.9}$$

With the frequency offset, the correlation at zero delays becomes

$$E\left[\check{\mathcal{R}}(0)\right] = E\left| \left\{ \frac{1}{M} \sum_{n=0}^{M-1} [s(n)\exp(-j2\pi\varepsilon n) + w(n)] \ [s(n)\exp(-j2\pi\varepsilon n) + w(n)]^* \right\} \right|^2 \tag{2.10}$$

$$= \sigma_s^4 + \sigma_w^4 + \frac{2M+1}{M}\sigma_s^2\sigma_w^2 \approx \sigma_s^4 + \sigma_w^4 + 2\sigma_s^2\sigma_w^2$$

and at T_N;

$$\begin{aligned} E[\check{\mathcal{R}}(T_N)] &= E\left| \begin{array}{c} \frac{1}{M}\sum_{n=0}^{M-1}[s(n)\exp(-j2\pi\varepsilon n) + w(t)] \\ \cdot [s(n-T_N)\exp[-j2\pi\varepsilon(n-T_N)] + w(n-T_N)]^* \end{array} \right|^2 \\ &\approx \left(\frac{G}{N+G}\right)^2 \sigma_s^4 \end{aligned} \tag{2.11}$$

The normalized mean value $E\left[\check{\mathcal{R}}_{nor}(T_N)\right]$ can be approximated as

$$E\left[\check{\mathcal{R}}_{nor}(T_N)\right] \approx \frac{\left(\frac{G}{N+G}\right)^2 \sigma_s^4}{\sigma_s^4 + \sigma_w^4 + 2\sigma_s^2\sigma_w^2} = \frac{G^2}{(N+G)^2}\left(\frac{SNR}{1+SNR}\right)^2 \tag{2.12}$$

The pdf of the two hypothesis are chi-squared distributed instead of Gaussian because $\mathcal{R}(\tau)$ is the modular square of two Gaussian distributed signal. It is more complicated than the previous case. To simplify the problem, we still set the threshold as $\frac{E[\check{\mathcal{R}}_{nor}(T_N)]}{2}$ (The mean value $E\left[\check{\mathcal{R}}_{nor}(T_N)\right]$ is given in equation (2.12)).

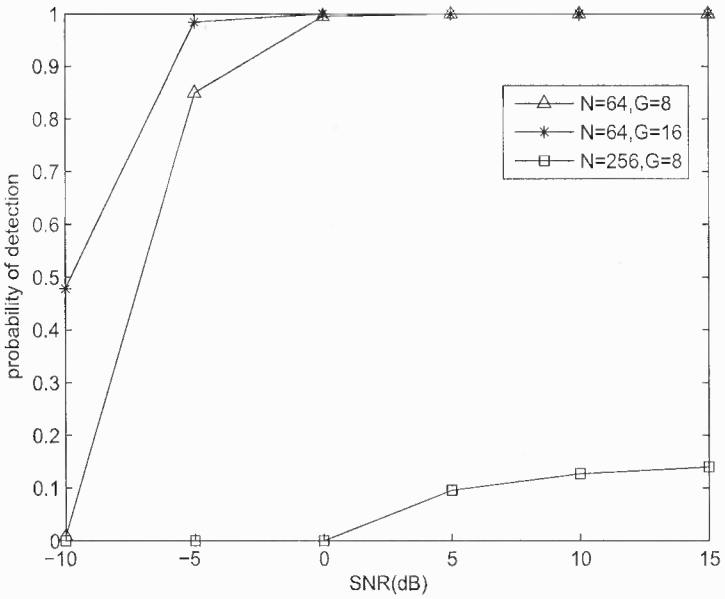

Figure 2.6 Probability of detection for OFDM signals with different N and G.

2.8 Simulation results

Monte Carlo simulations are conducted to test the performance of the above scheme under different scenarios. The observed duration is 1.2ms. Each OFDM burst contains 10 data symbols and 2 preambles. The symbol duration for OFDM symbol is 4 μs.

First, we assume that no frequency offset and pulse shaping exist. Different number of subcarriers or CP length are used in test. The threshold is set as in (2.5). The number of runs is 1000. In the simulation, OFDM signal is transmitted through AWGN and 1.2ms data samples are collected. With the correlation test (equation (2.1)), when the first correlation peak is within 2 samples of the length of the data part of OFDM symbol, we decide that the detection is successful.As shown in Fig. 2.6, the larger the CP length, the better the performance of the detection.

Second, we take as a frequency offset of $0.3 \times 2\pi$ (per sample). The number of subcarriers is 64 and the length of CP is 16. The threshold is set according to equation

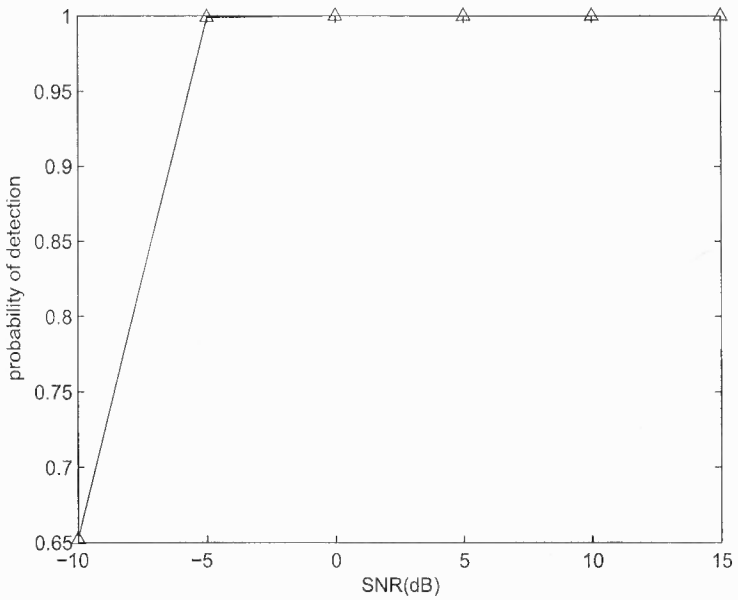

Figure 2.7 Probability of detection for OFDM signals with frequency offset.

(2.12). As shown in Fig. 2.7, the modified scheme according to (2.12) has a similar performance as the scheme according to (2.1).

Third, raised cosine pulse shaping is used. Finding the first group of correlation peaks by setting the threshold according to equation (2.9), then select the peak with the maximum magnitude. Similar to the previous tests, when the index of the peak is within 2 samples of the length of the data part of OFDM symbol, we conclude the detection is successful.

Similarly, we apply single carrier signal (without training symbols). and take time slot duration of $50\mu s$, which contains 200 symbols. We repeat the above three scenarios for this single carrier signal, and consider failed detection if there is a peak over the threshold; otherwise, it is considered successful.

Last, we apply single carrier signal with training symbols, with the same time slot duration of $50\mu s$, of 200 symbols in each time slot. This constitute number of training symbols per TS of 16%. We repeat the above three scenarios for this single carrier signal with training symbols. If there is multiple peak over the threshold, and the indices of the

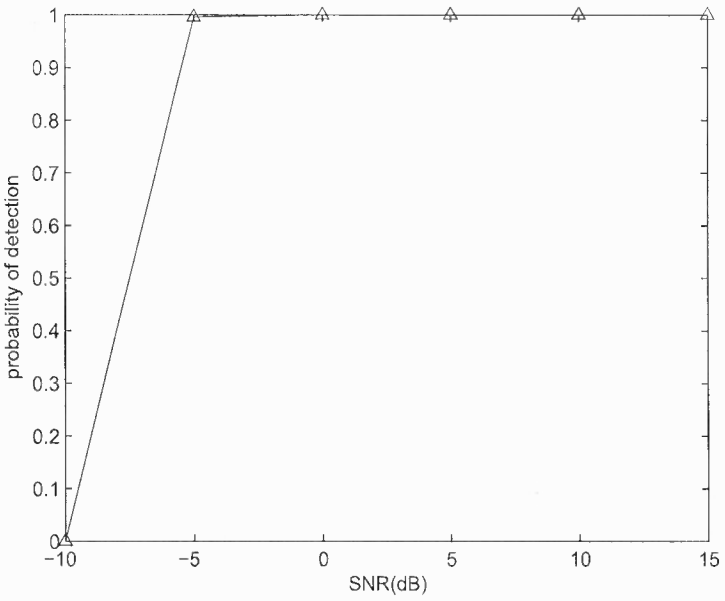

Figure 2.8 Probability of detection for OFDM signals with frequency offset and pulse shaping.

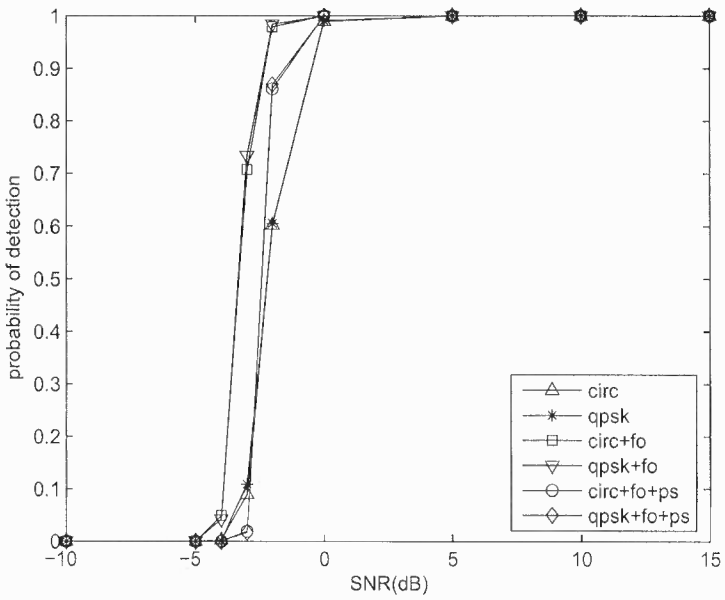

Figure 2.9 Probability of detection for single carrier signals without training symbols.

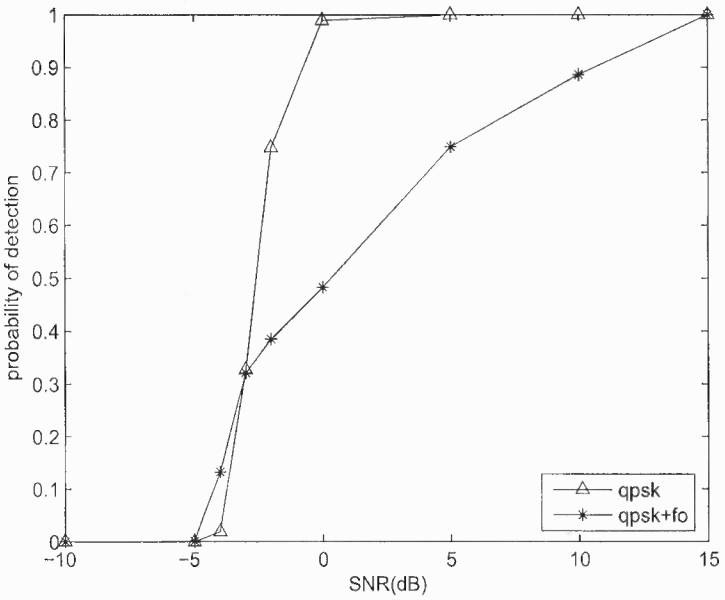

Figure 2.10 Probability of detection for single carrier signals with training symbols.

following peaks are of the first multiples, the detection is considered successful; otherwise, it is considered failed.

CHAPTER 3

FOURTH ORDER CUMULANTS BASED OFDM SIGNAL CLASSIFICATION

In this Chapter, we propose to use the fourth order cumulants to distinguish OFDM from single carrier signals.

We first show analytically that the value of $C_{40}(N)$ and $C_{42}(N)$ as a function of the number of subcarriers "N" of the OFDM signal and its SNR. We use these values as estimates of these functions, together with the estimates of the cumulants for different single carrier modulated signals as they were given in the literature [7] including SC-BC or by experiments we performed, as for others.

From all set of values we create thresholds detectors that compare the estimates of different groups using either one cumulant or both depending on the assumed environments which include timing offset, phase rotation, frequency offset of the received signals, and pulse shaping. To show robustness we use the variance of these cumulants.

Finally, in the Chapter, we use Monte Carlo simulations under different scenarios to examine the probability of distinguishing OFDM from different single carrier signals.

3.1 Signal Model and fourth order cumulants

The fourth-order cumulants can be defined as

$$C_{40} = cum\left(r\left(m\right), r\left(m\right), r\left(m\right), r\left(m\right)\right) \tag{3.1}$$

$$C_{41} = cum\left(r\left(m\right), r\left(m\right), r\left(m\right), r^{*}\left(m\right)\right) \tag{3.2}$$

$$C_{42} = cum\left(r\left(m\right), r\left(m\right), r^{*}\left(m\right), r^{*}\left(m\right)\right) \tag{3.3}$$

where $r(m)$ is the received sample sequence. For the zero-mean modulated signal, cum can be written as

$$\begin{aligned} cum(wxyz) &= E(wxyz) - E(wx)E(yz) \\ &\quad - E(wy)E(xz) - (wz)E(xy) \end{aligned} \tag{3.4}$$

The cumulants can be estimated from the sample estimates which are given by [7]

$$\hat{C}_{40} = \frac{1}{M}\sum_{m=0}^{M-1} r^4(m) - 3\hat{C}_{20}^2 \tag{3.5}$$

$$\hat{C}_{41} = \frac{1}{M}\sum_{m=0}^{M-1} r^3(m)\, r^*(m) - 3\hat{C}_{20}\hat{C}_{21} \tag{3.6}$$

$$\hat{C}_{42} = \frac{1}{M}\sum_{m=0}^{M-1} |r(m)|^4 - \left|\hat{C}_{20}\right|^2 - 2\hat{C}_{21}^2 \tag{3.7}$$

where M is the length of the observed data samples. $\hat{C}_{20}$ and $\hat{C}_{21}$ are given by [7]

$$\hat{C}_{21} = \frac{1}{M}\sum_{m=0}^{M-1} |r(m)|^2 \tag{3.8}$$

$$\hat{C}_{20} = \frac{1}{M}\sum_{m=0}^{M-1} r^2(m) \tag{3.9}$$

Apparently, $\hat{C}_{21}$ measure the average power of the received signal. In practice, we estimate the normalized cumulants [7]

$$\tilde{C}_{4k} = \hat{C}_{4k}/\hat{C}_{21}^2 \tag{3.10}$$

In the case of noisy data, $\hat{C}_{21}$ must be replaced by $\hat{C}_{21} - \hat{C}_{21,w}$, where $\hat{C}_{21,w}$ is an estimate of the variance of the additive noise $w(m)$.

In the following, we will use $\hat{C}_{40}$ and $\hat{C}_{42}$ for the detection problem. In Table 3.1, the theoretical values are obtained by computing the expectation of the signal in noise-free scenarios, under the constraint of unit energy [7].

Table 3.1 The theoretical cumulant statistics C_{40} and C_{42} for various constellation types.

constellation	C_{40}	C_{42}
BPSK	-2	-2
QPSK	1	-1
8PSK	0	-1
QAM16	-0.68	-0.68
QAM64	-0.62	-0.62
CIRC16	-1.36	-0.30
OFDM	0	0

We start by comparing cumulants of OFDM with that of Gaussian distributed signal. Using simulation with 50 OFDM symbols, 64 subcarriers, and 16 CP length, we have $\hat{C}_{40} = -0.009 - j0.005$ and $\hat{C}_{42} = 0.018$. When the number of subcarriers changed to 256, CP length is 16, $\hat{C}_{40} = -0.004 - j0.002$ and $\hat{C}_{42} = 0.005$. With complex Gaussian distributed signal generated by MATLAB, for the same length of the observed sequence, $\hat{C}_{40} = -0.002 + j0.001$ and $\hat{C}_{42} = 0.002$. This shows that, the difference between cumulants of OFDM signal and the Gaussian distributed signal is small compared to the difference in cumulants among OFDM and other SC signals.

3.2 Cases with timing, frequency offset, phase rotation and pulse shaping filtering

3.2.1 Effect of timing offset, phase rotation, and frequency offset

The timing offset does not affect the cumulants based detection scheme because we are summing over all the samples in the observed window.

From its definition, $\hat{C}_{42}$ is a combination of the absolute values of different terms, hence it is real. Also one can show [7] that C_{40} will have a complex multiplier $exp\,(j4\phi)$, where ϕ is a phase rotation of the signal. Therefore phase rotation will not affect $\left|\hat{C}_{40}\right|$ and $\hat{C}_{42}$.

The effect of the frequency offset has not been thoroughly discussed in [7] [1]. In this report, we consider the case when the frequency offset which is caused by the mismatch of the oscillator at receiver and the transmitter is considerably large. For example, when the frequency offset is $\varepsilon = 0.3 \times 2\pi$ per sample (radial frequency), we have $\hat{C}_{40}$ and $\hat{C}_{42}$ given in Table 3.2. This value is the same for any frequency offset except π or $\frac{\pi}{2}$.

Table 3.2 The theoretical cumulant statistics C_{40} and C_{42} for various constellation types with frequency offset $0.3 \times 2\pi$.

constellation	C_{40}	C_{42}
BPSK	0	-1
QPSK	0	-1
8PSK	0	-1
QAM16	0	-0.68
QAM64	0	-0.62
CIRC16	0	-0.30
OFDM	0	0

With frequency offset, we notice from Table 3.2 that in comparison to Table 3.1, C_{40} becomes zeros for all constellation, while C_{42} stays the same except for BPSK. That is, frequency offset eliminates the difference in C_{40} between different constellation, and hence it can not be used to distinguish different SC signals. Instead here we can use C_{42} to distinguish OFDM from other SC constellations. Note however that the difference in C_{42} between OFDM and Circ16 is the smallest.

[1] Swami conducted simulations to test the effect of a very small frequency offset.

On the other hand without frequency offset (Table 3.1), we may use C_{40} to distinguish MPSK($M > 4$) signals or OFDM from other signal and then use C_{42} to distinguish between OFDM and MPSK($M > 4$) signals.

3.2.2 Effect of pulse shaping

In practice, pulse shaping filters specifically, raised cosine are applied. This will result in change in the phase and magnitudes of the signal samples, and thus change the values of the cumulants.

For the case where no phase rotation but frequency offset are present, we present in Table 3.3 the simulated cumulant statistics with different roll-off factors. Due to using the simulated cumulant statistics, instead of theoretical values, the value of the cumulants for different roll-off factors are different for Table 3.1 and Table 3.2.

Table 3.3 The simulated cumulant statistics $\hat{C}_{40}$ and $\hat{C}_{42}$ for various constellation types with various roll-off factors with no rotation or frequency offset (number of samples=4000).

	roll-off = 0		roll off = 0.5		roll off = 1	
constellation	$\hat{C}_{40}$	$\hat{C}_{42}$	$\hat{C}_{40}$	$\hat{C}_{42}$	$\hat{C}_{40}$	$\hat{C}_{42}$
BPSK	−1.38	−1.38	−1.69	−1.69	−1.74	−1.74
QPSK	−0.69	−0.69	−0.93	−0.82	−1.18	−0.77
8PSK	0	−0.69	0	−0.82	0	−0.77
QAM16	−0.47	−0.47	−0.63	−0.52	−0.80	−0.39
QAM64	−0.43	−0.43	−0.57	−0.47	−0.73	−0.32
CIRC16	−0.94	−0.20	−1.26	−0.17	−1.60	0.06
OFDM	0	−0.01	0	0.08	0	0.39

A simple way to distinguish OFDM signal from the other signals is to employ the sum of $\hat{C}_{40}$ and $\hat{C}_{42}$. Without prior information of the roll-off factor, one use to define

the threshold, the sum, $\hat{C}_{40} + \hat{C}_{42}$, of that constellation and that roll-off factor, which is closest to that of OFDM at all roll-off (lower bound). From Table 3.3 this corresponds to 8PSK signal with roll-off factor 0, which equals to -0.69. Other single carrier signal has values even less than -0.69. For that roll-off, the value of $\hat{C}_{40} + \hat{C}_{42}$ for the OFDM signal with roll-off 0 is -0.01. Therefore, according to the detection theory, we should set the threshold as a half of the distance between $\hat{C}_{40} + \hat{C}_{42}$ of 8PSK and OFDM [2], which is $(-0.69 + 0.01)/2 = -0.34$. Therefore, when $\hat{C}_{40} + \hat{C}_{42} > -0.34$, we declare the signal is OFDM. Otherwise, it is SC.

If frequency offset exist, we notice from Table 3.2 that only the value of $\hat{C}_{42}$ is non-zero which can be used for our detection. Without prior knowledge of the roll-off factors, we notice from Table 3.4 that when the roll-off factor is 1, Circ16 signals have $\hat{C}_{42}$ equals to 0.06, which is already larger than that of OFDM signal with roll-off 0 (-0.01). Hence, it is impossible to distinguish between Circ16 and OFDM signals for such case by using $\hat{C}_{42}$.

Restricting the roll-off factor to no larger than 0.5 (which is almost true for most of the practical system), then according to Table 3.4, and using $\hat{C}_{42}$ alone, the closest case happens for distinguishing between Circ16 signal with roll-off factor 0.5 and OFDM signals with roll-off 0.

Therefore, for this case to distinguish OFDM signal from Circ16 signal, we can set the threshold as $(-0.17 + 0.01)/2 = -0.08$. "-0.17" corresponds to the sum of $\hat{C}_{40}$ and $\hat{C}_{42}$ for Circ16 signal with roll-off 0.5. [3] While "-0.01" is the value of $\hat{C}_{40} + \hat{C}_{42}$ for OFDM signal with roll-off 0. Hence, when $\hat{C}_{40} + \hat{C}_{42} > (-0.17 + 0.01)/2 = -0.08$, we declare the signal is OFDM. Otherwise, it is SC, including Circ16.

---

[2]This is the asymptotic threshold since we assume the sample variance for different signal constellations are the same [7].

[3]Similar to the case without frequency offset, $\hat{C}_{40} + \hat{C}_{42}$ is used. Actually, only $\hat{C}_{42}$ is non-zero.

Table 3.4 The simulated cumulant statistics $\hat{C}_{40}$ and $\hat{C}_{42}$ for various constellation types with various roll-off factors with frequency offset $\varepsilon = 0.3 \times 2\pi$ (number of samples=4000).

	rolloff = 0		roll off = 0.5		roll off = 1	
constellation	$\hat{C}_{40}$	$\hat{C}_{42}$	$\hat{C}_{40}$	$\hat{C}_{42}$	$\hat{C}_{40}$	$\hat{C}_{42}$
BPSK	0	−0.38	0	−0.70	0	−0.74
QPSK	0	−0.69	0	−0.82	0	−0.77
8PSK	0	−0.69	0	−0.82	0	−0.77
QAM16	0	−0.47	0	−0.52	0	−0.39
QAM64	0	−0.43	0	−0.47	0	−0.32
CIRC16	0	−0.20	0	−0.17	0	0.06
OFDM	0	−0.01	0	0.08	0	0.39

3.3 The mean and variance analysis

For the evaluation of the mean and variance of $\hat{C}_{40}$ and $\hat{C}_{42}$ we start by calculating the real value of C_{40} and C_{42} for an OFDM symbol which given by

$$r(n) = \frac{1}{\sqrt{N}} \sum_{k=0}^{N-1} X_k e^{\frac{j2\pi kn}{N}} \ , \ 0 \leq n \leq N-1 \tag{3.11}$$

where N is the number of subcarriers. X_k are the data symbols drawing from some constellation. in the following analysis we restrict X_k to be BPSK symbols.

3.3.1 Calculated values of C_{40} and C_{42} of OFDM signal

Value of $C_{40}(N)$ According to (3.4) we can write $C_{40}(n, N)$ as

$$C_{40}(n, N) = E\{r^4(n)\} - 3E\{r^2(n)\}^2 \tag{3.12}$$

It can easily shown that

$$E\{r^2(n)\} = \begin{cases} 1 & ,n = 0, \frac{N}{2} \\ 0 & ,o.w. \end{cases} \tag{3.13}$$

while

$$E\{r^4(n)\} = \begin{cases} 3 - \frac{2}{N} & ,n = 0, \frac{N}{2} \\ -\frac{2}{N} & ,n = \frac{N}{4}, \frac{3N}{4} \\ 0 & ,o.w. \end{cases} \tag{3.14}$$

Thus the value of $C_{40}(n, N)$ is given by

$$C_{40}(n, N) = \begin{cases} -\frac{2}{N} & ,n = 0, \frac{N}{4}, \frac{N}{2}, \frac{3N}{4} \\ 0 & ,o.w. \end{cases} \tag{3.15}$$

Averaging over the OFDM symbol $(0 \leq n \leq N-1)$ we get

$$C_{40}(N) = \frac{4}{N} \cdot \left(-\frac{2}{N}\right) = -\frac{8}{N^2} \tag{3.16}$$

Value of $C_{42}(N)$ Following the same steps for $C_{42}(n, N)$ it can be shown that

$$\begin{aligned} C_{42}(n, N) &= E\{|r(n)|^4\} - |E\{r^2(n)\}|^2 - 2E\{|r(n)|^2\}^2 = \\ &= -\tfrac{2}{N} \end{aligned} \tag{3.17}$$

Thus, after averaging we get

$$C_{42}(N) = -\frac{2}{N} \tag{3.18}$$

3.3.2 Mean and Variance of $\hat{C}_{40}$ and $\hat{C}_{42}$ of OFDM signals

By its definition (given by (3.5) and (3.7)) $\hat{C}_{40}$ and $\hat{C}_{42}$ are sample estimates. Sample estimate is known to be an unbiased estimator hence the mean values of $\hat{C}_{40}$ and $\hat{C}_{42}$ are

given by (3.16) and (3.18) respectively. In [7] the variances of $\hat{C}_{40}$ and $\hat{C}_{42}$ were derived for general signals and are given by

$$M \cdot var[\hat{C}_{40}] = m_{84} - |m_{40}|^2, \tag{3.19}$$

and for C_{42} in (3.7) calculate estimated C_{21} term complicates the variance calculation which is approximated by

$$M \cdot var[\hat{C}_{42}] \approx [m_{84} - m_{42}^2] + 4m_{21}[3m_{42}m_{21} - 2m_{63} + 2m_{21}^3] \tag{3.20}$$

where M is the number of samples and $m_{k,m} = E[y^{k-m}(y)^{*^m}]$ is the mean of $C_{k,m}$. An asymptotical approach is used to ease the derivation of this term. By assuming that the number of subcarriers N is large we omitted all terms that are $O(1/N^d)$ for $d > 0$, i.e. consider only terms that are $O(1)$. Using combinatorics reasoning it is easy to show that

$$m_{84} = 24 \tag{3.21}$$

and following the same steps it can be shown that

$$m_{63} = 6 \tag{3.22}$$

Similarly, we have

$$\begin{aligned} m_{40} &\approx 0 \\ m_{42} &\approx 2 \\ m_{21} &= 1 \end{aligned} \tag{3.23}$$

Putting it all together we conclude that

$$\begin{aligned} var[\hat{C}_{40}] &\approx 24/M \\ var[\hat{C}_{42}] &\approx 4/M \end{aligned} \tag{3.24}$$

We can conclude that the mean values of C_{40} and C_{42} are indeed goes to zero for large N as expected from an OFDM symbol which is approximated as Gaussian. The variance is shown not to vary substantially with N.

3.4 Simulation

Monte Carlo simulations were conducted to test the performance of the above scheme under different scenarios. The length of the observed symbols was 4000 for single carrier signals. For OFDM signals, there were 50 OFDM symbols, each with 64 subcarriers and CP length 16, resulting in 4000 observed data samples for detection. For SC-BC signals, there were 50 SC-BC symbols, each with data block length 64 and CP length 16, also resulting in 4000 observed data samples for detection.

First, we assume that neither frequency offset nor pulse shaping is used (referring to Table 3.1). We first use $\hat{C}_{40}$ to successfully distinguish the other modulation types from OFDM or8PSK signal (since only OFDM and 8PSK signal have a zero $\hat{C}_{40}$). then we use $\hat{C}_{42}$ to distinguish OFDM from 8PSK signal. According to Table 3.1, we set the threshold as -0.5. When $\hat{C}_{42} > -0.5$, we declare the signal is OFDM. Otherwise, it is 8PSK signal. OFDM and 8PSK, 8PSK SC-BC signal are transmitted respectively, each of which implementing Monte Carlo simulation experiments of 1000 runs resulting in Probability of detection as in Fig.3.1.

Second, assuming that a frequency offset of $0.3 \times 2\pi$ (per sample, normalized to the sampling frequency at the receiver) is used. Then from Table 3.2, we can only use the nonzero $\hat{C}_{42}$, and a threshold of $(-0.3 - 0)/2 = -0.15$. When $\hat{C}_{42} > -0.15$, we declare the signal is OFDM. Otherwise, it is SC signal. With a Monte Carlo of 1000 runs, the probability of detection is given in Fig.3.2. As it is shown, the detection of the SC-BC signals has the similar performance as SC signals.

Third, assuming that a frequency offset of $0.3 \times 2\pi$ (per sample) and raised cosine pulse shaping with roll-off factor of 0.25 is used. Without prior knowledge of the roll-

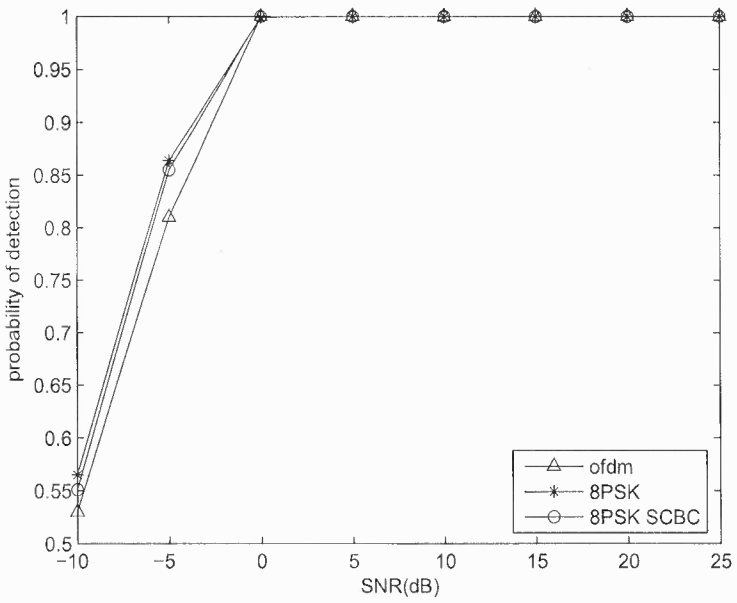

Figure 3.1 Probability of detection for OFDM signal vs 8PSK signal.

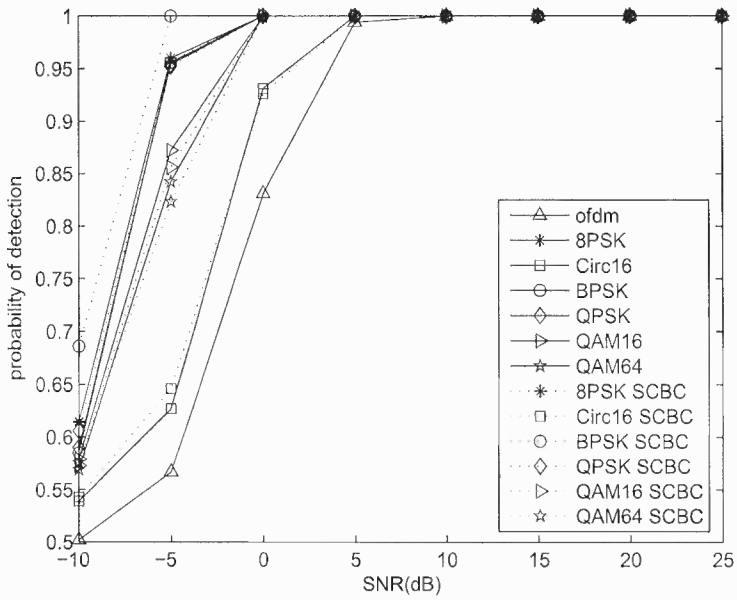

Figure 3.2 Probability of detection for OFDM signal vs SC signal with frequency offset 0.3.

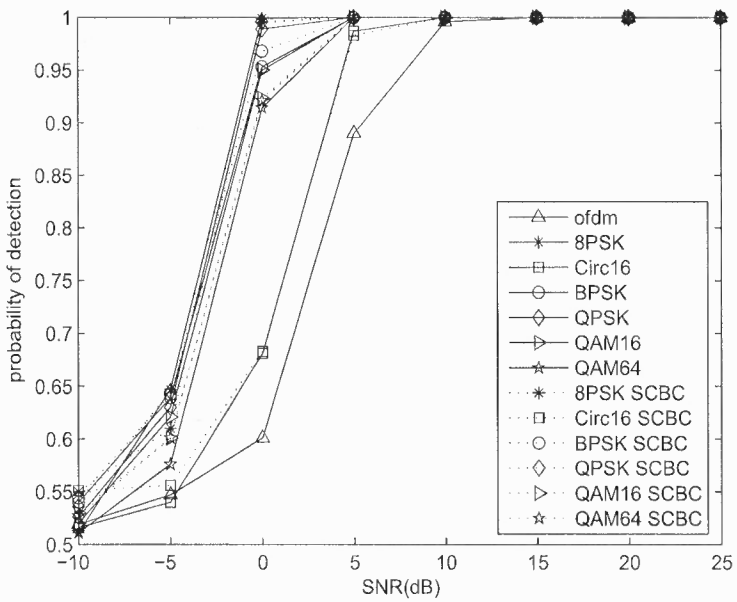

Figure 3.3 Probability of detection for OFDM signal vs SC signal with frequency offset 0.3 and pulse shaping (roll-off factor 0.25).

off factor, we set the threshold according to Table 3.4 and as discussed in section 3.2 it equals $(-0.17 + 0.01)/2 = -0.08$. When $\hat{C}_{42} > -0.08$, we declare the signal is OFDM. Otherwise, it is SC signal. With a Monte Carlo of 1000 runs, the probability of detection is given in Fig.3.3.

Fourth, as shown in Fig.3.4, assuming that a frequency offset of $0.3 \times 2\pi$ (per sample) and also raised cosine pulse shaping is used, but with roll-off factor 0.5. The threshold is set again to $(-0.17 + 0.01)/2 = -0.08$ according to Table 3.4. When $\hat{C}_{42} > -0.08$, we declare the signal is OFDM. Otherwise, it is SC signal. With a Monte Carlo of 1000 runs, the probability of detection is given in Fig.3.4.

3.5 Proof that C_{40} of SC constellations with frequency offset are zeros

According to [7] (see Table 3.1 for 8PSK), the fourth order cumulant C_{40} is zero for MPSK($M > 4$) signals.

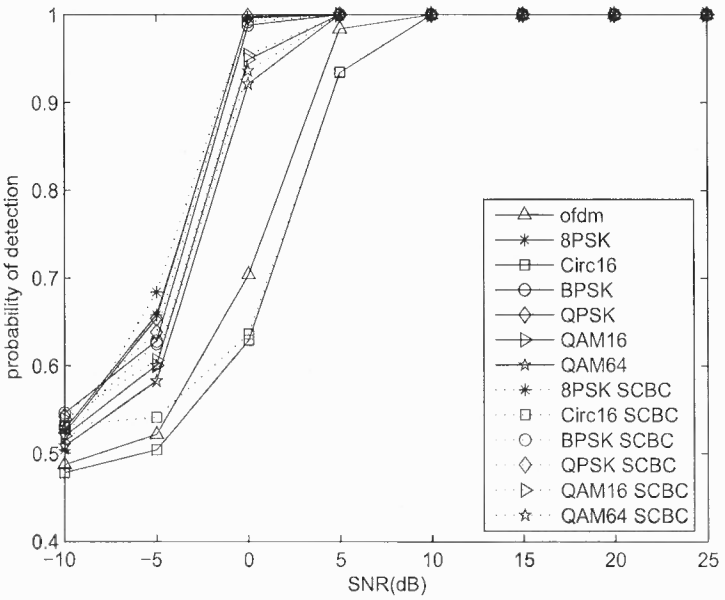

Figure 3.4 Probability of detection for OFDM signal vs SC signal with frequency offset $0.3 \times 2\pi$ and pulse shaping (roll-off factor 0.5).

For QPSK signals, when the normalized frequency offset equals to π or $\frac{\pi}{2}$, the constellation will not change. On the other hand, when the normalized frequency offset is not equal to π or $\frac{\pi}{2}$, the constellation of the signals with frequency offset will form a circle similar to the constellation of MPSK($M > 4$) signals (as shown in Fig.3.5), and hence, the cumulant C_{40} is zero.

For BPSK signals, when the normalized frequency offset equals to π, its constellation will not change. However, when the normalized frequency offset equals $\frac{\pi}{2}$, the constellation of the BPSK signals changes to that of QPSK signals which according to Table 3.1, given $C_{40} = 1$. On the other hand, similar to the QPSK signals, when the normalized frequency offset is equal to π or $\frac{\pi}{2}$, the constellation of the signals will form a circle similar to the constellation of MPSK($M > 4$) signals (as shown in Fig. 3.5), and hence, the cumulant C_{40} is zero.

For other signal constellations (QAM or Circ), we can regard the signals as PSK signals with multi-level magnitude. Similarly, when the normalized frequency offset is not

equal to π or $\frac{\pi}{2}$, the constellation of the signals form several circle which corresponds to the constellation of several MPSK($M > 4$) signals with different magnitudes (as shown in Fig. 3.5), and hence, the cumulant C_{40} is zero.

3.6 Proof that C_{42} of SC constellations with frequency offset stays the same

From its definition, $\hat{C}_{42}$ is a combination of the absolute values of different terms, hence it is real. According to Swami's paper, $C_{42} = -1$ for MPSK($M > 2$). In such cases, when the frequency offset is present, since the signal sample's absolute value does not change, the cumulant C_{42} stays the same, i.e, $C_{42} = -1$.

For BPSK signals, when the normalized frequency offset equals to π, the constellation will not change, i.e, $C_{42} = -2$ as in Table 3.1. For other frequency offset, the constellation of the BPSK signals changes to that of MPSK($M > 2$) signals, for which $C_{42} = -1$ (see Table 3.2 for BPSK).

For other signal constellations (QAM or Circ), we can regard the signals as MPSK($M > 2$) with multi-level magnitude, therefore, the constellation of the signals with frequency offset will form several circle which corresponds to the constellation of several MPSK($M > 4$) signals with different magnitudes. Hence, the cumulant C_{42} stays the same as in Table 3.1.

3.7 Summation and discussion

It is shown from above sections, the fourth cumulant based AMC we proposed for OFDM system has several limitations.

First, the threshold is subject to the pool of AMC candidates. For example, when Circ16 signal is not present, in the worst case (Table 3.4), the threshold can be set $-0.32 + 0.01/2 = -0.155$ instead of -0.08. Actually, this problem is inherent in the AMC of OFDM signals. Generally, in the case of modulation classification of a particular signal from a bunch of signal candidates, we may apply the Neyman-Pearson theorem where

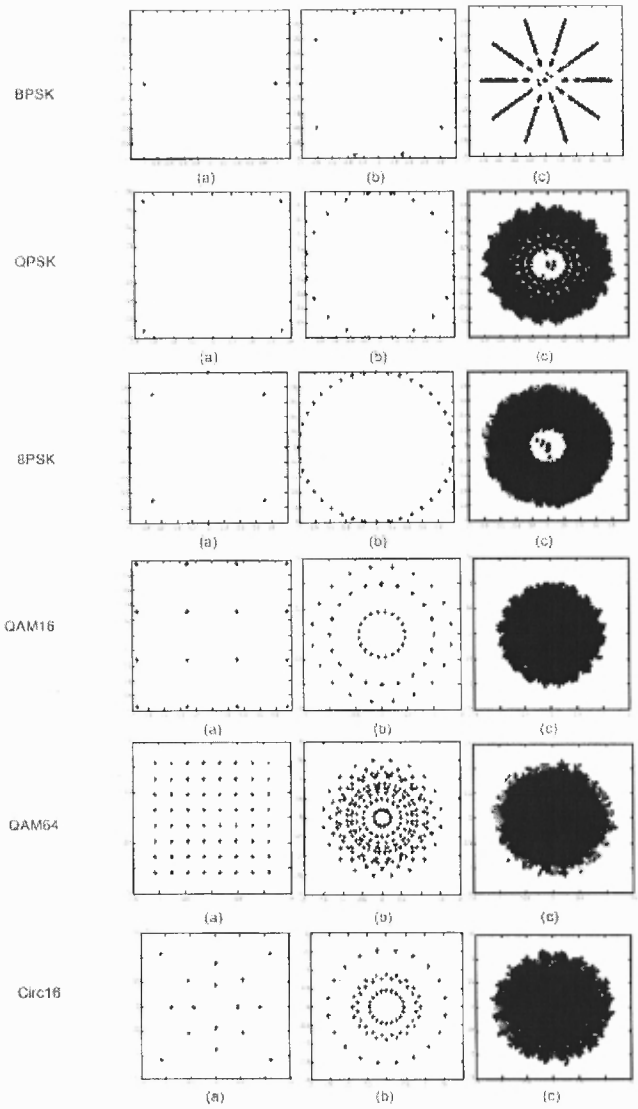

Figure 3.5 The constellation diagrams for various modulation types (a) original (b) with frequency offset (c) after raised cosine pulse shaping (roll-off = 0.5).

the probability density function (pdf) of that particular signal is known. While exact pdf expression for OFDM signal is extraordinary complicated, the approximation of the pdf of OFDM signal as Gaussian seems promising. However, previous Gaussianity based OFDM AMC methods fail in high SNR scenarios due to the fact of assuming OFDM signal is Gaussian distributed.

Second, the pulse shaping filtering will introduce correlation between the cumulants and thus deteriorate the performance. As we discussed in section 3.2, without restricting the roll-off factor, it is impossible to distinguish OFDM with Circ16 signal. A possible way to solve this problem is to whiten the fourth order cumulants using the Giannakis-Tsatsanis normality-test [13]. This is the same as proposed by Akmouche in [6] and as we discussed in Chapter 1, are very complicated. The impact of the fading channel is similar to that of pulse shaping due to the correlation introduced between samples and also between fourth order cumulants.

CHAPTER 4

BLIND OFDM SIGNALS PARAMETERS ESTIMATION

4.1 Introduction

After identifying the OFDM signals, blind OFDM parameters as well as the synchronization parameter estimation process is conducted thereafter needed for blind demodulation.

Blind estimation of OFDM signals has been widely explored in [1], [15], [16], [17], [18]. Most of which ([1], [15]) focused on the synchronization parameters or on one or two other parameters [16], [17]. According to our knowledge, to date a more complete OFDM signal parameters extraction has only been discussed in [14] and [18]. Both papers employed the correlation method to explore the system parameters of OFDM systems at the assumption of a known sampling frequency. Although it is not clearly emphasized, the method proposed in [18] can not perform well when the symbol timing is not synchronized.

In this chapter, we propose a blind estimation process that consider the complete system parameters and synchronization parameters for OFDM demodulation. The proposed blind estimation process is divided into three steps [1]: sampling frequency estimation, number of subcarriers estimation, joint estimation of CP length and timing/frequency estimation. First, using the cyclostationarity introduced by the oversampling, we employ the cyclostationarity test algorithm proposed by Dandawaté and Giannakis for the sampling frequency estimation [19]. In the second step, a simple correlation method is used to extract the number of subcarriers. Last, the length of the cyclic prefix (CP) as well as the timing and frequency offset are jointly estimated by using the cyclostationarity test [19], [1], [15].

[1]This is the first version of the work on OFDM blind estimation, which has been published in [12].

4.2 Cyclostationarity in the received OFDM signals

A signal $x(t)$ is called second-order cyclostationary if its time-varying correlation function [2]

$$R(t,\tau) = E[x(t)\,x^*(t+\tau)] \tag{4.1}$$

is periodic in t for a given delay τ. Denote M as the length of the data. The cyclic-correlation at cycle frequency α, $C(\alpha,\tau)$, is the Fourier series of $R(t,\tau)$ with respect to time t [19], given by (note that t here is integer)

$$C(\alpha,\tau) = \lim_{M\to\infty}\frac{1}{M}\sum_{t=0}^{M} R(t,\tau)\exp(-j\alpha t) \tag{4.2}$$

Let $x(t)$ be the received OFDM signal, which can be given by

$$x(t) = \sum_{m} s(m)\,h(t-mT_b) + w(t) \tag{4.3}$$

where $s(m)$ is the transmitted OFDM signal with CP. T_b is the received signal duration of one sample in time domain. $h(t)$ results from the transmitting and receiving filters and the fading channel. $w(t)$ is additive white Gaussian noise (AWGN) with variance σ_w^2.

To simplify the derivation, we assume that the transmitted signal have a rectangular pulse shape and the channel is AWGN. We assume that $q = T_b/T_b'$, the over-sampling factor, is large enough. The oversampled sequence $x(n)$ is obtained by oversampling the received signal with sampling frequency $1/T_b'$; i.e.

$$x(n) = \sum_{m} s(m)\,g(n-mq) + w(n) \tag{4.4}$$

[2] In literature, E$[x(t)x(t+\tau)]$, ie. without conjugation is also considered.

where we used $T_b' = 1$. $g(l)$ is the rectangular pulse given by

$$g(l) = \begin{cases} 1, & 0 \leq l \leq q \\ 0, & otherwise \end{cases} \tag{4.5}$$

Suppose $q > 2$, the discrete time-varying correlation function $R(n, \tau)$ at $\tau = 1$ [3] will be periodic with period equals q (when q is an integer number) or almost-periodic (when q is a fractional number) with period q, that is

$$R(n + lq, 1) = R(n, 1) \tag{4.6}$$

where l is any integer larger than 1. Note that since the received signal is now change to discrete sequence, we will use the discrete number to indicate the time delay τ without specific mention.

For example, when q is an integer, and since the OFDM signal $s(m)$ is independent of the noise, the signal power is σ_s^2, $R(n, \tau)$ will be a rectangular pulse train given by

$$R(n, 1) = \begin{cases} \sigma_s^2, & 0 \leq n \bmod q < q - 1 \\ 0, & n \bmod q = q - 1 \end{cases} \tag{4.7}$$

Obviously, the above function is a periodic function with period q. Therefore, when we choose the delay $q > \tau = 1$, the discrete time-varying correlation function $R(n, \tau)$ will be a periodic function with period q.

Actually, due to the introduction of CP, the OFDM signal itself is cyclostationary [1]. The time-varying correlation function of the OFDM signal $s(m)$ is periodic having rectangular pulse shape of a period $T_{all} = T_s + T_{cp}$, where $T_{cp} = GT_b$, the duration of the CP part. $T_s = NT_b$ is the useful OFDM symbol duration. N is the number of subcarriers. G is the length of the CP.

[3] τ is a integer here after sampling in the receiver.

4.3 Blind estimation of system parameters

4.3.1 Sampling frequency estimation

The first step of the blind estimation process is to extract the sampling frequency or the oversampling factor q. We employ the existing cyclic spectrum analysis method proposed by Dandawaté and Giannakis [19].

If the signal is cyclostationary with cyclic-frequency α (or oversampling frequency when $q > 1$) for delay τ, the estimator gives by

$$\widehat{\alpha} = \arg\max_{\alpha} \left[\hat{c}\left(\alpha, \tau\right) \hat{Y}^{-1} \hat{c}\left(\alpha, \tau\right)^{T} \right] \tag{4.8}$$

where $\hat{c}\left(\alpha, \tau\right)$ is given by

$$\hat{c}\left(\alpha, \tau\right) = \left[\begin{array}{cc} \mathrm{Re}\left(\hat{C}\left(\alpha, \tau\right)\right) & \mathrm{Im}\left(\hat{C}\left(\alpha, \tau\right)\right) \end{array} \right] \tag{4.9}$$

$\hat{C}\left(\alpha, \tau\right)$ is the estimate of $C\left(\alpha, \tau\right)$, the cyclic-correlation at cycle frequency α, which is given by

$$\hat{C}\left(\alpha, \tau\right) = \frac{1}{M} \sum_{t=0}^{M} x\left(t\right) x^{*}\left(t + \tau\right) \exp\left(-j\alpha t\right) \tag{4.10}$$

and $\hat{Y}$ is the asymptotic covariance matrix of the estimator $\hat{C}\left(\alpha, \tau\right)$, which can be computed by using the equations given in [19],

$$\hat{Y} = \left[\begin{array}{cc} \mathrm{Re}\{\frac{\mathbf{Q}_{2c} + \mathbf{Q}_{2c}^{(*)}}{2}\} & \mathrm{Im}\{\frac{\mathbf{Q}_{2c} - \mathbf{Q}_{2c}^{(*)}}{2}\} \\ \mathrm{Im}\{\frac{\mathbf{Q}_{2c} + \mathbf{Q}_{2c}^{(*)}}{2}\} & \mathrm{Re}\{\frac{\mathbf{Q}_{2c} - \mathbf{Q}_{2c}^{(*)}}{2}\} \end{array} \right] \tag{4.11}$$

where $\mathbf{Q}_{2c}$ and $\mathbf{Q}_{2c}^{(*)}$ are given by

$$\mathbf{Q}_{2c} = S\left(2\alpha, \alpha\right) = \frac{1}{Mb} \sum_{i=-(b-1)/2}^{(b-1)/2} W\left(i\right) C\left(\alpha - \frac{2\pi i}{M}, 1\right) C\left(\alpha + \frac{2\pi i}{M}, 1\right) \tag{4.12}$$

$$\mathbf{Q}_{2c}^{(*)} = S\left(0, -\alpha\right) = \frac{1}{Mb} \sum_{i=-(b-1)/2}^{(b-1)/2} W\left(i\right) C^{*}\left(\alpha + \frac{2\pi i}{M}, 1\right) C\left(\alpha + \frac{2\pi i}{M}, 1\right) \tag{4.13}$$

$W(i)$ is a spectral window of length b.

Note that we used $\tau = 1$. From the previous section, the oversampled received signal will be cyclostationary when $\tau < q$. It is shown that $\tau = 1$ is enough for cyclostationarity test [32].

Subsequently, the oversampling factor q will be given by

$$\widehat{q} = \frac{2\pi}{\widehat{\alpha}} \tag{4.14}$$

where $\widehat{\alpha}$ is the estimated cyclic frequency in radian with oversampling q. Using FFT for the cyclic spectrum analysis, the above equation can be rewritten as

$$\widehat{q} = \frac{P}{\widehat{K}} \tag{4.15}$$

where P is the FFT size, $\widehat{K}$ is the index of the peak value.

4.3.2 Estimation of the number of subcarriers

The target of this sub-section is to estimate the data part duration of an OFDM symbol, T_s. Combined with the sampling frequency we estimated in the last section, we can get the number of subcarriers given by $N = \lfloor T_s/T_b \rceil$.

Due to the correlation introduced by the CP in OFDM signal, a simpler estimator for the data part duration T_s can then be given by

$$\widehat{T_s} = \arg\max_{l>0} \left[\left| \left(\sum_{k=0}^{M} x(k)\, x^*(k+l) \right) \right| \right] T_b' \tag{4.16}$$

4.3.3 Joint estimation of CP length, frequency and timing offset

The joint estimation of CP length and the timing/frequency offset is presented in this sub-section. Since the OFDM signal itself is a cyclostationary signal at a delay $\tau = T_s$, when T_s was estimated from the previous sub-section, we can employ (4.8) with $\tau = T_s$ for estimating the corresponding cyclo-frequency or symbol duration T_{all}, and find the $T_{cp} = T_{all} - T_s$.

Also from [1] and [15], the frequency and timing offset can be obtained by using the cyclostationary statistics. The frequency estimator we will use here are different from theirs, though the performance are approximately the same as these two. We assume the signal at this step is already downsampled and as the above, is rectangular pulse shaping under AWGN channels. Considering the timing offset ν and the frequency offset ε, the signal can be given by

$$x(k) = s(k-\nu)\exp(-j2\pi\varepsilon k/N) + w(k) \tag{4.17}$$

Note that we may consider the correlation term in (4.16) as the cyclic-correlation at cycle frequency 0. Due to the introduction of the CP, when the delay $\tau = N$, the correlation term can be rewritten as

$$\sum_{k=0}^{n} x(k)\, x^*(k+N) = \exp(-j2\pi\varepsilon) \sum_{k-\nu\in I} |s(k-\nu)|^2 + Z(\cdot) \tag{4.18}$$

where I is the set of k which are inside the CP or, $I = \{k | 0 \le (k-\nu) \mod N + G < G\}$, and

$$\begin{aligned} Z(\cdot) = & \sum_{k-\nu\notin I} x(k)\, x^*(k+N) \\ & + \sum_{k-\nu\in I} w^*(k+N)\, s(k-\nu)\exp(-j2\pi\varepsilon k/N) \\ & + \sum_{k-\nu\in I} w(k)\, s^*(k-\nu+N)\exp[j2\pi(\varepsilon k/N+\varepsilon)] \end{aligned} \tag{4.19}$$

With the assumption that the noise is independent from the signal and the signal outside of CP is independent, $Z(\cdot)$ can be approximated due to the central limit theorem as Gaussian noise. When the number of OFDM symbols for the estimation is large, the frequency offset ε can be given by

$$\widehat{\varepsilon} = -\frac{1}{2\pi N}\arg\hat{C}\left(0, \widehat{N}\right) \tag{4.20}$$

where $\hat{C}\left(0,\widehat{N}\right)$ is the estimate of the cyclic-correlation at cycle frequency 0 and delay $\widehat{N}$. Note $\hat{C}\left(0,\widehat{N}\right)$ can also be given by (4.18).

After obtaining the frequency offset as in (18), we use eqn.(21) of [1] to obtain the timing offset $\widehat{\nu}$, i.e.

$$\widehat{\nu} = \lfloor -\frac{\widehat{T_{all}}}{2\pi} \arg\left[C\left(\alpha,\widehat{N}\right)\exp\left(-j2\pi\widehat{\varepsilon}\right)\right]\rceil \tag{4.21}$$

where $\widehat{T_{all}}$ was estimated earlier.

According to the standards [8], [9], the maximum CP length is $1/4$ of the useful symbol duration. For example, when $N = 64$, $G = 16$, and the FFT size for the cyclic spectrum analysis is 1024, the peak will appear around the index $\lfloor 1024/\left(N+G\right)\rceil \simeq 13$. Since at this step, we already know the number of subcarriers N, the peak we expected will be smaller than $\lfloor 1024/N\rceil$. Using such prior information of the CP length, the performance of the estimator can be drastically improved. Also, to improve the resolution of the cyclo-period estimation, larger FFT size for the cyclic spectrum can also be employed.

As shown in the Fig. 4.1, Cyclostationarity test was conducted when $N = 64$, $G = 16$, timing offset $\nu = 36$, normalized frequency offset $\varepsilon = 0.3$, $SNR = 25dB$, and the FFT size for the cyclic spectrum analysis is 4096. The received signal duration used was around 100 OFDM symbols. Using the estimator given in (4.8), (4.20) and (4.21), we get the estimated cyclo-period $\widehat{T_{all}} = \lfloor 4096/51\rceil = 80$, the estimated frequency offset $\widehat{\varepsilon} = 0.30$, the estimated timing offset $\widehat{\nu} = 36$. Note from Fig. 4.1, there are three peaks clustered together, corresponding to the cyclic-frequency and its multiple. Without prior information about the CP length, the performance of the estimator will deteriorate due to the existence of such multiple peaks in the cyclic correlation spectrum.

4.4 Simulation

Monte Carlo simulations are conducted to test the performance of the above estimators under different scenarios. First, the performance of the each of the estimators is tested

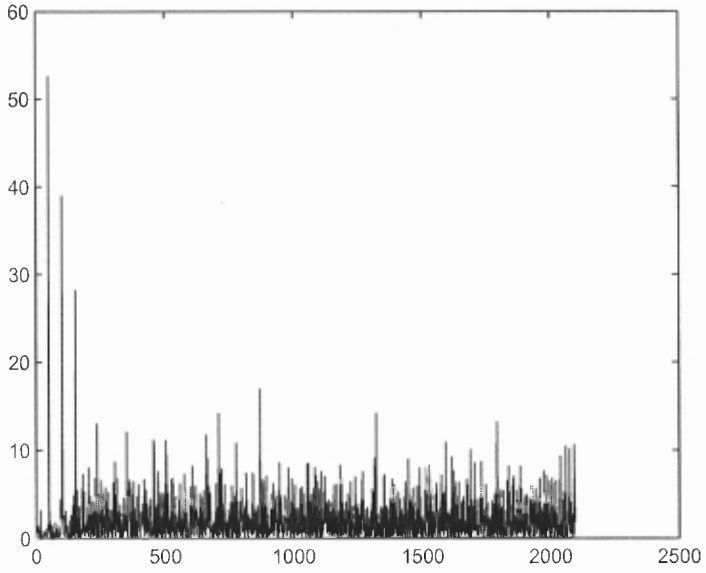

Figure 4.1 Cyclostationarity test for CP length estimator at fixed $\tau = T_s$.

independently in different scenarios. In the first case, AWGN channel with ideal rectangular pulse shaping is used with $N = 64$, $G = 16$, $q = 5/2$, $\nu = 20T_b$, $\varepsilon = 0.3$ and the number of runs was 1000. The received data used for estimation is around 50 OFDM symbols. The normalized mean square error (NMSE) of the estimated oversampling factor q and the frequency offset, the absolute sample deviation of the number of subcarriers N, and the symbol duration $(N + G)$ as well as the timing offset ν under different SNRs are measured and shown in Fig. 4.2. As it can be seen, the correlation based method for the estimate of N is quite robust even with low SNRs. The estimator for q based on cyclostationarity test is not good enough when the noise is larger than a certain value, while the estimator for $(N + G)$ based on cyclostationarity test is robust. Note that the FFT size for cyclostationarity test will affect the performance. This will consequently results in an error floor in the timing offset estimate.

In the second set of simulation, a square raised cosine filter with roll-off equals to 0.25 is used in the transmitter. We carry out the simulations under slow timing varying multipath

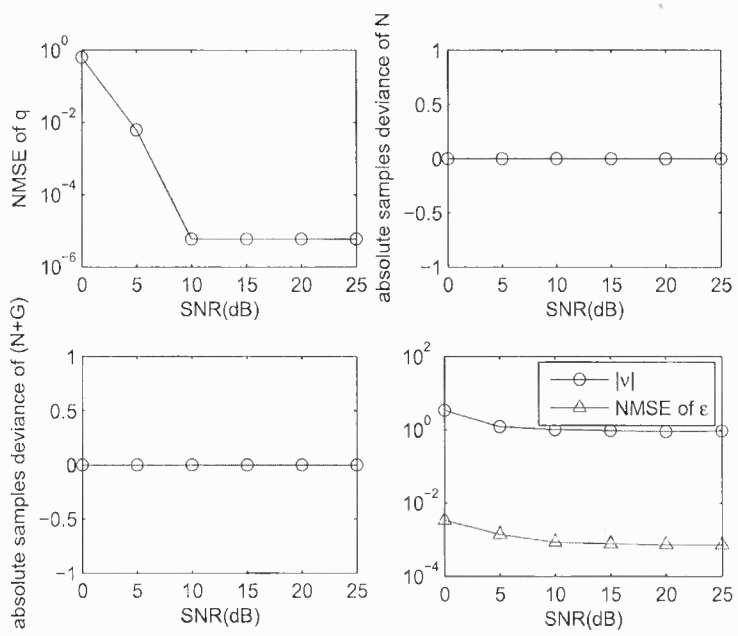

Figure 4.2 Performance of the estimator of oversampling factor q, number of subcarriers N, symbol duration T_{all}, timing offset ν, frequency offset ε under AWGN channel.

channels. Fig. 4.3 shows that the performance of all the estimators will deteriorate somewhat. The timing offset estimator will have an error floor corresponding to the delay due to the raised cosine pulse filter.

To evaluate the overall performance of our proposed estimators, a chain test is performed under the above three different scenarios. The system parameters we used is $N = 64$, $G = 16$, $q = 3$, $\nu = 20T_b$, $\varepsilon = 0.3$. The number of runs is 1000. The received data used for estimation is around 50 symbols. The performance of the estimator is as shown in the Fig. 4.4 and 4.5, respectively. It is shown that the performance of the sampling frequency estimator is very crucial.

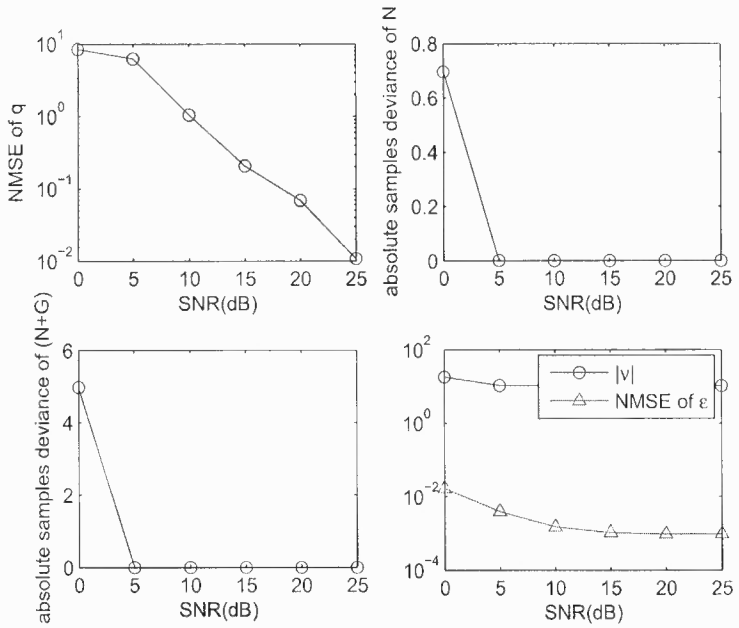

Figure 4.3 Performance of the estimator of oversampling factor q, number of subcarriers N, symbol duration T_{all}, timing offset ν, frequency offset ε with raised cosine pulse shaping under multipath channel.

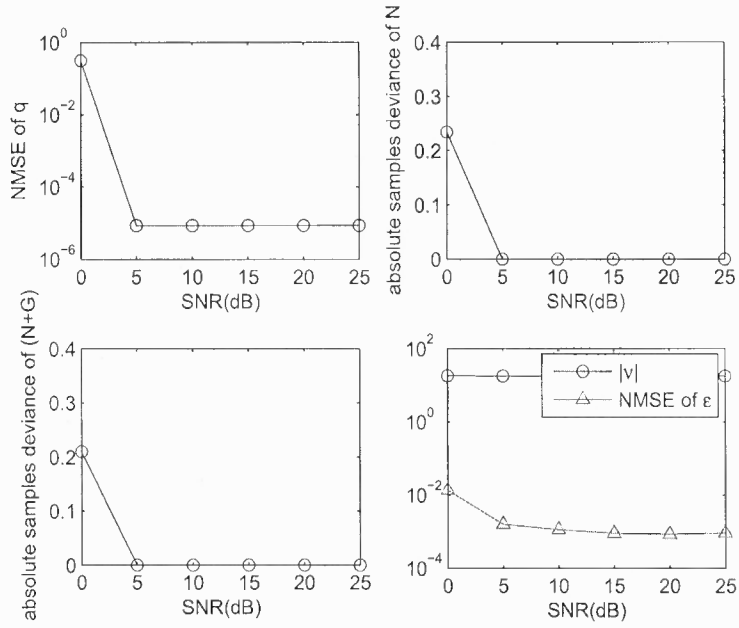

Figure 4.4 Performance of the chain estimator of oversampling factor q, with number of subcarriers N, symbol duration T_{all}, timing offset ν, frequency offset ε under AWGN channel.

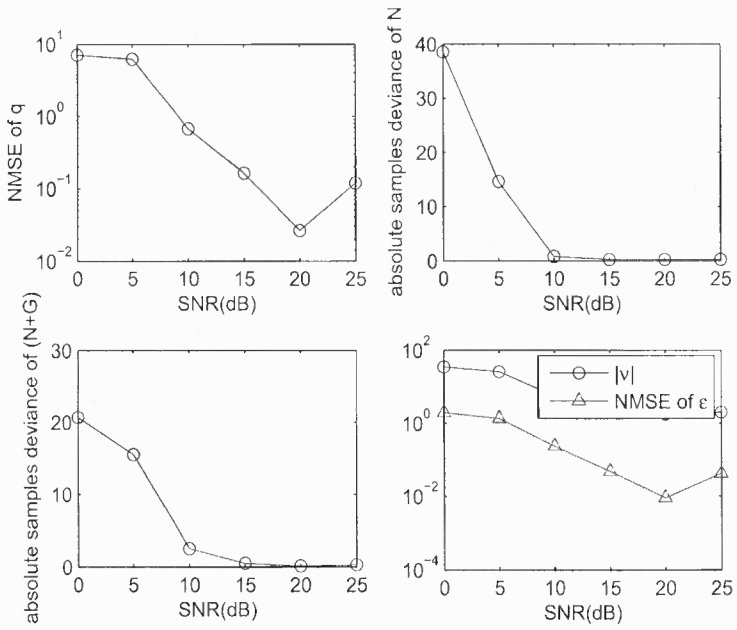

Figure 4.5 Performance of the chain estimator of oversampling factor q, with number of subcarriers N, symbol duration T_{all}, timing offset ν, frequency offset ε with raised cosine filtering under multipath channel.

Part II

SECOND ORDER CYCLOSTATIONARITY AND APPLICATIONS

CHAPTER 5

A SIMPLE METHOD TO ENHANCE THE DETECTION OF SECOND ORDER CYCLOSTATIONARITY

5.1 Introduction

Cyclostationarity is an important feature of wireless communication signals and many other man made processes. Exploration of cyclostationarity started in the 1950s, when Bennett applied it in synchronization algorithms for communications systems [26]. The detection of cyclostationarity of communication signals has been studied by Gardner [27], [28]. Giannakis and Dandawaté proposed statistical tests to show the existence of cyclostationarity [19].

The detection of cyclostationarity has been explored and applied in many areas in literature [27]- [38]. It can be used for symbol rate estimation in traditional modulation classification [32]- [33]. In the recent development of modulation classification, it has been used to estimate the OFDM system parameters as well as MIMO classification [12]- [20]. With the development of cognitive radio, problems like spectrum sensing requires a strong and reliable cyclostationarity detection scheme [35]- [37]. Cyclostationarity was also applied for estimating frequency offset, timing recovery and channel equalization [30]- [31]. More papers on the application about cyclostationarity have been listed by E. Serpedin and el. [38]. Hence improving capability of detecting cyclostationarity will ease performing these processes.

In this Chapter, we consider a scheme to enhance the performance of detecting (probability of detections) the second order cyclostationarity of the received communication signal. By noticing that the second order time varying auto-correlation of the received communication signal contains a cyclostationary real part and a non-cyclostationary complex part, we propose to combine the positive part and the negative part of the *cyclo-spectrum*. (Note that we use the term "cyclo-spectrum" to denote the Fourier transform of the time

varying correlation function. Different from this, it has been called cyclic autocorrelation or cyclic covariance in [28] and [19] respectively. We use the term "cyclo-spectrum" to emphasize its feature in frequency domain.) We note that the DFT at the positive and the negative cyclic frequencies of the real cyclostationary part is conjugate to each other, while the DFT of the non-cyclostationary part (noise part), which is complex, does not have such feature. This property is similar to having cyclostationary part from two different bases. Therefore, it presents extra degree of freedom that can enhance detection performance of the second order cyclostationarity.

5.2 Signal Model and second order Cyclostationarity

The signal model and the definition of second order cyclostationarity have been discussed in section 4.2 in Chapter 4.

Originally proposed for the detection of cyclostationarity in signals, Dandawaté and Giannakis [19] proposed a generalized ML (maximum likelihood) method. This method can also be used to estimate the cyclic frequency $\hat{\alpha}$ [32].

Define $\hat{C}(\alpha, \tau_i)$ as the estimate of $C(\alpha, \tau_i)$, the *cyclo-spectrum* at cyclic frequency α with delay τ_i, which is given by

$$\hat{C}(\alpha, \tau_i) = \frac{1}{M} \sum_{t=0}^{M-1} x(t)\, x^*(t + \tau_i) \exp(-j\alpha t) \tag{5.1}$$

and $\hat{c}(\alpha, \vec{\tau})$ by the vector of dimension $2p$,

$$\begin{aligned} \hat{c}(\alpha, \vec{\tau}) &= \left[\begin{array}{cc} \mathrm{Re}\left(\hat{C}(\alpha, \vec{\tau})\right) & \mathrm{Im}\left(\hat{C}(\alpha, \vec{\tau})\right) \end{array} \right] \\ &= \left[\begin{array}{cccccc} \mathrm{Re}\left(\hat{C}(\alpha, \tau_1)\right) & \mathrm{Im}\left(\hat{C}(\alpha, \tau_1)\right) & \ldots & \mathrm{Re}\left(\hat{C}(\alpha, \tau_p)\right) & \mathrm{Im}\left(\hat{C}(\alpha, \tau_p)\right) \end{array} \right] \end{aligned} \tag{5.2}$$

where $\vec{\tau}$ is a vector of τ. Since the *cyclo-spectrum* for different τ have the same cyclic frequency $\hat{\alpha}$ [19], the estimator (5.3) prewhitens the *cyclo-spectrums* $C(\alpha, \tau_i)$, $i = 1, \ldots, p$,

before combining them together. The cyclic frequency estimator for delay $\vec{\tau}$ is given by

$$\hat{\alpha} = \arg\max_{\alpha}[\hat{c}(\alpha, \vec{\tau})\hat{Y}^{-1}\hat{c}(\alpha, \vec{\tau})^{H}] \tag{5.3}$$

where $\hat{Y}$ is of size $2p \times 2p$ is the asymptotic covariance matrix of the estimator $\hat{c}\,(\alpha, \vec{\tau})$, which can be computed by using the equations (16) and (17) given in [19] ($\hat{Y}$ of size 2×2 is given in equation (4.11) in Chapter 4).

As noticed from (5.3), the scheme proposed by Dandawaté and Giannakis [19] combines the *cyclo-spectrums* at different delay τ to enhance the detection probability of the cyclostationarity test. In the following, we present a new method for enhancing the cyclostationarity of the received signal by combining the information contained in the positive and negative frequency part of the *cyclo-spectrum*.

5.3 New methods to enhance the second order cyclostationarity

5.3.1 direct combining schemes

To simplify the derivation, we assume first that *no pulse shaping filtering* is used in the transmitter, hence the received signal $x(t)$ oversampled with $q > 1$ is given by

$$x\,(n) = \sum_{m} s\,(m)\, g\,(n - mq) + w\,(n) \tag{5.4}$$

$$m = 0, 1, ...; n = 0, 1, ...;$$

where we normalize the sample duration at the receiver, T_b' to 1. $g\,(l)$ is the rectangular pulse given by

$$g(l) = \begin{cases} 1, & 0 \leq l < q,\ l \text{ is an integer} \\ 0, & otherwise \end{cases} \tag{5.5}$$

The discrete time-varying correlation function $R(n, \tau)$ at $\tau = 1$ [1] will be periodic with period q (when q is an integer) or almost-periodic [2] (when q is a fractional number)

[1] τ is taken as integer after sampling in the receiver.

[2] To simplify the derivation, we only consider the periodic case.

[19].That is,

$$R(n+lq,1) = R(n,1) \tag{5.6}$$

when l is any integer. Hence the choice of $\tau = 1$ does not restrict generality. Note that since the received signal is now changed to discrete sequence, we will use the discrete number to indicate the time delay without specific mentioning.

For example, when q is an integer, and since the signal $s(m)$ is independent of the noise, $R(n,1)$ will be a rectangular pulse train given by

$$R(n,1) = \begin{cases} \sigma_s^2, & 0 \le [(n-\nu) \bmod q] < q-1 \\ 0, & [(n-\nu) \bmod q] = q-1 \end{cases} \tag{5.7}$$

where ν is the timing offset, $\nu = 0, \cdots, q-1$, though we will assume $\nu = 0$ in our derivation Obviously, the above function is a periodic function with period q.

In practice, the estimate of the time-varying correlation function, $\hat{R}(n,1)$ is given by

$$\begin{aligned} \hat{R}(n,1) &= x(n)x^*(n+1) \\ &= [x(n) - w(n)]\,[x(n+1) - -w(n+1)]^* \\ &+ w(n)w^*(n+1) + [x(n) - w(n)]\,w^*(n+1) + w(n)\,[x(n+1) - w(n+1)]^* \end{aligned} \tag{5.8}$$

where $n = 0, \cdots M-1$, with M is the length of the observed data samples. Note that the estimate of the time-varying correlation function contains four terms. The first results from the signal, which we denote as $\hat{R}_s(n,1)$. We split $\hat{R}_s(n,1)$ into two complementary sequences: $\hat{R}_{ps}(n,1)$ and $\hat{R}_{nps}(n,1)$. The first shown to be *cyclostationary sequence*, which we call the cyclostationary signal part, is defined as

$$\begin{aligned} &\hat{R}_{ps}(n,1) \\ &= \begin{cases} [x(n) - w(n)] \cdot [x(n+1) - w(n+1)]^*, & 0 \le [(n-\nu) \bmod q] < q-1 \\ 0, & [(n-\nu) \bmod q] = q-1 \end{cases} \end{aligned} \tag{5.9}$$

Clearly, when the received signal is oversampled, the expectation of the $\hat{R}_{ps}(n,1)$ is periodic and is given by (5.7).

The other part of $\hat{R}_s(n,1)$ is non-cyclostationary, which we call the *non-cyclostationary signal part*, is defined as

$$\hat{R}_{nps}(n,1) \tag{5.10}$$
$$= \begin{cases} 0, & 0 \leq [(n-\nu) \bmod q] < q-1 \\ [x(n)-w(n)]\cdot[x(n+1)-w(n+1)]^*, & [(n-\nu) \bmod q] = q-1 \end{cases}$$

The expectation of $\hat{R}_{nps}(n,1)$ is zero for all n due to the fact that the signal $s(m)$ and $s(l)$, $m \neq l$, are independent from each other.

To conduct cyclostationarity test, we use at the front end of the receivers a wide band filter, causing the noise samples be independent and thus contributes to the non-cyclostationary part of $\hat{R}(n,1)$. The *non-cyclostationary sequence noise part* (the other three terms of (5.8)) is given by

$$\hat{R}_{npn}(n,1) = w(n)w^*(n+1) + [x(n)-w(n)]\,w^*(n+1) \tag{5.11}$$
$$+ w(n)\,[x(n+1)-w(n+1)]^*$$

The expectation of $\hat{R}_{npn}(n,1)$ is zero for all n.

As an example of the sequence of (12), (13) and (14), for OFDM systems, when the oversampling factor $q=3$, timing synchronized ($\nu=0$), the sequence of the oversampled signal is given by $[s(0), s(0), s(0), s(1), s(1), ...]$, then the received signal $x(n)$, $n = 0, ...,$ is given by

$$x(n) = \begin{bmatrix} s(0)+w(0), s(0)+w(1), s(0)+w(2), \\ s(1)+w(3), s(1)+w(4), ... \end{bmatrix} \tag{5.12}$$

The *cyclostationary signal part* of the time-varying correlation, $\hat{R}_{ps}(n,1)$, $n=0,...,$ is given by

$$\hat{R}_{ps}(n,1)=\left[|s(0)|^2,|s(0)|^2,0,|s(1)|^2,|s(1)|^2,...\right] \tag{5.13}$$

while the sequence of the *non-cyclostationary signal part* $\hat{R}_{nps}(n,1)$, $n=0,...,$ is given by

$$\hat{R}_{nps}(n,1)=[0,0,s(0)s^*(1),0,0,...] \tag{5.14}$$

The *non-cyclostationary noise part* $\hat{R}_{npn}(n,1)$, $n=0,...,$ is given by

$$\hat{R}_{npn}(n,1)=\begin{bmatrix} w(0)w^*(1)+s(0)w^*(1)+s^*(0)w(0), \\ w(1)w^*(2)+s(0)w^*(2)+s^*(0)w(1), \\ w(2)w^*(3)+s(0)w^*(3)+s^*(1)w(2),... \end{bmatrix} \tag{5.15}$$

We note from (5.13) that the cyclostationary sequence, $\hat{R}_{ps}(n,1)$ is real while from (17) and (18) the non-cyclostationary part, $\hat{R}_{nps}(n,1)$ and $\hat{R}_{npn}(n,1)$ are complex. According to the property of DFT, the Fourier transform of a real periodic sequence has symmetric feature, that is, $F(-\alpha)=F^*(\alpha)$, where $F(\alpha)$ denotes the DFT at frequency α. Hence, the DFT of $\hat{R}_{ps}(n,1)$ will have the aforementioned symmetry; while the non-cyclostationary parts, $\hat{R}_{nps}(n,1)$ and $\hat{R}_{npn}(n,1)$ are complex and aperiodic which does not have the above symmetries. Note that these conclusions can also be applied to the case where delay $\tau>1$.

Straightforwardly going to frequency domain, the detection of cyclostationarity will be enhanced by combining the positive frequency part with the negative frequency part of the *cyclo-spectrum*. This is a simple method which we call the *direct combining scheme*. In fact, with this approach, the cyclic frequency estimator is given by

$$\hat{\alpha}=\arg\max_{\alpha}\kappa_1(\alpha,\tau)=\arg\max_{\alpha}[\left|\hat{C}'(\alpha,\tau)+\hat{C}'^*(-\alpha,\tau)\right|^2] \tag{5.16}$$

where $\hat{C}'(\alpha, \tau)$ is half of the *cyclo-spectrum* of (8.17) with α positive, and $\hat{C}'(-\alpha, \tau)$ is the other half corresponds to α negative, $\alpha \in [0, \pi]$. $\kappa_1(\alpha)$ is the cost function for this scheme. Note that $\hat{\alpha}$ is a function of τ.

5.3.2 prewhiten combining scheme

In [19], Dandawaté and Giannakis proposed a generalized maximum likelihood scheme to estimate the cyclic frequency by combining the *cyclo-spectrum*s for p different delay τ (5.3), which can be regarded as prewhiten before combining. In the following, we apply this approach to combine the corresponding negative frequency part and the positive frequency part of the *cyclo-spectrum* together i.e with $p = 1$. Note that the asymptotic covariance matrix $\hat{Y}$ in (5.3) is estimated by using the *cyclo-spectrum* vector $\hat{c}(\alpha)$ [3]. We propose two ways to obtain the covariance matrix $\hat{Y}$. First, we present a method which uses the exact covariance matrix of the *cyclo-spectrum* $\hat{C}'(\alpha)$. Then we use the asymptotic estimates of $\hat{Y}$ similar to the method proposed by Dandawaté and Giannakis. To distinguish these two methods from the method proposed in previous, we call in the following two methods as prewhitening combining methods.

Assuming that the FFT which generates the *cyclo-spectrum* has size M, which is the same as the length of the observed sequence, when $(M \bmod q) = 0$ or the period q fits the measurement M, the *cyclo-spectrum* of $\hat{R}_{ps}(n, 1)$ has peaks only at indices $\alpha = lM/q$ and zeros elsewhere. l is an integer. This is because the Fourier transform of a periodic signal is an impulse train in the frequency domain with the impulse values proportional to the discrete Fourier series. To simplify the derivation, we can approximate the *cyclo-spectrum* of $\hat{R}_{ps}(n, 1)$ will generate peaks only at indices $\alpha = 2\pi/q$ and zeros elsewhere when the observed sequence is long enough (more periods of data is taken in the measurement.) The *cyclo-spectrum* of $\hat{R}_{ps}(n, 1)$ can be expressed by using the Fourier transform of one

[3]Note that we dropped the dependence of τ as we took it to equal to one.

period of the cyclostationary sequence, which is given by

$$\hat{C}_{ps}(\alpha) = \sum_{l=0}^{q-1} Z_l \delta\left(\alpha - \frac{2l\pi}{q}\right) \tag{5.17}$$

where $\delta(\cdot)$ is a delta function. Z_l, $l = 0, \cdots, q-1$, is the lth sample of the DFT of one period of the periodic sequence $\left[\overbrace{\sigma_s^2, \cdots, \sigma_s^2}^{q-\nu-1}, 0, \overbrace{\sigma_s^2, \cdots, \sigma_s^2}^{\nu}\right]$. To simplify the derivation, in the following, we assume the signal is timing synchronized, or $\nu = 0$. When $\nu \neq 0$, the above sequence will be rotated accordingly, and thus change the value of Z_l.

The noise in the *cyclo-spectrum* is due to the non-cyclostationary part which is the overall result of $\hat{R}_{nps}(n,1)$ and $\hat{R}_{npn}(n,1)$. Since the signal is independent of the noise, it is possible to find directly the *cyclo-spectrum* noise introduced by $\hat{R}_{nps}(n,1)$ and $\hat{R}_{npn}(n,1)$ separately. When $\nu = 0$, from (5.10), the DFT of $\hat{R}_{nps}(n,1)$ is given by

$$\hat{C}_{nps}(\alpha) = \frac{1}{M} \sum_{k=0}^{\lfloor M/q \rfloor - 1} s(k)\, s^*(k+1) \cdot \exp(-jq\alpha k) \exp[-j\alpha(q-1)] \tag{5.18}$$

Note that when $\nu \neq 0$, according the property of the DFT, $\hat{C}_{nps}(\alpha)$ will have an additional exponential term on the right corresponding to the non-zero timing offset ν. Since both $\hat{C}_{nps}(\alpha)$ and $\hat{C}^*_{nps}(-\alpha)$ are complex, and $\mathrm{Re}[\hat{C}^*_{nps}(-\alpha)] = \mathrm{Re}[\hat{C}_{nps}(-\alpha)]$, $\mathrm{Im}[\hat{C}^*_{nps}(-\alpha)] = -\mathrm{Im}[\hat{C}_{nps}(\alpha)]$, the covariance matrix of $\hat{C}_{nps}(\alpha)$ and $\hat{C}^*_{nps}(-\alpha)$, cov_{nps} is given by

$$cov_{nps}(\alpha) = \begin{bmatrix} (\hat{c}_{r+})^2 & \hat{c}_{r+}\hat{c}_{r-} & \hat{c}_{r+}\hat{c}_{i+} & \hat{c}_{r+}\hat{c}_{i-} \\ \hat{c}_{r+}\hat{c}_{r-} & (\hat{c}_{r-})^2 & \hat{c}_{r-}\hat{c}_{i+} & \hat{c}_{r-}\hat{c}_{i-} \\ \hat{c}_{r+}\hat{c}_{i+} & \hat{c}_{r-}\hat{c}_{i+} & (\hat{c}_{i+})^2 & \hat{c}_{i+}\hat{c}_{i-} \\ \hat{c}_{r+}\hat{c}_{i-} & \hat{c}_{r-}\hat{c}_{i-} & \hat{c}_{i+}\hat{c}_{i-} & (\hat{c}_{i-})^2 \end{bmatrix} \tag{5.19}$$

where

$$\begin{aligned} \hat{c}_{r+} &= \mathrm{Re}[\hat{C}_{nps}(\alpha)] \\ &= \frac{1}{M} \sum_{k=0}^{\lfloor M/q \rfloor - 1} \left\{ \begin{array}{l} z_r(k) \cos[q\alpha k + \alpha(q-1)] \\ +z_i(k) \sin[q\alpha k + \alpha(q-1)] \end{array} \right\} \end{aligned} \tag{5.20}$$

$$\hat{c}_{r-} = \mathrm{Re}[\hat{C}_{nps}(-\alpha)] \tag{5.21}$$
$$= \frac{1}{M}\sum_{k=0}^{\lfloor M/q \rfloor - 1}\left\{\begin{array}{l} z_r(k)\cos[q\alpha k + \alpha(q-1)] \\ -z_i(k)\sin[q\alpha k + \alpha(q-1)] \end{array}\right\}$$

$$\hat{c}_{i+} = \mathrm{Im}[\hat{C}_{nps}(\alpha)] \tag{5.22}$$
$$= \frac{1}{M}\sum_{k=0}^{\lfloor M/q \rfloor - 1}\left\{\begin{array}{l} -z_r(k)\sin[q\alpha k + \alpha(q-1)] \\ +z_i(k)\cos[q\alpha k + \alpha(q-1)] \end{array}\right\}$$

$$\hat{c}_{i-} = -\mathrm{Im}[\hat{C}_{nps}(-\alpha)] \tag{5.23}$$
$$= \frac{1}{M}\sum_{k=0}^{\lfloor M/q \rfloor - 1}\left\{\begin{array}{l} -z_r(k)\sin[q\alpha k + \alpha(q-1)] \\ -z_i(k)\cos[q\alpha k + \alpha(q-1)] \end{array}\right\}$$

Note that $z_r(k) = \mathrm{Re}[s(k)s^*(k+1)]$ and $z_i(k) = \mathrm{Im}[s(k)s^*(k+1)]$. $\mathrm{E}[z_r(l)z_r(m)] = \mathrm{E}[z_i(l)z_i(m)] = 0$, $l \neq m$, since the signal $s(k)$ is i.i.d. $\mathrm{E}[z_r^2(k)] = \mathrm{E}[z_i^2(k)] = \frac{\sigma_s^4}{2}$ and $\mathrm{E}[z_r(k)z_i(k)] = 0$ since the real and imaginary part of the signal $s(k)$ is also i.i.d. Through mathematical manipulation, we have

$$\mathrm{E}\left[(\hat{c}_{r+})^2\right] \tag{5.24}$$
$$= \mathrm{E}\left\{\mathrm{Re}\left[\frac{1}{M}\sum_{k=0}^{\lfloor M/q \rfloor - 1}\left\{\begin{array}{l} z_r(k)\cos[q\alpha k + \alpha(q-1)] \\ -z_i(k)\sin[q\alpha k + \alpha(q-1)] \end{array}\right\}\right]^2\right\}$$
$$= \frac{1}{M^2}\sum_{k=0}^{\lfloor M/q \rfloor - 1}\mathrm{E}\left[z_r^2(k)\right]\cos^2[q\alpha k + \alpha(q-1)]$$
$$+ \mathrm{E}\left[z_i^2(k)\right]\sin^2[q\alpha k + \alpha(q-1)]$$
$$= \frac{\sigma_s^4}{2Mq}$$

Similarly, we can get

$$\mathrm{E}\left[(\hat{c}_{r+})^2\right] = \mathrm{E}\left[(\hat{c}_{r-})^2\right] = \mathrm{E}\left[(\hat{c}_{i+})^2\right] = \mathrm{E}\left[(\hat{c}_{i-})^2\right] = \frac{\sigma_s^4}{2Mq} \tag{5.25}$$

$$\mathrm{E}\left[\hat{c}_{r+}\hat{c}_{i+}\right] = \mathrm{E}\left[\hat{c}_{r-}\hat{c}_{i-}\right] = 0 \tag{5.26}$$

$$\begin{aligned}\mathrm{E}\left[\hat{c}_{r+}\hat{c}_{r-}\right] &= -\mathrm{E}\left[\hat{c}_{i+}\hat{c}_{i-}\right] \\ &= \frac{\sigma_s^4}{2Mq}\sum_{k=0}^{\lfloor M/q\rfloor-1}\cos\left[2q\alpha k + 2\alpha\left(q-1\right)\right]\end{aligned} \tag{5.27}$$

and

$$\begin{aligned}\mathrm{E}\left[\hat{c}_{r+}\hat{c}_{i-}\right] &= \mathrm{E}\left[\hat{c}_{r-}\hat{c}_{i+}\right] \\ &= -\frac{\sigma_s^4}{2Mq}\sum_{k=0}^{\lfloor M/q\rfloor-1}\sin\left[2qk\alpha + 2\left(q-1\right)\alpha\right]\end{aligned} \tag{5.28}$$

Note that except at the cyclic frequency $l\pi/q$, where l is an integer, all the non-diagonal entries of the covariance matrix $cov_{nps}(\alpha)$ given by (5.19) are approximately zeros, that is, the *cyclo-spectrum* noise generated by the signal is almost white.

Similarly from (14), we can get $\hat{C}_{npn}\left(\alpha\right)$, the DFT of $\hat{R}_{npn}(n,1)$, and the covariance matrix of $\hat{C}_{npn}\left(\alpha\right)$ and $\hat{C}^*_{npn}\left(-\alpha\right)$, cov_{npn}. Except the frequency at 0, $\pm\pi$, $cov_{npn}(\alpha)$ is given by

$$cov_{npn}(\alpha) = \frac{\sigma_w^4}{2M}\mathbf{I}_4 + cov_{npn2}(\alpha) \tag{5.29}$$

where $\mathbf{I}_4$ is the unit matrix of size 4, and $cov_{npn2}(\alpha)$ is the covariance matrix generated by the cross term of the signal and noise, which is a 4×4 matrix given by

$$cov_{npn2}(\alpha) = \begin{bmatrix} \varsigma_{11}(\alpha) & \varsigma_{12}(\alpha) & \varsigma_{13}(\alpha) & \varsigma_{14}(\alpha) \\ \varsigma_{12}(\alpha) & \varsigma_{22}(\alpha) & \varsigma_{23}(\alpha) & \varsigma_{24}(\alpha) \\ \varsigma_{13}(\alpha) & \varsigma_{23}(\alpha) & \varsigma_{33}(\alpha) & \varsigma_{34}(\alpha) \\ \varsigma_{14}(\alpha) & \varsigma_{24}(\alpha) & \varsigma_{34}(\alpha) & \varsigma_{44}(\alpha) \end{bmatrix} \tag{5.30}$$

where

$$\varsigma_{11}(\alpha) = \varsigma_{22}(\alpha) \tag{5.31}$$
$$= \frac{\sigma_s^2\sigma_w^2}{Mq}\left\{q + \sum_{k=0}^{\lfloor M/q\rfloor-1}\sum_{i=0}^{q-2}\cos\left[(2i+1)\,\alpha + 2qk\alpha\right]\right\}$$

$$\varsigma_{33}(\alpha) = \varsigma_{44}(\alpha) \tag{5.32}$$
$$= -\frac{\sigma_s^2\sigma_w^2}{Mq}\left\{q - \sum_{k=0}^{\lfloor M/q\rfloor-1}\sum_{i=0}^{q-2}\cos\left[(2i+1)\,\alpha + 2qk\alpha\right]\right\}$$

$$\varsigma_{12}(\alpha) = \varsigma_{34}(\alpha) = -\frac{\sigma_s^2\sigma_w^2}{Mq}\cos\alpha \tag{5.33}$$

$$\varsigma_{13}(\alpha) = \varsigma_{24}(\alpha) = -\frac{\sigma_s^2\sigma_w^2}{Mq}\sum_{k=0}^{\lfloor M/q\rfloor-1}\sum_{i=0}^{q-2}\sin\left[(2i+1)\,\alpha + 2qk\alpha\right] \tag{5.34}$$

and

$$\varsigma_{14}(\alpha) = \varsigma_{23}(\alpha) = 0 \tag{5.35}$$

In summary, the first term on the RHS of (5.29) is diagonal, which means that the *cyclo-spectrum* noise from the additive noise $w(n)$ is white (except the frequency at $0, \pm\pi$) [4]. However, the second term on the RHS of (5.29) is not diagonal, meaning that the cross term of the signal and noise will bring correlated *cyclo-spectrum* noise. Similar to (5.3, the cyclic frequency estimator using prewhiten combining scheme is given by

$$\hat{\alpha} = \arg\max_{\alpha}\kappa_2(\alpha) \tag{5.36}$$
$$= \arg\max_{\alpha}[\hat{c}'(\alpha)\left[cov_{nps}(\alpha) + cov_{npn}(\alpha)\right]^{-1}\hat{c}'(\alpha)^H] \tag{5.37}$$

[4]The oversampling factor $q \neq 2$ will insure that cyclic frequency is not equal to $\pm\pi$.

where as in (5.2)

$$\hat{c}'(\alpha) = \begin{bmatrix} \mathrm{Re}\left(\hat{C}'(\alpha)\right) & \mathrm{Re}\left(\hat{C}'(-\alpha)\right) \ldots \\ \mathrm{Im}\left(\hat{C}'(\alpha)\right) & -\mathrm{Im}\left(\hat{C}'(-\alpha)\right) \end{bmatrix} \tag{5.38}$$

except $\hat{C}'(\alpha)$ is only half of the *cyclo-spectrum.* (The prime identifies this fact). [5].

In the above prewhiten scheme, the covariance matrix is derived theoretically. According to (5.19) and (5.29), to calculate the covariance matrix, we need the prior knowledge of oversampling factor q, timing offset ν, signal power σ_s^2 and noise power σ_w^2. Dandawaté and Giannakis avoid this difficulty by evaluating the covariance matrix experimentally without resorting to the particular information of other parameters except the *cyclo-spectrum* itself. Following their approach, we will present a modified and more practical prewhiten combining scheme next.

We directly apply Dandawaté and Giannakis's scheme to get the covariance matrix for the negative and positive half of the *cyclo-spectrum.* Note that $x(n)x^*(n+\tau)$ and $x(n+\tau)x^*(n)$ are conjugate to each other. If the positive part of the Fourier transform of $x(n)x^*(n+\tau)$ is $\hat{C}'(\alpha)$, then according to the properties of Fourier transform, the positive part of the Fourier transform of $x(n+\tau)x^*(n)$ will be $\hat{C}'^*(-\alpha)$. Therefore, by calculating the covariance matrix of the cyclo-spectrums of $x(n)x^*(n+\tau)$ and $x(n+\tau)x^*(n)$, we can get the covariance matrix of $\hat{C}'(\alpha)$ and $\hat{C}'^*(-\alpha)$ without exact calculation using the prior knowledge of q, ν, σ_s^2 and σ_w^2. Later in simulation, to distinguish from the previous proposed prewhiten combining scheme, we will call this scheme as the experimental prewhiten combining scheme, while the previously proposed one as theoretical prewhiten combining scheme.

[5]We only consider one cyclo-spectrum with negative and positive parts to combine, which corresponds to $p = 1$ for (5.2) in [19]. When $p > 1$, for each cyclo-spectrum, it can be divided into two parts, negative and positive, to combine as in (5.2).

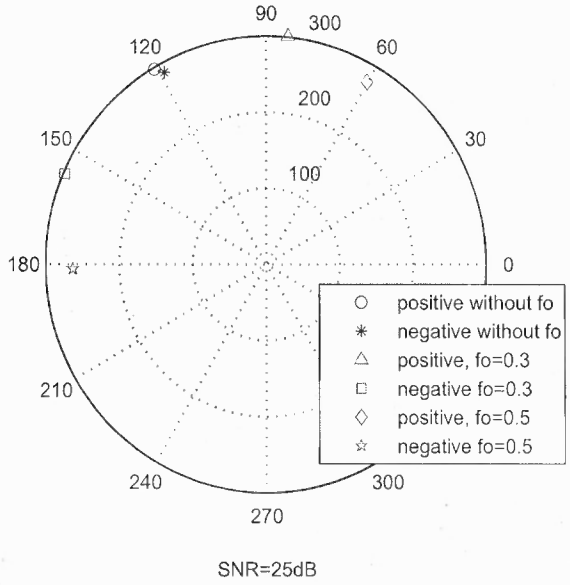

Figure 5.1 Polar graph of the cyclo-spectrum at $\alpha = \pm\pi/3$ for cases with or without frequency offset, q=3, SNR=25dB .

5.4 Cases with frequency offset

We have not considered the effect of frequency offset in the above section. The frequency offset will introduce a complex multiplicative in the received data samples. In a block fading scenario, where the frequency offset maintains the same for a block of samples, the time-varying correlation function $R(t,\tau)$ in a block changes to

$$R(t,\tau) = \mathrm{E}[x(t)x^*(t+\tau)]\exp(j2\pi\varepsilon\tau) \tag{5.39}$$

where ε is the sample frequency offset for the block. The signal is block cyclostationary and have block *cyclo-spectrum*. However, due to introduction of the complex multiplicative, "$\exp(j2\pi\varepsilon\tau)$", the second order time varying auto-correlation of the cyclostationary signal part is not real any more. Therefore, the above methods will fail since the *cyclo-spectrum* of the positive frequency part and the negative frequency part does not have the symmetric property any more. Instead, the cyclo-spectrum of $\hat{C}'(\alpha,\tau)$ and $\hat{C}'^*(-\alpha)$ will be symmetrically

located around the cyclo-spectrum of the cases without frequency offset, as shown in Fig.5.1.

Hence, the multiplication of $\hat{C}'(\alpha,\tau)$ and $\hat{C}'^{*}(-\alpha)$ will correct the angle of the cyclo-statistics introduced by the frequency offset. A modified scheme for the cases with frequency offset is given by

$$\hat{\alpha} = \arg\max_{\alpha}\kappa_3(\alpha,\tau) = \arg\max_{\alpha}[\left|\hat{C}'(\alpha,\tau)\cdot\hat{C}'^{*}(-\alpha,\tau)\right|^2] \tag{5.40}$$

where $\kappa_3(\alpha)$ is the cost function for this scheme.

5.5 Cases with pulse shaping

In practice, pulse shaping filtering is applied for spectral management. For the second order cyclostationarity test, the pulse shaping filter will introduce correlations between successive samples and thus degrade its performance.

To simplify the derivation, we assume the cyclostationarity test is conducted before the pulse shaping match filtering in the receiver. Similar to the no pulse shaping filter case, we can get the mean value and the covariance matrix of the cyclic spectrum noise due to the periodic and aperiodic signal and noise. It was also found that for the pulse shaping case, the theoretical derivation of the prewhiten scheme is very complicated. Therefore, in simulation with pulse shaping, we only test the performance of the direct combining and the experimental prewhiten combining scheme which use the estimated asymptotic covariance matrix.

5.6 Simulation

Monte Carlo simulations are conducted to test the performance of the above methods(5000 trails for each point). In the first scenario, no pulse shaping is used in the transmitter. The received signal is oversampled with $q = 3$ (In the half *cyclo-spectrum*, there will be only one peak. When $q > 3$, there will be multiple peaks in the *cyclo-spectrum*, and hence

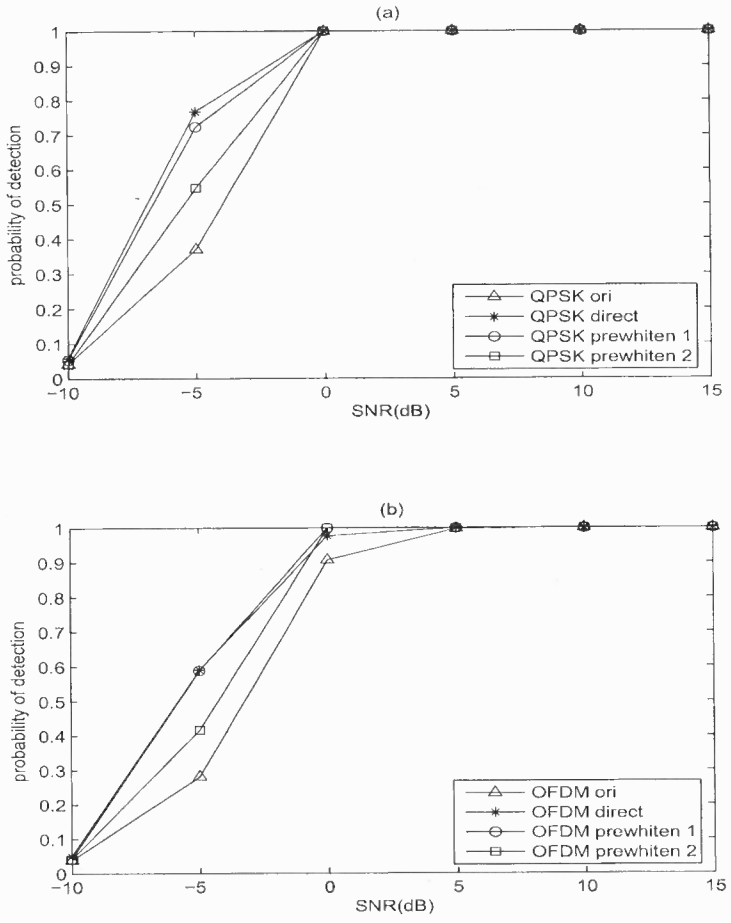

Figure 5.2 Probability of detection for the scenario without pulse shaping filtering.

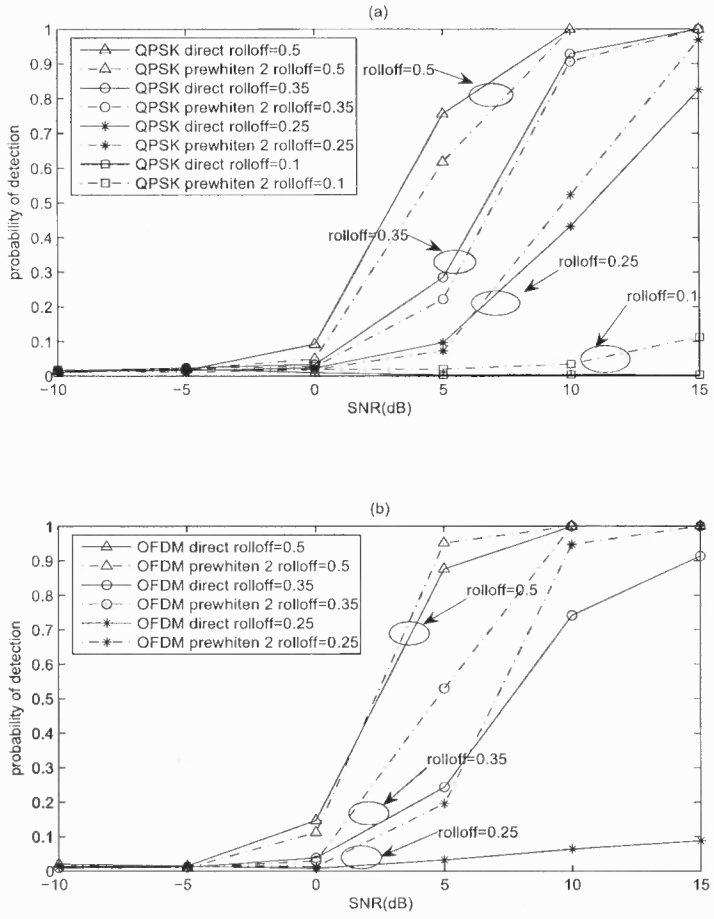

Figure 5.3 Probability of detection for the scenario with pulse shaping filtering.

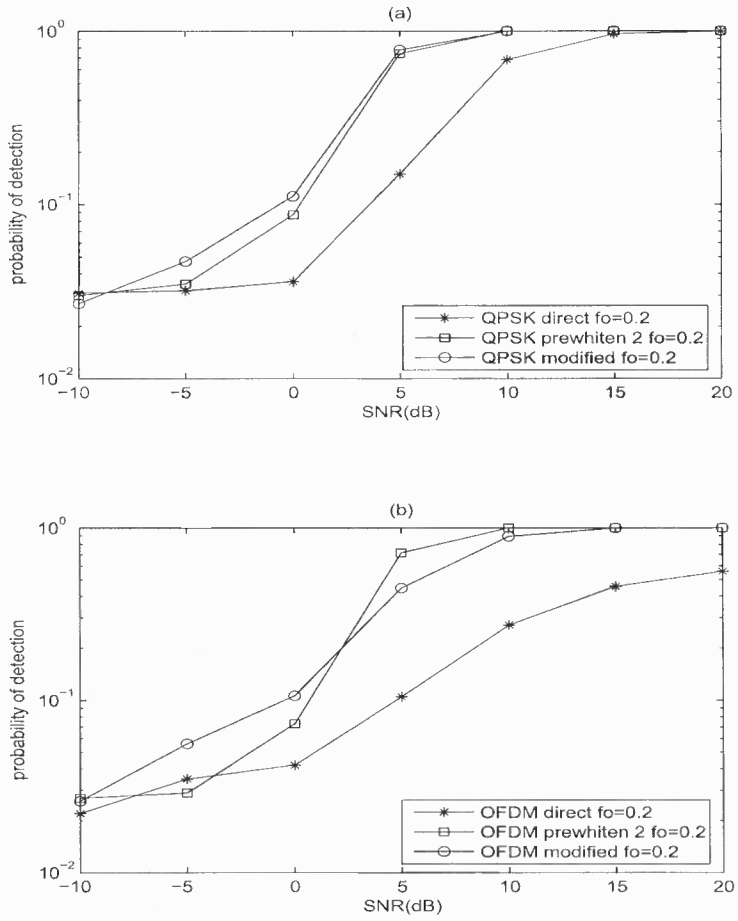

Figure 5.4 Probability of detection for the scenario with frequency offset $\varepsilon = 0.2$ without pulse shaping filtering.

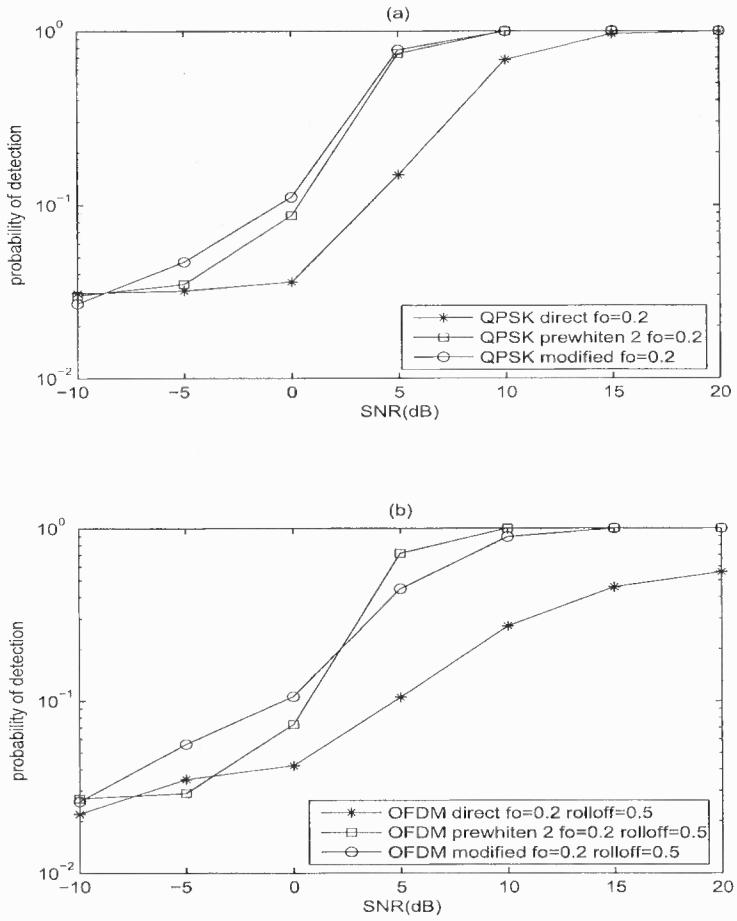

Figure 5.5 Probability of detection for the scenario with frequency offset $\varepsilon = 0.2$ with pulse shaping filtering.

need an approximate range to detect the peak corresponding to the oversampling rate.) The methods, direct combining (*direct*) and prewhiten combining schemes are applied respectively. Note that we apply two methods for the prewhiten combining scheme; one is the theoretical prewhiten combining scheme which uses the exact covariance we derived (prewhiten 1) and the other is experimental combining scheme which uses the asymptotic covariance matrix (prewhiten 2) [19]. We also applied the original algorithm in [19] (*ori*) *without using our schemes* but for fairness, with the search range limited to half of the *cyclo-spectrum*. QPSK and OFDM modulation are used. The number of the received symbols for cyclostationarity test was 1000. The detection is considered successful when the absolute cyclic frequency $\hat{\alpha}$ is detected within $2\pi \cdot (3/M)$ error. As it is shown in Fig.5.2, for both OFDM and QPSK, all the schemes outperform the original scheme. The direct combining scheme has almost similar detection performance as the theoretical prewhiten (prewhiten 1) combining schemes. The performance of the theoretical prewhiten combining scheme is also better than the experimental scheme. The reason is for the latter, the covariance matrix is only an asymptotic estimation of the actual covariance matrix.

In the second set of simulation, raised cosine pulse shaping is added in the transmitter. The oversampling rate is again $q = 3$. The delay of the filter is 10 taps. Two methods, direct combining (direct) and the second prewhiten combining schemes (prewhiten 2) are applied respectively. All the parameters and test conditions are as in the case of no pulse shape. As it is shown in Fig.5.3, for QPSK signals, the performance of the direct combining scheme is better. For OFDM signals, the performance of the prewhiten combining scheme is better. The reason is that for QPSK signals, the cyclostationary signal part of the cyclo-spectrum $\hat{R}_{ps}(n,1)$ is already periodic sequence without statistical expectation. While for OFDM signals, only the statistical expectation of $\hat{R}_{ps}(n,1)$ is periodic sequence. And thus, it may result in additional cyclo-spectrum noise which degrades the detection performance, especially for the direct combining scheme.

In the third set of simulation, frequency offset $\varepsilon = 0.2$ (the frequency offset per sample will be ε/q) is introduced in the receiver. All the parameters and test conditions

are as in the previous cases. Three methods, direct combining (direct) (equation (5.16)), the second prewhiten combining scheme (prewhiten 2) and the modified scheme (equation (5.40)) are applied respectively. As it is shown in Fig.5.4, both the direct scheme and the second prewhiten scheme have a degraded performance due to the frequency offset. The modified scheme will outperform the direct and the second prewhiten schemes for the case of QPSK modulation. For the case of OFDM modulation, the second prewhiten combining scheme will have a better performance when SNR is high. It is due to that the additional cyclo-spectrum noise introduced in OFDM case may be correlated and thus degrade the performance of the modified scheme.

Last, with the same frequency offset, raised cosine pulse shaping with rolloff factor as 0.5 is added in the transmitter. The parameters and test conditions are as in the previous cases. Three methods, direct combining (direct) (equation (5.16)), the second prewhiten combining scheme (prewhiten 2) and the modified scheme (equation (5.40)) are applied respectively. As it is shown in Fig.5.5, the performance is like the above simulation, where both the direct scheme and the second prewhiten scheme have a degraded performance and for the case of OFDM modulation, the second prewhiten combining scheme will have a better performance in high SNR scenario.

5.7 Proof that *cyclo-spectrum* noise introduced by $\hat{R}_{nps}(n,1)$ and $\hat{R}_{npn}(n,1)$ are independent

To prove that the cyclo-spectrum noise introduced by $\hat{R}_{nps}(n,1)$ and $\hat{R}_{npn}(n,1)$ are independent, that is,

$$\mathrm{E}\left[\hat{C}_{nps}(\alpha)\,\hat{C}_{npn}(\alpha)\right] = \mathrm{E}\left\{\sum_{n=0}^{M-1}\hat{R}_{nps}(n,1)\exp(-j\alpha n)\sum_{m=0}^{M-1}\hat{R}_{npn}(m,1)\exp(-j\alpha m)\right\} \tag{5.41}$$

$$= \mathrm{E}\sum_{n=0}^{M-1}\sum_{m=0}^{M-1}\hat{R}_{nps}(n,1)\hat{R}_{npn}(m,1)\exp(-j\alpha n - j\alpha m) = 0$$

The sufficient condition for the independence of $\hat{C}_{nps}(\alpha)$ and $\hat{C}_{npn}(\alpha)$ is that $\hat{R}_{nps}(n,1)$ and $\hat{R}_{npn}(n,1)$ are independent of each other for any n, that is:

$$\mathrm{E}\left[\hat{R}_{nps}(n,1)\hat{R}_{npn}(n,1)\right] = 0 \text{ for any } n \tag{5.42}$$

From (5.10) and (5.11), it can be shown straightforwardly that (5.42) is satisfied for any n. Hence, it is proved that the *cyclo-spectrum* noise introduced by $\hat{R}_{nps}(n,1)$ and $\hat{R}_{npn}(n,1)$ are independent from each other and can be analyzed separately.

5.8 Proof of approximating zeros for $\sum_{k=0}^{\lfloor M-1/q \rfloor} \cos\left[2qk\alpha + 2(q-1)\alpha\right]$ and $\sum_{k=0}^{\lfloor M-1/q \rfloor} \sin\left[2qk\alpha + 2(q-1)\alpha\right]$ when $\alpha \neq l\pi/q$

First, when $(M \bmod q) = 0$, $\alpha = \frac{2\pi l}{M}$, $l = 0, ..., M-1$, we have

$$\begin{aligned}
&\sum_{k=0}^{\lfloor M/q \rfloor - 1} \cos\left[2qk\alpha + 2(q-1)\alpha\right] \qquad (5.43)\\
&= \sum_{k=0}^{\lfloor M/q \rfloor - 1} \frac{\exp\left\{-j\left[2qk\alpha + 2(q-1)\alpha\right]\right\} + \exp\left\{j\left[2qk\alpha + 2(q-1)\alpha\right]\right\}}{2}\\
&= \begin{cases} \frac{\exp[-j2(q-1)\alpha]\exp[-j(M-q)\alpha]}{2}\frac{\sin(M\alpha)}{\sin(q\alpha)} + \frac{\exp[j2(q-1)\alpha]\exp[j(M-q)\alpha]}{2}\frac{\sin(M\alpha)}{\sin(q\alpha)}, & \alpha = l\pi/q \\ 0, & \alpha \neq l\pi/q \end{cases}\\
&= \begin{cases} \cos\left[2(q-1)\alpha + (M-q)\alpha\right]\frac{\sin(M\alpha)}{\sin(q\alpha)}, & \alpha = l\pi/q \\ 0, & \alpha \neq l\pi/q \end{cases}
\end{aligned}$$

Similarly, we have

$$\begin{aligned}
&\sum_{k=0}^{\lfloor M/q \rfloor - 1} \sin\left[2qk\alpha + 2(q-1)\alpha\right] \qquad (5.44)\\
&= \sum_{k=0}^{\lfloor M/q \rfloor - 1} \frac{\exp\left\{j\left[2qk\alpha + 2(q-1)\alpha\right]\right\} - \exp\left\{-j\left[2qk\alpha + 2(q-1)\alpha\right]\right\}}{2j}\\
&= \begin{cases} \frac{\exp[j2(q-1)\alpha]\exp[j(M-q)\alpha]}{2j}\frac{\sin(M\alpha)}{\sin(q\alpha)} - \frac{\exp[-j2(q-1)\alpha]\exp[-j(M-q)\alpha]}{2j}\frac{\sin(M\alpha)}{\sin(q\alpha)}, & \alpha = l\pi/q \\ 0, & \alpha \neq l\pi/q \end{cases}
\end{aligned}$$

$$= \begin{cases} \sin\left[2\left(q-1\right)\alpha + \left(M-q\right)\alpha\right] \frac{\sin(M\alpha)}{\sin(q\alpha)}, & \alpha = l\pi/q \\ 0, & \alpha \neq l\pi/q \end{cases}$$

When $(M \bmod q) \neq 0$, M is large enough, the difference between $\alpha = \frac{2\pi l}{M}$ and $\alpha' = \frac{2\pi l}{M'}$ is very small. Note $M' = \lfloor M/q \rfloor q$. Hence, we have that $\sum_{k=0}^{\lfloor M-1/q \rfloor} \cos\left[2qk\alpha + 2\left(q-1\right)\alpha\right]$ and $\sum_{k=0}^{\lfloor M-1/q \rfloor} \sin\left[2qk\alpha + 2\left(q-1\right)\alpha\right]$ are approximately zeros when $\alpha \neq l\pi/q$.

5.9 Derivation of $cov_{npn}(\alpha)$

The DFT of $\hat{R}_{npn}(n,1)$ is given by

$$\begin{aligned} \hat{C}_{npn}\left(\alpha\right) &= \frac{1}{M}\sum_{n=0}^{M-1} \hat{R}_{npn}(n,1)\exp\left(-j\alpha n\right) \qquad (5.45) \\ &= \frac{1}{M}\sum_{n=0}^{M-1} \left\{ \begin{array}{c} w(n)w^*(n+1) + \left[x(n) - w\left(n\right)\right] w^*(n+1) \\ +w(n)\left[x(n+1) - w\left(n+1\right)\right]^* \end{array} \right\} \exp\left(-j\alpha n\right) \\ &= \frac{1}{M}\sum_{n=0}^{M-1} w(n)w^*(n+1)\exp\left(-j\alpha n\right) \\ &+ \frac{1}{M}\sum_{n=0}^{M-1} \left\{\left[x(n) - w\left(n\right)\right] w^*(n+1) + w(n)\left[x(n+1) - w\left(n+1\right)\right]^*\right\}\exp\left(-j\alpha n\right) \\ &= \hat{C}_{npn1}\left(\alpha\right) + \hat{C}_{npn2}\left(\alpha\right) \end{aligned}$$

The first term on the RHS is caused by the additive noise. The second term on the RHS is due to the cross term of the signal and the additive noise. Since the signal is independent of the noise, we can analyze the covariance matrix of these two terms separately.

For the first term $\hat{C}_{npn1}(\alpha)$, the covariance matrix of $\hat{C}_{npn1}(\alpha)$ and $\hat{C}^*_{npn1}(-\alpha)$ can be given by

$$cov_{npn1}(\alpha) = \mathrm{E}\left\{ \begin{array}{l} \left[\begin{array}{cccc} \mathrm{Re}\left[\hat{C}_{npn1}(\alpha)\right] & \mathrm{Re}\left[\hat{C}^*_{npn1}(-\alpha)\right] & \mathrm{Im}\left[\hat{C}_{npn1}(\alpha)\right] & \mathrm{Im}\left[\hat{C}^*_{npn1}(-\alpha)\right] \end{array} \right]_T \\ \cdot \left[\begin{array}{cccc} \mathrm{Re}\left[\hat{C}_{npn1}(\alpha)\right] & \mathrm{Re}\left[\hat{C}^*_{npn1}(-\alpha)\right] & \mathrm{Im}\left[\hat{C}_{npn1}(\alpha)\right] & \mathrm{Im}\left[\hat{C}^*_{npn1}(-\alpha)\right] \end{array} \right] \end{array} \right\}^T \tag{5.46}$$

$$= \mathrm{E}\left\{ \begin{array}{l} \left[\begin{array}{cccc} \mathrm{Re}\left[\hat{C}_{npn1}(\alpha)\right] & \mathrm{Re}\left[\hat{C}_{npn1}(-\alpha)\right] & \mathrm{Im}\left[\hat{C}_{npn1}(\alpha)\right] & -\mathrm{Im}\left[\hat{C}_{npn1}(-\alpha)\right] \end{array} \right] \\ \cdot \left[\begin{array}{cccc} \mathrm{Re}\left[\hat{C}_{npn1}(\alpha)\right] & \mathrm{Re}\left[\hat{C}_{npn1}(-\alpha)\right] & \mathrm{Im}\left[\hat{C}_{npn1}(\alpha)\right] & -\mathrm{Im}\left[\hat{C}_{npn1}(-\alpha)\right] \end{array} \right] \end{array} \right\}^T$$

$$= \mathrm{E}\left[\begin{array}{cccc} \left(\hat{c}_{n1r+}\right)^2 & \hat{c}_{n1r+}\hat{c}_{n1r-} & \hat{c}_{n1r+}\hat{c}_{n1i+} & \hat{c}_{n1r+}\hat{c}_{n1i-} \\ \hat{c}_{n1r+}\hat{c}_{n1r-} & \left(\hat{c}_{n1r-}\right)^2 & \hat{c}_{n1r-}\hat{c}_{n1i+} & \hat{c}_{n1r-}\hat{c}_{n1i-} \\ \hat{c}_{n1r+}\hat{c}_{n1i+} & \hat{c}_{n1r-}\hat{c}_{n1i+} & \left(\hat{c}_{n1i+}\right)^2 & \hat{c}_{n1i+}\hat{c}_{n1i-} \\ \hat{c}_{n1r+}\hat{c}_{n1i-} & \hat{c}_{n1r-}\hat{c}_{n1i-} & \hat{c}_{n1i+}\hat{c}_{n1i-} & \left(\hat{c}_{n1i-}\right)^2 \end{array} \right]$$

where

$$\begin{aligned} \hat{c}_{n1r+} &= \mathrm{Re}\left[\hat{C}_{npn1}(\alpha)\right] \\ &= \mathrm{Re}\left\{\frac{1}{M}\sum_{n=0}^{M-1} w(n)w^*(n+1)\exp(-j\alpha n)\right\} \\ &= \frac{1}{M}\mathrm{Re}\left\{\sum_{n=0}^{M-1}\left[\nu_r(n)+j\nu_i(n)\right]\left[\cos(-\alpha n)+j\sin(-\alpha n)\right]\right\} \\ &= \frac{1}{M}\sum_{n=0}^{M-1}\left\{\nu_r(n)\cos(\alpha n)+\nu_i(n)\sin(\alpha n)\right\} \end{aligned} \tag{5.47}$$

$$\begin{aligned} \hat{c}_{n1r-} &= \mathrm{Re}\left[\hat{C}_{npn1}(-\alpha)\right] \\ &= \mathrm{Re}\left\{\frac{1}{M}\sum_{n=0}^{M-1} w(n)w^*(n+1)\exp(j\alpha n)\right\} \\ &= \frac{1}{M}\sum_{n=0}^{M-1}\left\{\nu_r(n)\cos(\alpha n)-\nu_i(n)\sin(\alpha n)\right\} \end{aligned} \tag{5.48}$$

$$\begin{aligned}\hat{c}_{n1i+} &= \mathrm{Im}[\hat{C}_{npn1}(\alpha)] \\ &= \mathrm{Im}\left\{\frac{1}{M}\sum_{n=0}^{M-1} w(n)w^*(n+1)\exp(-j\alpha n)\right\} \\ &= \frac{1}{M}\sum_{n=0}^{M-1}\{\nu_r(n)\sin(\alpha n)+\nu_i(n)\cos(\alpha n)\}\end{aligned} \tag{5.49}$$

$$\begin{aligned}\hat{c}_{n1i-} &= -\mathrm{Im}[\hat{C}_{npn1}(-\alpha)] \\ &= -\mathrm{Im}\left\{\frac{1}{M}\sum_{n=0}^{M-1} w(n)w^*(n+1)\exp(j\alpha n)\right\} \\ &= \frac{1}{M}\sum_{n=0}^{M-1}\{-\nu_r(n)\sin(\alpha n)-\nu_i(n)\cos(\alpha n)\}\end{aligned} \tag{5.50}$$

Note that $\nu_r(n) = \mathrm{Re}[w(n)w^*(n+1)]$ and $\nu_i(n) = \mathrm{Im}[w(n)w^*(n+1)]$. $\mathrm{E}[\nu_r(n)\nu_r(m)] = \mathrm{E}[\nu_i(n)\nu_i(m)] = 0$, $n \neq m$, as the noise $w(n)$ is i.i.d. $\mathrm{E}[\nu_r^2(n)] = \mathrm{E}[\nu_i^2(n)] = \frac{\sigma_w^4}{2}$ and $\mathrm{E}[\nu_r(n)\nu_i(n)] = 0$ since the real and imaginary part of the noise $w(n)$ is also i.i.d. Through mathematical manipulation, we have

$$\begin{aligned}\mathrm{E}\left[(\hat{c}_{n1r+})^2\right] &= \mathrm{E}\left\{\left[\frac{1}{M}\sum_{n=0}^{M-1}\{\nu_r(n)\cos(\alpha n)+\nu_i(n)\sin(\alpha n)\}\right]^2\right\} \\ &= \frac{1}{M^2}\mathrm{E}\left\{\begin{array}{c}\sum_{n=0}^{M-1}\{\nu_r(n)\cos(\alpha n)+\nu_i(n)\sin(\alpha n)\}^2 \\ +\sum_{n=0,n\neq m}^{M-1}\{\nu_r(n)\cos(\alpha n)+\nu_i(n)\sin(\alpha n)\} \\ \cdot\sum_{m=0}^{M-1}\{\nu_r(m)\cos(\alpha m)+\nu_i(m)\sin(\alpha m)\}\end{array}\right\} \\ &= \frac{\sigma_w^4}{2M}\end{aligned} \tag{5.51}$$

Similarly, we can get

$$\mathrm{E}\left[(\hat{c}_{n1r+})^2\right] = \mathrm{E}\left[(\hat{c}_{n1r-})^2\right] = \mathrm{E}\left[(\hat{c}_{n1i+})^2\right] = \mathrm{E}\left[(\hat{c}_{n1i-})^2\right] = \frac{\sigma_w^4}{2M} \tag{5.52}$$

$$\mathrm{E}[\hat{c}_{n1r+}\hat{c}_{n1i+}] = \mathrm{E}\left\{\begin{array}{c}\left[\frac{1}{M}\sum_{n=0}^{M-1}\{\nu_r(n)\cos(\alpha n)+\nu_i(n)\sin(\alpha n)\}\right] \\ \cdot\left[\frac{1}{M}\sum_{m=0}^{M-1}\{-\nu_r(m)\sin(\alpha m)+\nu_i(m)\cos(\alpha m)\}\right]\end{array}\right\} \tag{5.53}$$

$$= \frac{1}{M^2}\mathrm{E}\left\{\begin{array}{c} \sum_{n=0}^{M-1}\left\{\nu_r(n)\cos(\alpha n)+\nu_i(n)\sin(\alpha n)\right\} \\ \cdot\left\{-\nu_r(n)\sin(\alpha n)+\nu_i(n)\cos(\alpha n)\right\} \\ +\sum_{n=0}^{M-1}\left\{\nu_r(n)\cos(\alpha n)+\nu_i(n)\sin(\alpha n)\right\} \\ \cdot\sum_{m=0}^{M-1}\left\{-\nu_r(m)\sin(\alpha m)+\nu_i(m)\cos(\alpha m)\right\} \end{array}\right\}$$

$$= 0$$

$$= \mathrm{E}\left[\hat{c}_{n1r-}\hat{c}_{n1i-}\right]$$

$$\mathrm{E}\left[\hat{c}_{n1r+}\hat{c}_{n1r-}\right] = \mathrm{E}\left\{\begin{array}{c} \left[\frac{1}{M}\sum_{n=0}^{M-1}\left\{\nu_r(n)\cos(\alpha n)+\nu_i(n)\sin(\alpha n)\right\}\right] \\ \cdot\left[\frac{1}{M}\sum_{m=0}^{M-1}\left\{\nu_r(m)\cos(\alpha m)-\nu_i(m)\sin(\alpha m)\right\}\right] \end{array}\right\} \tag{5.54}$$

$$= \frac{1}{M^2}\mathrm{E}\left\{\begin{array}{c} \sum_{n=0}^{M-1}\left\{\nu_r(n)\cos(\alpha n)+\nu_i(n)\sin(\alpha n)\right\} \\ \cdot\left\{\nu_r(n)\cos(\alpha n)-\nu_i(n)\sin(\alpha n)\right\} \\ +\sum_{n=0,n\neq m}^{M-1}\left\{\nu_r(n)\cos(\alpha n)+\nu_i(n)\sin(\alpha n)\right\} \\ \cdot\sum_{m=0}^{M-1}\left\{\nu_r(m)\cos(\alpha m)-\nu_i(m)\sin(\alpha m)\right\} \end{array}\right\}$$

$$= \frac{\sigma_s^4}{2M}\sum_{n=0}^{M-1}\cos(2\alpha n)$$

$$= -\mathrm{E}\left[\hat{c}_{n1i+}\hat{c}_{n1i-}\right]$$

and

$$\mathrm{E}\left[\hat{c}_{n1r+}\hat{c}_{n1i-}\right] = \mathrm{E}\left\{\begin{array}{c} \left[\frac{1}{M}\sum_{n=0}^{M-1}\left\{\nu_r(n)\cos(\alpha n)+\nu_i(n)\sin(\alpha n)\right\}\right] \\ \cdot\left[\frac{1}{M}\sum_{m=0}^{M-1}\left\{-\nu_r(m)\sin(\alpha m)-\nu_i(m)\cos(\alpha m)\right\}\right] \end{array}\right\} \tag{5.55}$$

$$= \frac{1}{M^2}\mathrm{E}\left\{\begin{array}{c} \sum_{n=0}^{M-1}\left\{\nu_r(n)\cos(\alpha n)+\nu_i(n)\sin(\alpha n)\right\} \\ \cdot\left\{-\nu_r(n)\sin(\alpha n)-\nu_i(n)\cos(\alpha n)\right\} \\ +\sum_{n=0}^{M-1}\left\{\nu_r(n)\cos(\alpha n)+\nu_i(n)\sin(\alpha n)\right\} \\ \cdot\sum_{m=0}^{M-1}\left\{-\nu_r(m)\sin(\alpha m)-\nu_i(m)\cos(\alpha m)\right\} \end{array}\right\}$$

$$= -\frac{\sigma_w^4}{2M} \sum_{k=0}^{\lfloor M/q \rfloor - 1} \sin(2\alpha n)$$

$$= \mathrm{E}\left[\hat{c}_{n1r-}\hat{c}_{n1i+}\right]$$

According to Appendix B, it is shown that except at the cyclic frequency $l\pi$, where l is an integer, all the non-diagonal entries of the covariance matrix $cov_{npn1}(\alpha)$ are approximately zeros, that is, the *cyclo-spectrum* noise generated by the additive noise only is almost white.

For the second term $\hat{C}_{npn2}(\alpha)$, the covariance matrix of $\hat{C}_{npn2}(\alpha)$ and $\hat{C}^*_{npn2}(-\alpha)$ can be given by

$$cov_{npn2}(\alpha) = \mathrm{E}\left\{ \begin{array}{l} \left[\begin{array}{cccc} \mathrm{Re}\left[\hat{C}_{npn2}(\alpha)\right] & \mathrm{Re}\left[\hat{C}^*_{npn2}(-\alpha)\right] & \mathrm{Im}\left[\hat{C}_{npn2}(\alpha)\right] & \mathrm{Im}\left[\hat{C}^*_{npn2}(-\alpha)\right] \end{array} \right] \\ \cdot \left[\begin{array}{cccc} \mathrm{Re}\left[\hat{C}_{npn2}(\alpha)\right] & \mathrm{Re}\left[\hat{C}^*_{npn2}(-\alpha)\right] & \mathrm{Im}\left[\hat{C}_{npn2}(\alpha)\right] & \mathrm{Im}\left[\hat{C}^*_{npn2}(-\alpha)\right] \end{array} \right]^T \end{array} \right\} \tag{5.56}$$

$$= \mathrm{E}\left\{ \begin{array}{l} \left[\begin{array}{cccc} \mathrm{Re}\left[\hat{C}_{npn2}(\alpha)\right] & \mathrm{Re}\left[\hat{C}_{npn2}(-\alpha)\right] & \mathrm{Im}\left[\hat{C}_{npn2}(\alpha)\right] & -\mathrm{Im}\left[\hat{C}_{npn2}(-\alpha)\right] \end{array} \right] \\ \cdot \left[\begin{array}{cccc} \mathrm{Re}\left[\hat{C}_{npn2}(\alpha)\right] & \mathrm{Re}\left[\hat{C}_{npn2}(-\alpha)\right] & \mathrm{Im}\left[\hat{C}_{npn2}(\alpha)\right] & -\mathrm{Im}\left[\hat{C}_{npn2}(-\alpha)\right] \end{array} \right]^T \end{array} \right.$$

$$= \mathrm{E}\begin{bmatrix} (\hat{c}_{n2r+})^2 & \hat{c}_{n2r+}\hat{c}_{n2r-} & \hat{c}_{n2r+}\hat{c}_{n2i+} & \hat{c}_{n2r+}\hat{c}_{n2i-} \\ \hat{c}_{n2r+}\hat{c}_{n2r-} & (\hat{c}_{n2r-})^2 & \hat{c}_{n2r-}\hat{c}_{n2i+} & \hat{c}_{n2r-}\hat{c}_{n2i-} \\ \hat{c}_{n2r+}\hat{c}_{n2i+} & \hat{c}_{n2r-}\hat{c}_{n2i+} & (\hat{c}_{n2i+})^2 & \hat{c}_{n2i+}\hat{c}_{n2i-} \\ \hat{c}_{n2r+}\hat{c}_{n2i-} & \hat{c}_{n2r-}\hat{c}_{n2i-} & \hat{c}_{n2i+}\hat{c}_{n2i-} & (\hat{c}_{n2i-})^2 \end{bmatrix}$$

$$= \begin{bmatrix} \varsigma_{11}(\alpha) & \varsigma_{12}(\alpha) & \varsigma_{13}(\alpha) & \varsigma_{14}(\alpha) \\ \varsigma_{12}(\alpha) & \varsigma_{22}(\alpha) & \varsigma_{23}(\alpha) & \varsigma_{24}(\alpha) \\ \varsigma_{13}(\alpha) & \varsigma_{23}(\alpha) & \varsigma_{33}(\alpha) & \varsigma_{34}(\alpha) \\ \varsigma_{14}(\alpha) & \varsigma_{24}(\alpha) & \varsigma_{34}(\alpha) & \varsigma_{44}(\alpha) \end{bmatrix}$$

where

$$\hat{c}_{n2r+} = \mathrm{Re}\left[\hat{C}_{npn2}(\alpha)\right] \tag{5.57}$$

$$= \mathrm{Re}\left\{\frac{1}{M}\sum_{n=0}^{M-1}\left[x(n)-w\left(n\right)\right]w^{*}(n+1)+w(n)\left[x(n+1)-w\left(n+1\right)\right]^{*}\exp\left(-j\alpha n\right)\right\}$$

$$= \frac{1}{M}\mathrm{Re}\left\{\sum_{n=0}^{M-1}\left[\mu_r\left(n\right)+j\mu_i\left(n\right)\right]\left[\cos\left(-\alpha n\right)+j\sin\left(-\alpha n\right)\right]\right\}$$

$$= \frac{1}{M}\sum_{n=0}^{M-1}\left\{\mu_r\left(n\right)\cos\left(\alpha n\right)+\mu_i\left(n\right)\sin\left(\alpha n\right)\right\}$$

$$\hat{c}_{n2r-} = \mathrm{Re}\left[\hat{C}_{npn2}\left(-\alpha\right)\right] \tag{5.58}$$

$$= \mathrm{Re}\left\{\frac{1}{M}\sum_{n=0}^{M-1}\left[x(n)-w\left(n\right)\right]w^{*}(n+1)+w(n)\left[x(n+1)-w\left(n+1\right)\right]^{*}\exp\left(j\alpha n\right)\right\}$$

$$= \frac{1}{M}\sum_{n=0}^{M-1}\left\{\mu_r\left(n\right)\cos\left(\alpha n\right)-\mu_i\left(n\right)\sin\left(\alpha n\right)\right\}$$

$$\hat{c}_{n2i+} = \mathrm{Im}[\hat{C}_{npn2}\left(\alpha\right)] \tag{5.59}$$

$$= \mathrm{Im}\left\{\frac{1}{M}\sum_{n=0}^{M-1}\left[x(n)-w\left(n\right)\right]w^{*}(n+1)+w(n)\left[x(n+1)-w\left(n+1\right)\right]^{*}\exp\left(-j\alpha n\right)\right\}$$

$$= \frac{1}{M}\sum_{n=0}^{M-1}\left\{-\mu_r\left(n\right)\sin\left(\alpha n\right)+\mu_i\left(n\right)\cos\left(\alpha n\right)\right\}$$

$$\hat{c}_{n2i-} = -\mathrm{Im}[\hat{C}_{npn2}\left(-\alpha\right)] \tag{5.60}$$

$$= -\mathrm{Im}\left\{\frac{1}{M}\sum_{n=0}^{M-1}\left[x(n)-w\left(n\right)\right]w^{*}(n+1)+w(n)\left[x(n+1)-w\left(n+1\right)\right]^{*}\exp\left(j\alpha n\right)\right\}$$

$$= \frac{1}{M}\sum_{n=0}^{M-1}\left\{-\mu_r\left(n\right)\sin\left(\alpha n\right)-\mu_i\left(n\right)\cos\left(\alpha n\right)\right\}$$

Note that $\mu_r\left(n\right) = \mathrm{Re}\left\{\left[x(n)-w\left(n\right)\right]w^{*}(n+1)+w(n)\left[x(n+1)-w\left(n+1\right)\right]^{*}\right\}$ and $\mu_i\left(n\right) = \mathrm{Im}\left\{\left[x(n)-w\left(n\right)\right]w^{*}(n+1)+w(n)\left[x(n+1)-w\left(n+1\right)\right]^{*}\right\}$. $\mathrm{E}\left[\mu_r^2\left(n\right)\right] = \mathrm{E}\left[\mu_i^2\left(n\right)\right] = \sigma_s^2\sigma_w^2$ and $\mathrm{E}\left[\mu_r\left(n\right)\mu_i\left(n\right)\right] = 0$ since the real and imaginary part of the noise $w\left(k\right)$ is also i.i.d. Different from the case for the cyclo spectrum noise introduced by the

additive noise only, for the cross term of the signal and noise, we have

$$\begin{aligned} \mathrm{E}\left[\mu_r(n)\,\mu_r(m)\right] &= -\mathrm{E}\left[\mu_i(n)\,\mu_i(m)\right] \\ &= \begin{cases} \frac{\sigma_s^2\sigma_w^2}{2}, & 0 < |n-m| \le q-2, [(n,m)\,\mathrm{E}q] \ne q-1 \\ 0, & others \end{cases} \end{aligned} \tag{5.61}$$

Through mathematical manipulation, we have

$$\begin{aligned} \mathrm{E}\left[(\hat{c}_{n2r+})^2\right] &= \mathrm{E}\left\{\left[\frac{1}{M}\sum_{n=0}^{M-1}\left\{\mu_r(n)\cos(\alpha n)+\mu_i(n)\sin(\alpha n)\right\}\right]^2\right\} \\ &= \frac{1}{M^2}\mathrm{E}\left\{\begin{array}{c} \sum_{n=0}^{M-1}\left\{\mu_r(n)\cos(\alpha n)+\mu_i(n)\sin(\alpha n)\right\}^2 \\ +\sum_{n=0,n\ne m}^{M-1}\left\{\mu_r(n)\cos(\alpha n)+\mu_i(n)\sin(\alpha n)\right\} \\ \cdot\sum_{m=0}^{M-1}\left\{\mu_r(m)\cos(\alpha m)+\mu_i(m)\sin(\alpha m)\right\} \end{array}\right\} \\ &= \frac{\sigma_s^2\sigma_w^2}{Mq}\left\{q+\sum_{k=0}^{\lfloor M/q\rfloor-1}\sum_{i=0}^{q-2}\cos\left[(2i+1)\,\alpha+2qk\alpha\right]\right\} \\ &= \mathrm{E}\left[(\hat{c}_{n2r-})^2\right] \end{aligned} \tag{5.62}$$

Similarly, we can get

$$\mathrm{E}\left[(\hat{c}_{n2i+})^2\right] = \mathrm{E}\left[(\hat{c}_{n2i-})^2\right] = \frac{\sigma_s^2\sigma_w^2}{Mq}\left\{q-\sum_{k=0}^{\lfloor M/q\rfloor-1}\sum_{i=0}^{q-2}\cos\left[(2i+1)\,\alpha+2qk\alpha\right]\right\} \tag{5.63}$$

$$\begin{aligned} \mathrm{E}\left[\hat{c}_{n2r+}\hat{c}_{n2i+}\right] &= \mathrm{E}\left\{\begin{array}{c} \left[\frac{1}{M}\sum_{n=0}^{M-1}\left\{\mu_r(n)\cos(\alpha n)+\mu_i(n)\sin(\alpha n)\right\}\right] \\ \cdot\left[\frac{1}{M}\sum_{m=0}^{M-1}\left\{\mu_r(m)\sin(\alpha m)+\mu_i(m)\cos(\alpha m)\right\}\right] \end{array}\right\} \\ &= \frac{1}{M^2}\mathrm{E}\left\{\begin{array}{c} \sum_{n=0}^{M-1}\left\{\mu_r(n)\cos(\alpha n)+\mu_i(n)\sin(\alpha n)\right\} \\ \cdot\left\{\mu_r(n)\sin(\alpha n)+\mu_i(n)\cos(\alpha n)\right\} \\ +\sum_{n=0,n\ne m}^{M-1}\left\{\mu_r(n)\cos(\alpha n)+\mu_i(n)\sin(\alpha n)\right\} \\ \cdot\sum_{m=0}^{M-1}\left\{\mu_r(m)\sin(\alpha m)+\mu_i(m)\cos(\alpha m)\right\} \end{array}\right\} \\ &= \frac{\sigma_s^2\sigma_w^2}{M}\sum_{n=0}^{M-1}\sin(2\alpha n)+\frac{\sigma_s^2\sigma_w^2}{2M^2} \end{aligned} \tag{5.64}$$

$$\cdot \sum_{n=0}^{M-1} \sum_{m=0,|n-m|=1,\left[(n,m) \bmod q\right]\neq q-1}^{M-1} \{\cos(\alpha m)\sin(\alpha n)+\sin(\alpha m)\cos(\alpha n)\}$$

$$= \frac{\sigma_s^2\sigma_w^2}{Mq}\left\{ q\sum_{n=0}^{M-1}\sin(2\alpha n) + \sum_{k=0}^{\lfloor M/q\rfloor-1}\sum_{i=0}^{q-2}\sin\left[(2i+1)\alpha+2qk\alpha\right]\right\}$$

$$= \mathrm{E}\left[\hat{c}_{n2r-}\hat{c}_{n2i-}\right]$$

$$\mathrm{E}\left[\hat{c}_{n2r+}\hat{c}_{n2i-}\right] = \mathrm{E}\left\{\begin{array}{c}\left[\frac{1}{M}\sum_{n=0}^{M-1}\{\mu_r(n)\cos(\alpha n)+\mu_i(n)\sin(\alpha n)\}\right] \\ \cdot\left[\frac{1}{M}\sum_{m=0}^{M-1}\{-\mu_r(m)\sin(\alpha m)-\mu_i(m)\cos(\alpha m)\}\right]\end{array}\right\} \tag{5.65}$$

$$= \frac{1}{M^2}\mathrm{E}\left\{\begin{array}{c}\sum_{n=0}^{M-1}\{\mu_r(n)\cos(\alpha n)+\mu_i(n)\sin(\alpha n)\} \\ \cdot\{-\mu_r(n)\sin(\alpha n)-\mu_i(n)\cos(\alpha n)\} \\ +\sum_{n=0,n\neq m}^{M-1}\{\mu_r(n)\cos(\alpha n)+\mu_i(n)\sin(\alpha n)\} \\ \cdot\sum_{m=0}^{M-1}\{-\mu_r(m)\sin(\alpha m)-\mu_i(m)\cos(\alpha m)\}\end{array}\right\}$$

$$= \frac{\sigma_s^2\sigma_w^2}{M}\sum_{n=0}^{M-1}\sin(2\alpha n) + \frac{\sigma_s^2\sigma_w^2}{2M^2}$$

$$\cdot \sum_{n=0}^{M-1} \sum_{m=0,|n-m|=1,\left[(n,m) \bmod q\right]\neq q-1}^{M-1} \{\cos(\alpha m)\sin(\alpha n)-\sin(\alpha m)\cos(\alpha n)\}$$

$$= -\frac{\sigma_s^2\sigma_w^2}{M}\sum_{n=0}^{M-1}\sin(2\alpha n) = \mathrm{E}\left[\hat{c}_{n2r-}\hat{c}_{n2i+}\right]$$

and

$$\mathrm{E}\left[\hat{c}_{n2r+}\hat{c}_{n2r-}\right] = \mathrm{E}\left\{\begin{array}{c}\left[\frac{1}{M}\sum_{n=0}^{M-1}\{\mu_r(n)\cos(\alpha n)+\mu_i(n)\sin(\alpha n)\}\right] \\ \cdot\left[\frac{1}{M}\sum_{m=0}^{M-1}\{\mu_r(m)\cos(\alpha m)-\mu_i(m)\sin(\alpha m)\}\right]\end{array}\right\} \tag{5.66}$$

$$= \frac{1}{M^2}\mathrm{E}\left\{\begin{array}{c}\sum_{n=0}^{M-1}\{\mu_r(n)\cos(\alpha n)+\mu_i(n)\sin(\alpha n)\} \\ \cdot\{\mu_r(n)\cos(\alpha n)-\mu_i(n)\sin(\alpha n)\} \\ +\sum_{n=0,n\neq m}^{M-1}\{\mu_r(n)\cos(\alpha n)+\mu_i(n)\sin(\alpha n)\} \\ \cdot\sum_{m=0}^{M-1}\{\mu_r(m)\cos(\alpha m)-\mu_i(m)\sin(\alpha m)\}\end{array}\right\}$$

$$= \frac{\sigma_s^2\sigma_w^2}{M}\sum_{n=0}^{M-1}\cos(2\alpha n) + \frac{\sigma_s^2\sigma_w^2}{2M^2}$$

$$\cdot \sum_{n=0}^{M-1} \sum_{m=0,|n-m|=1,[(n,m) \bmod q]\neq q-1} \{\cos(\alpha m)\cos(\alpha n) + \sin(\alpha m)\sin(\alpha n)\}$$

$$= \frac{\sigma_s^2\sigma_w^2}{Mq}\left[q\sum_{n=0}^{M-1}\cos(2\alpha n) + \cos\alpha\right] = \mathrm{E}\left[\hat{c}_{n2i+}\hat{c}_{n2i-}\right]$$

The overall covariance matrix $cov_{npn}(\alpha)$ is the sum of $cov_{npn1}(\alpha)$ and $cov_{npn2}(\alpha)$. Except the frequency at 0, $\pm\pi$, $cov_{npn}(\alpha)$ is given by

$$cov_{npn}(\alpha) = \frac{\sigma_w^4}{2M}\mathbf{I}_4 + cov_{npn2}(\alpha) \tag{5.67}$$

where $\mathbf{I}_4$ is the unit matrix of size 4.

CHAPTER 6

REVISITING THE TIMING AND FREQUENCY OFFSET ESTIMATION BASED ON CYCLOSTATIONARITY

6.1 Introduction

The increased demand for more bandwidth, and the rapid emergence of cognitive radio had attracted more interests at both industry and academia in blind synchronization schemes. Particularly, among the blind synchronization schemes proposed, there is a group of timing and frequency offset estimators that explore the second-order cyclostationarity.

Cyclostatioanrity based synchronization schemes dates back to the 1950s, when Bennett proposed to use these synchronization algorithms for **single carrier** communications systems [26]. In [7] and [41], the square law based synchronization were applied. But due to the introduction of the noise term in the squared cyclostationarity of the signal, the method in [41] results in deteriorated performance. The method proposed by Ghogho and el. [7] combined delay "1" and delay "0" (square law) cyclostationarity to improve performance, but it requires additional computations. The method of Scott [42] which is later extended by Gini and Giannakis [30], uses delay "1" based second order cyclostationarity. However, in both [42] and [30], the estimation of the timing offset requires frequency offset estimate first. Therefore, it has a propagation error caused by the frequency offset error. In this paper, we propose a new method where a new timing estimation scheme is presented without the required frequency offset estimate. That is, the timing and frequency offset estimators are independent and result in an enhanced performance [1].

Due to the inherent cyclostationarity in **OFDM signal**, second order cyclostationarity based blind synchronization schemes have also been applied in these systems [1]- [?]. The estimators for timing and frequency proposed in these articles are extension of those for

[1]There are many other works that deal with the time difference problems which used correlation (see Gardner's [51]).

the single carrier system [41]- [30], which are not independent. Extended to OFDM, it is shown that our new method also has an improved time and frequency offset estimation.

6.2 Signal model

The received **single carrier** signal is given by [30]

$$x(n) = h(n)e^{-j(2\pi\varepsilon Tn/q+\theta)} \sum_m s(m)g(n-mq-\nu) + w(n) \tag{6.1}$$

$h(n)$ is the flat channel fading; The introduced frequency, timing and phase offset are ε, ν and θ respectively; q is the oversampling rate, while T is the symbol period. W.l.g, T is normalized to "1". $s(m)$ is the information symbols. $g(n) = g_{tx}(t) * g_{rx}(t) \mid_{n=\lfloor tq/T \rceil}$, is the combined effect of the transmitter and receiver pulse shaping filters after oversampling, where $\lfloor \cdot \rceil$ is the integer operator. $w(n) = g_{rx}(n) * v(n)$ is the filtered noise, and $v(n)$ is complex white Gaussian noise. *Throughout the paper, we will make the following assumptions:*

(AS1) $h(n)$ is a zero-mean stationary sequence with real valued autocorrelation $R_h(\tau)$ when the channel is flat (slow) fading [42]. This was assumed by most of the cyclostationarity based synchronization scheme [7]- [?].

(AS2) $g_{tx}(t)$ and $g_{rx}(t)$ are real-valued pulse shaping filter, which is almost always true in practice.

The time-varying auto-correlation for delay τ;

$$R(n,\tau) = E\{x(n)x^*(n+\tau)\} \tag{6.2}$$

The cyclic correlation, $C(k,\tau)$, which is the Fourier series of $R(n,\tau)$ with period $P = q$, is given by [30];

$$C(k,\tau) = \frac{\sigma_s^2}{q} R_h(\tau) e^{j2\pi\varepsilon\tau/q} \sum_n g_{seq}(n-\nu,\tau) \cdot e^{-j2\pi kn/P} \tag{6.3}$$

$$+ R_w(\tau)\delta(k)$$

$$g_{seq}(n,\tau) = \sum_{l} g(n-lP)g^*(n+\tau-lP) \tag{6.4}$$

and k is the cyclic frequency. Suppose the combined pulse shaping filter $g(n)$ has $2dq$ taps. (when each is raised cosine filters. d is the delay factor of the filter) Then it can be shown that $g_{seq}(n,\tau)$ is a periodic sequence with period $P = q$. One period of $g_{seq}(n,\tau)$, $n = 0...q-1$ is given by

$$g_{seq}(n,\tau) = \sum_{l=0}^{2d-1} g(n-lq)g(n+\tau-lq) \tag{6.5}$$

6.3 Previous methods of timing and frequency estimation

Using Parseval's relation to rewrite the term $\sum_n g_{seq}(n)\cdot e^{-j2\pi kn/P}$, and compensate for the effect of pulse shaping filter, Gini and Giannakis [30] gave the modified cyclic correlation for **single carrier** as [2]

$$\begin{aligned}\varrho(k,\tau) &= C(k,\tau)\gamma^{-1}(k,\tau) \\ &= \frac{\sigma_s^2}{q}R_h(\tau)e^{j2\pi\varepsilon\tau/q}e^{-j2\pi k\nu/P} + \gamma^{-1}(k,\tau)R_w(\tau)\delta(k)\end{aligned} \tag{6.6}$$

where $\gamma(k,\tau)$ is given by

$$\gamma(k,\tau) = q\int_{-q/2}^{q/2} G^*(\beta-k)G(\beta)e^{-j2\pi\beta\tau/q}d\beta \tag{6.7}$$

and $G(f) = \sum_n g(n)exp(-j2\pi fn)$ is the Fourier Transform of $g(n)$. With this, the authors of [30] proposed the following frequency and timing estimators ((10) and (11) in [30]):

$$\hat{\varepsilon} = q\arg\{\varrho(k,\tau)\varrho(-k,\tau)\}/(4\pi\tau), k>0; \tau\in[1,q-1] \tag{6.8}$$

$$\hat{\nu} = -P\arg\{\varrho(k,\tau)e^{j2\pi\hat{\varepsilon}\tau/q}\}/(2\pi k), k>0; \tau\in[1,q-1] \tag{6.9}$$

[2] In simulation, as in [7], only the phase of $\gamma^{-1}(k,\tau)$ is compensated to avoid propagation error.

where $\arg\{\cdot\}$ stands for unwrapped phase of $(\cdot)$ [3]. Note that the above timing estimator, $\hat{\nu}$, is dependent of the frequency offset estimator, $\hat{\varepsilon}$. On the other hand, Ghogho and el. [7] proposed a different timing estimator which does not require the estimate of frequency offset;

$$\hat{\nu} = -P[\arg \varrho(k,0) - arg\varrho(-k,0)]/(4\pi k), \tag{6.10}$$

but it is obtained by using two computations at delay "0" cyclostationarity statistics.

There are other kind of timing and frequency offset estimators based on different kind of cyclic correlations. They are either dependent or more complicated due to the need of calculating two values of $\varrho(k,\tau)$.

Bölcskei [1] extended the previous estimators to **OFDM systems**, in which the frequency estimator as in (6.8). With no oversampling, $q = 1$ and the delay $\tau = N$, the number of subcarriers for OFDM system. The time estimator as in (6.9) except the period $P = N+G$, where G is the length of the cyclic prefix (CP).

$$\hat{\varepsilon} = \arg\{\varrho(k,N)\varrho(-k,N)\}/(4\pi N), k > 0; \tag{6.11}$$

$$\hat{\nu} = (N+G)\arg\{\varrho(k,\tau)e^{j2\pi\hat{\varepsilon}N}\}/(2\pi k), k > 0; \tag{6.12}$$

Obviously, the estimate of the timing still depends on the performance of the frequency estimator.

6.4 New method for timing and frequency estimation

From (AS2) we know that, for **single carrier** signal, $g(n)$ is real, and thus the sequence of $g_{seq}(n-\nu,\tau)$ in (6.3) is real. As a result, its Fourier series, $G_s(k,\tau) \triangleq \sum_n g_{seq}(n -$

[3]Note we have P in numerator for the timing offset estimator which is different from equation (11) in [30], where ν is already normalized with P.

$\nu, \tau)e^{-j2\pi kn/P}$, will be Hermitian symmetric, i.e. $G_s(-k,\tau) = G_s^*(k,\tau)$, and from (6.3),

$$\arg\{C(k,\tau)\} = 2\pi\varepsilon\tau/P + \arg\{G_s(k,\tau)\} \tag{6.13}$$

Since $G_s(k,\tau)$ is Hermitian symmetric, we have $\arg\{G_s(k,\tau)\} = -\arg\{G_s(-k,\tau)\}$ and we obtain when combining $\arg\{C(k,\tau)\}$ from (6.13) with $\arg\{C(-k,\tau)\}$.

$$\hat{\varepsilon} = \frac{q}{4\pi\tau}\arg\{C(k,\tau)C(-k,\tau)\} \tag{6.14}$$

This frequency offset estimator is similar to that proposed by Ghogho with assumption of real $g(n)$ (page 3 in [7]).

For timing estimator, we note from its definition that $G_s(k,\tau)$ depends on timing offset ν. Then by the shift property of the Fourier transform, we have,

$$\arg\{G_s(k,\tau)\} = -2\pi\nu k/P + arg\{G_{seq}(k,\tau)\} \tag{6.15}$$

where $G_{seq}(k,\tau) = F\{g_{seq}(n,\tau)\} = \sum_n g_{seq}(n,\tau)\cdot e^{-j2\pi kn/P}$. Note the second term on the RHS of (6.15) depends only on the pulse shaping filter, $g(n)$. Instead of calculating it in the frequency domain from (6.6)(as in [7]- [?]), we calculate it directly from (6.5) in the time domain. Substituting (6.15) into (6.13), and using similar method of canceling out the effect of the frequency offset, we obtain by using $\arg\{G_{seq}(k,\tau)\} = -\arg\{G_{seq}(-k,\tau)\}$

$$\hat{\nu} = -P\arg\{C(k,\tau)/(C(-k,\tau)G_{seq}^2(k,\tau))\}/(4\pi k) \tag{6.16}$$

For the **OFDM system**, whose number of subcarriers is N, and CP length is G, the cyclic correlation, $C(k,N)$, which is the Fourier series of $R(n,N)$ with period of $P = N+G$, is given by;

$$C(k,N) = \sigma_s^2 R_h(\tau)e^{j2\pi\epsilon N}\sum_n z_{seq}(n-\nu) \tag{6.17}$$
$$\cdot\, e^{-j2\pi kn/(N+G)} + R_w(\tau)\delta(k)$$

$z_{seq}(n)$ is a periodic rectangular sequence of period $N+G$ with rectangular window length G [1] [**?**]. Similar to the derivation above for single carrier signal(eqn. (6.15)), the angle of $G_s(k,\tau)$ is given by

$$\arg\{G_s(k,\tau)\} = -2\pi\nu k/(N+G) + arg\{\sum_l z_{seq}(l)\cdot e^{-j2\pi kl/(N+G)}\} \tag{6.18}$$

Through similar manipulations, the corresponding frequency and timing offset estimator obtained by the new method for OFDM systems are given by

$$\hat{\varepsilon} = \arg\{C(k,N)C(-k,N)\}/(4\pi N) \tag{6.19}$$

and

$$\hat{\nu} = -(N+G)\arg\{\frac{C(k,N)}{C(-k,N)G_z^2(k,N)}\}/(4\pi k) \tag{6.20}$$

where $G_z(k,N)$ is the Fourier Transform of the periodic sequence $z_{seq}(n)$.

6.5 Simulation

Monte Carlo simulations are conducted to test the performance of the above methods(1000 trials for each point).

In the *first scenario*, for **single carrier** signal, the transmit and receive filters were raised cosine filters with roll-off 0.5, and upsampling rate 8, delay 7. Single carrier QPSK symbols are assumed. Time-selective Rayleigh fading channel is assumed, with Doppler spread of $B_hT = 0.05$, where B_h is the bandwidth of $h(n)$. Same as in [43], the channel filter $h(n)$ is obtained by bilinearly transforming a third-order continuous-time all-pole filter, whose poles are the roots of the equation $(s^2 + 0.35\omega_0 s + \omega_0^2)(s+\omega_0) = 0$, where $\omega_0 = 2\pi B_h/1.2$. The time offset $\nu = 3$ samples and frequency offset $\varepsilon = 0.1$, are implemented. Normalized Mean Square Error (NMSE) is used to evaluate the performance. Three methods; *the one proposed by Gini and Giannakis with* $\tau = 1$*(GG-single) [30], the*

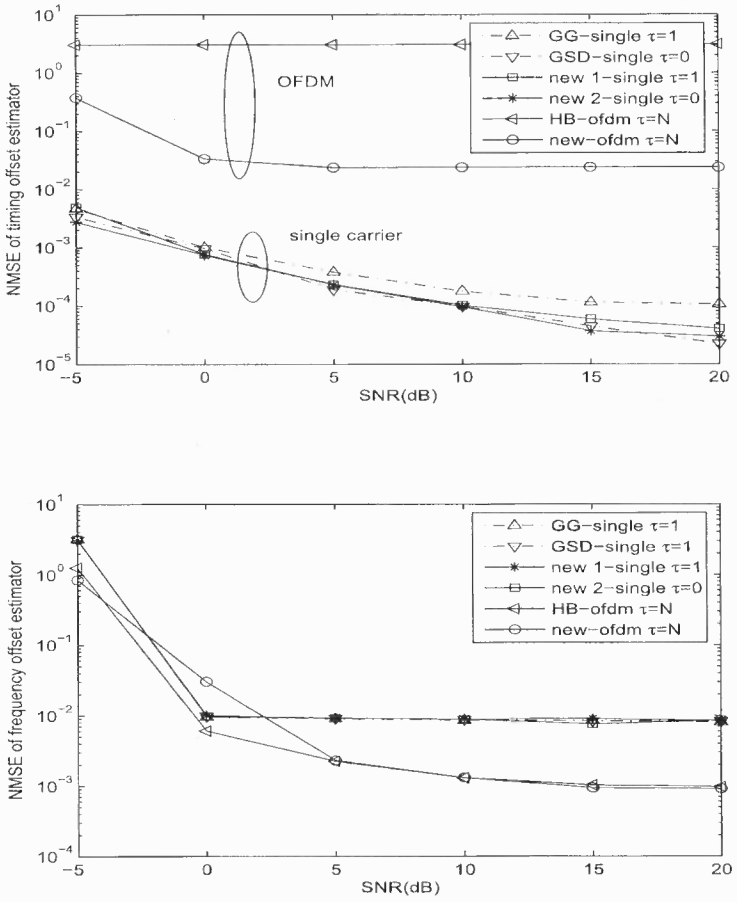

Figure 6.1 NMSE of ε and ν versus SNR for QPSK and OFDM in time-selective Rayleigh fading channel.

new proposed method with $\tau = 1$*(new 1-single), and the new proposed method with* $\tau = 0$ *(new 2-single)* are applied respectively. For the *timing estimator*, as shown in Fig. 6.1(a) (marked single carrier), the new proposed scheme (new 1 -single) outperforms the scheme proposed in [30] by almost 3dB when $SNR = 15dB$. The new method (eqn. (6.16)) applied to $\tau = 0$ (new 2 -single) has similar performance as Ghogho (GSD) [7].

In the *second scenario*, **CP-OFDM** signal is transmitted. The number of subcarriers was 64 with CP length equals 16. The frequency offset $\varepsilon = 0.1/64$ and time offset $\nu = 18$. Two methods; the one proposed by *Bölcskei (HB-ofdm)* (equation (20) and

(21) in [1]), the *new proposed method (new-ofdm)* (equation (6.19) and (6.20)) are applied respectively. We average the result over three cyclic frequencies ($k = 1, 2, 3$). As shown in Fig. 6.1(a) (marked OFDM), the new proposed scheme has much better timing estimation than the scheme proposed by Bölcskei [1]. The scheme proposed by Ghogho and el. can not work in OFDM systems, since for delay "0" the time-varying correlation is not even cyclostationary.

The frequency offset estimators (Fig. 6.1(b)) have almost the same performance for all the methods. Note that in the *first scenario* with **single carrier**, when using raised cosine pulse shaping filter, the Fourier transform of $g(n)$ only have non-zero values for cyclic frequencies at $k = 0, \pm 1$ [43]. Hence, we did not average the results over multiple cyclic frequencies, but we only used $k = 1$.

CHAPTER 7

BLIND ESTIMATION OF RAISED COSINE PULSE SHAPING BY USING SECOND ORDER CYCLOSTATIONARITY

7.1 Introduction

Chapter 7 discussed using the second order cyclostationarity in timing and frequency offset estimation. As it is shown in Chapter 7, when raised cosine pulse shaping is employed in the transmitter, the blind estimation of timing and frequency offset requires the knowledge of pulse shaping filter. However, in practice, especially in the non-cooperative environment, it is impossible to have such prior knowledge.

In this Chapter, we are going to explore the blind estimation of raised cosine pulse shaping filter. The problem can be explored in time or frequency domain. In time domain, a parametric model of the impulse response is required for the blind estimation. In [48], several methods are presented which employs the traditional channel estimation methods for pulse shaping filter estimation. Actually the estimation of the pulse shaping filter parameters has been combined into the channel estimation process. Compared to estimation in the time domain, blind estimation in the frequency domain appears more convenient for the raised cosine pulse shaping filter. This is due to the fact that the frequency response of a raised cosine pulse shaping filter depends only on one unknown variable, the roll-off factor.

Since we only focus on the raised cosine filter, we can narrow down our blind estimation to the roll-off factor estimation. The roll-off factor estimation has been explored in [49]. The authors in [49] presents an experimental method for the estimation of pulse shaping filter roll-off factor, where the roll-off factor is obtained through an approximate solution without exact theoretical proof.

In this Chapter, We propose to use the second order cyclostationarity for the roll-off factor estimation. We will explore the delay "0" and delay "1" cyclostationarity for the estimation purpose.

7.2 Raised cosine pulse shaping filter

The raised cosine pulse shaping filter is the most popular filter used in the area of digital communication. Depending on the available extra bandwidth, the raised cosine filter can be well defined using its roll-off factor. Its frequency domain function is given by [50],

$$H_{rc}(f) = \begin{cases} P, & |f| \leq \frac{1-\beta}{2P} \\ P\frac{1+\cos\left(\frac{\pi P}{\beta}\left[|f|-\frac{1-\beta}{2P}\right]\right)}{2}, & \frac{1-\beta}{2P} \leq |f| \leq \frac{1+\beta}{2P} \\ 0 & otherwise \end{cases} \tag{7.1}$$

where f is the frequency, $0 \leq \beta \leq 1$ is the roll-off factor.

The impulse response of the above filter is given by,

$$h_{rc}(n) = \frac{\sin\left(\frac{\pi n}{P}\right)}{\pi n}\frac{\cos\left(\frac{\pi \beta n}{P}\right)}{1-\frac{4\beta^2 n^2}{P^2}} \tag{7.2}$$

In practice, square root raised cosine filter is used in the transmitter and for the matched filtering, the corresponding square root raised cosine filter is used in the receiver. Their combined effect is that of a raised cosine filter given by (7.1).

The frequency domain function of a root raised cosine filter is given by [50],

$$H_{rrc}(f) = \begin{cases} \sqrt{P}, & |f| \leq \frac{1-\beta}{2P} \\ \sqrt{P}\cos\left(\frac{\pi P}{2\beta}\left[|f|-\frac{1-\beta}{2P}\right]\right), & \frac{1-\beta}{2P} \leq |f| \leq \frac{1+\beta}{2P} \\ 0 & otherwise \end{cases}$$

The impulse response of the root raised cosine filter can be given by,

$$h_{rrc}(n) = \begin{cases} 1-\beta+4\frac{\beta}{\pi}, & n=0 \\ \frac{\beta}{\sqrt{2}}\left[\begin{array}{c}\left(1+\frac{2}{\pi}\right)\sin\left(\frac{\pi}{4\beta}\right) \\ +\left(1-\frac{2}{\pi}\right)\cos\left(\frac{\pi}{4\beta}\right)\end{array}\right], & n=\pm\frac{P}{4\beta} \\ \frac{\sin\left[\pi\frac{n}{P}(1-\beta)\right]+4\beta\frac{n}{P}\cos\left[\pi\frac{n}{P}(1+\beta)\right]}{\pi\frac{n}{P}\left[1-\left(4\beta\frac{n}{P}\right)^2\right]} & otherwise \end{cases} \tag{7.3}$$

7.3 second order cyclostationarity for raised cosine pulse shaping

In Chapter 6, we find that the roll-off factor will affect the cyclostationarity test. For example, for QPSK signal, AWGN channel with SNR = 25dB, upsampling facor $P = 4$, filter delay is 100, the cyclo-spectrum for delay "1" and delay "0" are plotted in Fig. 7.1 and Fig. 7.2 respectively. As shown in the figures, it is obvious that the magnitude of the first peak (corresponds to frequency index "256") in cyclo-spectrum is related to the roll-off factor of the raised cosine filter [1]. The larger the roll-off factor, the larger the peaks at cyclic frequency $k = 1$. Note that when using raised cosine pulse shaping filter, the resulted cyclo-spectrum only has non-zero values for cyclic frequencies at $k = 0, \pm 1$ [43].

Denote the magnitude of the first peak in cyclo-spectrum as $|C(1,\tau)|$. τ is the delay. $C(1,0)$ and $C(1,1)$ are the first peak of the cyclo-spectrum at delay "0" and "1" respectively.

We recall in Chapter 7, the cyclo statistics $C(k,\tau)$ is given in (6.3). Specifically, the first peak in cyclo-spectrum $C(1,\tau)$ is given by

$$C(1,\tau) = \frac{\sigma_s^2}{P} R_h(\tau) e^{j2\pi\varepsilon\tau/P} \sum_n g_{seq}(n-\nu,\tau)\cdot e^{-j2\pi n/P} \tag{7.4}$$

Note that when $\tau = 0$, the term $e^{j2\pi\varepsilon\tau/P}$ is 1. That is, the delay "0" cyclo-spectrum $C(1,0)$ is independent of the frequency offset ε. To simplify the derivation, we first assume

[1] As we mentioned in Chapter 7, for the raised cosine pulse shaping case, the delay "0" and delay "1" time varying correlation functions are all cyclostationary.

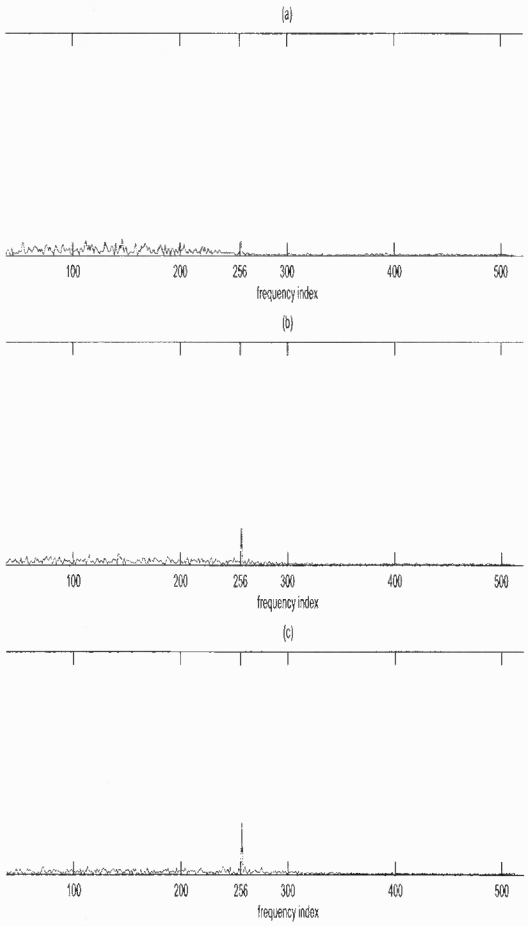

Figure 7.1 Magnitude of delay "1" cyclo-spectrum, $C(1,1)$ for roll-off factor (a) $\beta = 0.2$ (b) $\beta = 0.5$ (c) $\beta = 0.8$.

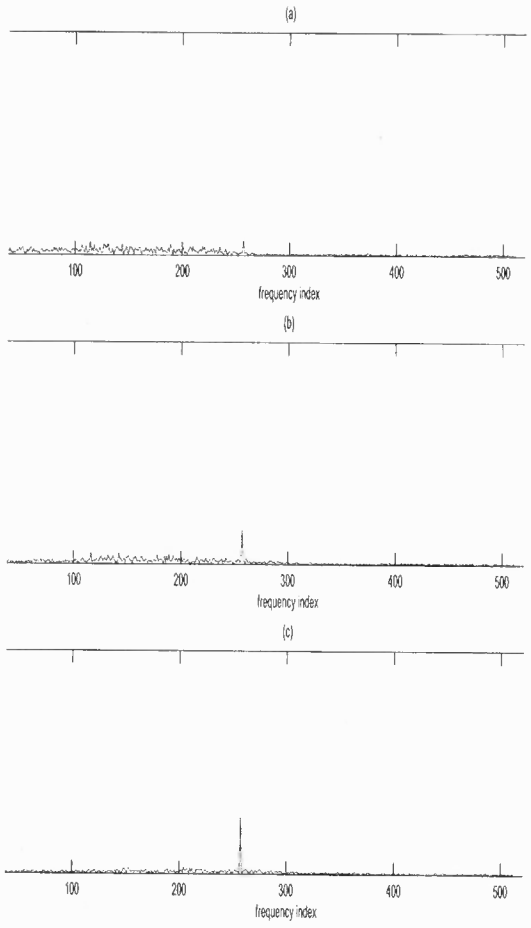

Figure 7.2 Magnitude of delay "1" cyclo-spectrum, $C(1,0)$ for roll-off factor (a) $\beta = 0.2$ (b) $\beta = 0.5$ (c) $\beta = 0.8$.

the AWGN channel with full synchronization. That is, the timing frequency offset are all zeros. Hence, $C(1,\tau)$ is simplified as

$$C(1,\tau) = \frac{\sigma_s^2}{P} \sum_n g_{seq}(n,\tau) \cdot e^{-j2\pi n/P} \tag{7.5}$$

It shows that the value of $C(1,\tau)$ depends on the Fourier transform of the periodic sequence $g_{seq}(n,\tau)$. The periodic sequence $g_{seq}(n,\tau)$, as derived in Chapter 7, depends on the delay τ, period P, and the impulse response of the pulse shaping filter.

$$g_{seq}(n,\tau) = \sum_l g(n-lP)g^*(n+\tau-lP)$$

Note that in this chapter, the pulse shaping filter $g(n)$ is not the convolution of the transmitter pulse shaping filter $g_{tx}(n)$ and the receiver pulse shaping filter $g_{rx}(n)$. Without the prior knowledge of the raise cosine pulse shaping filter, $g(n)$ is simply the transmitter filter $g_{tx}(n)$.

To further explore the relation of roll-off factor β and the mean value of $C(1,\tau)$, we show in Fig. 7.4 and Fig. 7.3 the relation of $C(1,\tau)$ vs. roll-off factor β with delay τ equals "0" and "1" for different upsampling factor P respectively.

Note to simplify the case, our simulation does not introduce any additive noise. Also, the coefficient $\frac{\sigma_s^2}{q}$ is removed for simplification. The equation (7.5) then become the Fourier transform of $g_{seq}(n,\tau)$. To differ from the previous notation, we will use $C_{ps}(1,\tau)$ to denote the value of $C(1,\tau)$ in such special case. [2]

$$C_{ps}(1,\tau) = \sum_n g_{seq}(n,\tau) \cdot e^{-j2\pi n/P} \tag{7.6}$$

We use the normalized magnitude, $|C_{ps}(1,\tau)|/|C_{ps}(0,\tau)|$, instead of the magnitude, $|C_{ps}(1,\tau)|$ due to the fact that different period P will cause different number of periods

[2]As shown in Chapter 6, when the size of FFT for cyclostationarity test M can be divided by P, the two are actually the same. When the size of FFT for cyclostationarity test can not be divided by P, there will be side-lobes around the peaks in cyclo-spectrum. To simplify the derivation, we assume that M can be divided by P.

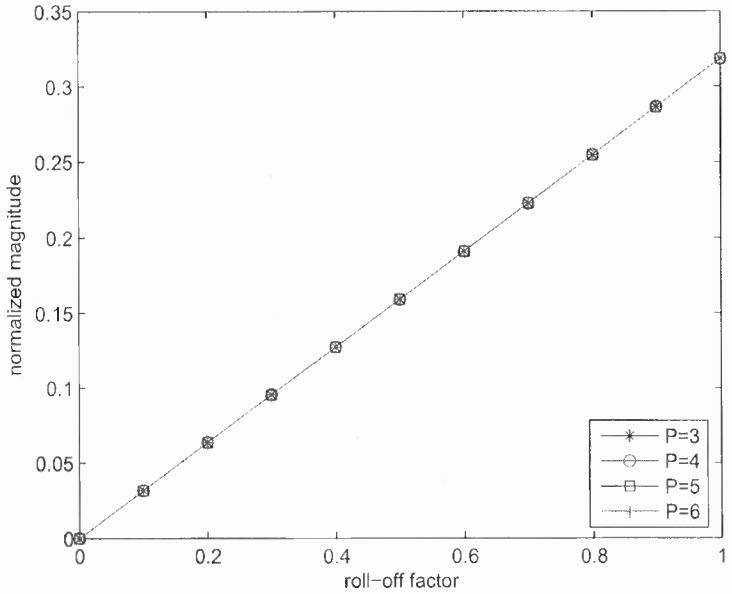

Figure 7.3 The normalized magnitude, $C_{ps}(1,0)/C_{ps}(0,0)$ vs. roll-off factor for $P = 3, 4, 5, 6$.

in a given observed window, and thus affect the magnitude of $C_{ps}(1,\tau)$. The normalized magnitude, however, is independent of the length of the observed window or the period of the cyclostationary sequence.

For delay "0" cyclo-spectrum, as it is shown in Fig. 7.3, the normalized magnitude, $|C_{ps}(1,0)|/|C_{ps}(0,0)|$, is linearly corresponding to the roll-off factors β. The slope of the line remains the same for different period P.

For delay "1" cyclo-spectrum, as it is shown in Fig. 7.4, similar to Fig. 7.3, the normalized magnitude, $|C_{ps}(1,1)|/|C_{ps}(0,1)|$, is almost linearly corresponding to the roll-off factors β. Different from Fig. 7.3, the slope of the line changes when the period P changes. The larger the period P, the smaller the slope of the line. While P is increasing, the gap between the lines due to different P is decreasing.

The number of delay taps in raised cosine pulse shaping filter, however, will not affect the normalized magnitude, $|C_{ps}(1,\tau)|/|C_{ps}(0,\tau)|$. In Fig. 7.5 and Fig. 7.6, the relation of $|C_{ps}(1,\tau)|/|C_{ps}(0,\tau)|$ vs. roll-off factor β for different delay taps are shown with delay τ

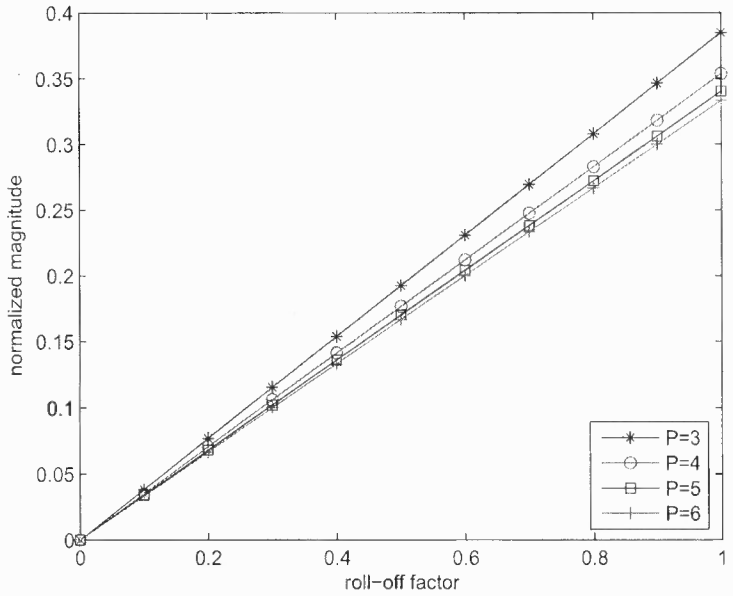

Figure 7.4 The normalized magnitude, $C_{ps}(\mathbf{1},1)/C_{ps}(0,\mathbf{1})$ vs. roll-off factor for $P = 3$, $4, 5, 6$.

equals "0" and "1" respectively. As it can be shown, when the number of delay taps is larger than 4, the value of the normalized magnitude, $|C_{ps}(1,\tau)|/|C_{ps}(0,\tau)|$ approaches to be the same. This fact indicates that the method based on cyclostationarity which we are going to proposed thereafter can not estimate the number of delay taps used in the transmitter filter. Later we will explain that the knowledge of the number of delay taps will not affect the synchronization scheme in Chapter 7.

7.4 Roll-off factor estimation based on second order cyclostationarity

7.4.1 Derivation of delay "0" and delay "1" second order cyclostationarity

In the previous section, we show the relation of the magnitude of the first peak in cyclo-spectrum, $|C_{ps}(1,\tau)|$ is related to the roll-off factor. In this section, we will prove theoretically $C_{ps}(1,\tau)$ as a function of the roll-off factor β.

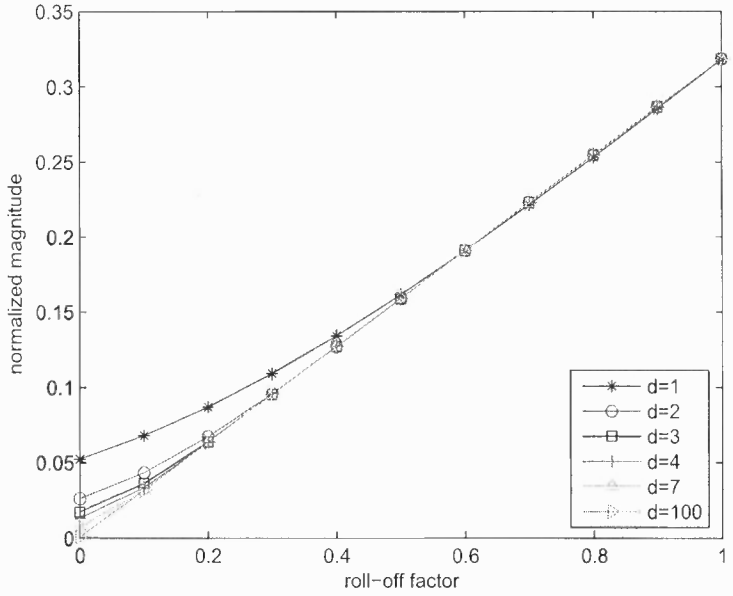

Figure 7.5 The normalized magnitude, $C_{ps}(1,0)/C_{ps}(0,0)$ vs. roll-off factor for number of delay taps $d = 1, 2, 3, 4, 7, 100$, $P = 4$.

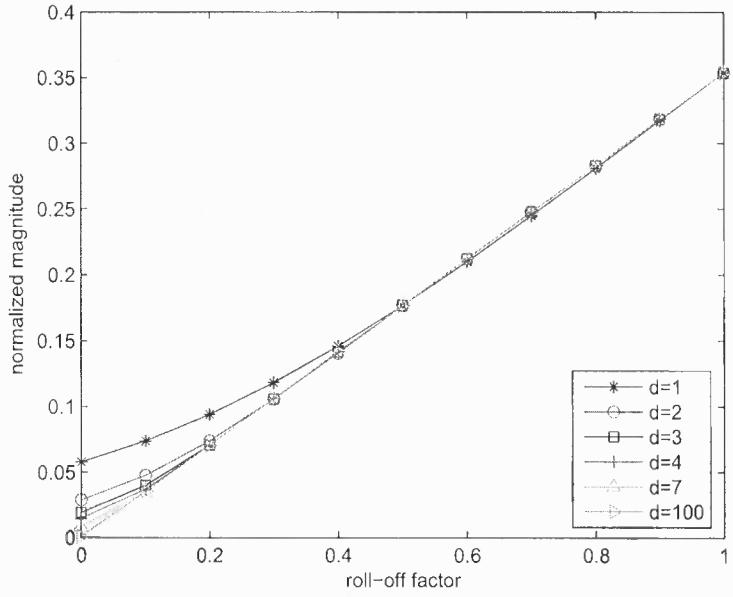

Figure 7.6 The normalized magnitude, $C_{ps}(1,1)/C_{ps}(0,1)$ vs. roll-off factor for number of delay taps $d = 1, 2, 3, 4, 7, 100$, $P = 4$.

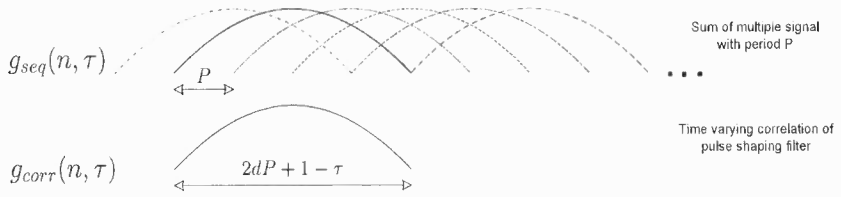

Figure 7.7 The periodic sequence $g_{seq}(n,\tau)$ with period P vs. time varying correlation $g_{corr}(n,\tau)$ with length $(2dP+1-\tau)$.

As in (6.4), $g_{seq}(n,\tau)$ is the periodic sequence with period P. From (6.5), it appears to be complicated to directly calculate the Fourier transform of $g_{seq}(n,\tau)$. Here, we propose a simple method using the time-frequency symmetry.[3]

In Fig. 7.7, the sequence $g_{seq}(n,\tau)$ is plotted. As shown, it is the sum of all the overlapping sequence $g_{corr}(n,\tau)$, where $g_{corr}(n,\tau)$ is simply the time-varying correlation of two transmitter pulse shaping filters. $g_{corr}(n,\tau)$ is given by

$$g_{corr}(n,\tau) = g_{tx}(n)g_{tx}^{*}(n-\tau) \tag{7.7}$$

For raised cosine pulse shaping filter with delay d and upsampling factor P, the length of $g_{corr}(n,\tau)$ is $(2dP+1-\tau)$, which is larger than P, the period of $g_{seq}(n,\tau)$. According to the Nyquist-Shannon sampling theorem, the signal that has been sampled can be perfectly reconstructed from the samples if the sampling rate exceeds twice of the highest frequency in the original signal. If the sampling rate is less than twice of the highest frequency, the signal can not be recovered from its samples. The frequency spectrum of the under-sampled signal will be overlapping each other with period 2π. Due to the time-frequency symmetry, as in Fig. 7.7, the overlapping signal of $g_{seq}(n,\tau)$ with period P indicates its Fourier transform, $C_{ps}(k,\tau)$ is under-sampled.

[3]In [30], it is calculated directly using Parceval's theorem. This is equivalent to the method we propose hereafter. The method we will use, however, can be used to explain some other fact as well.

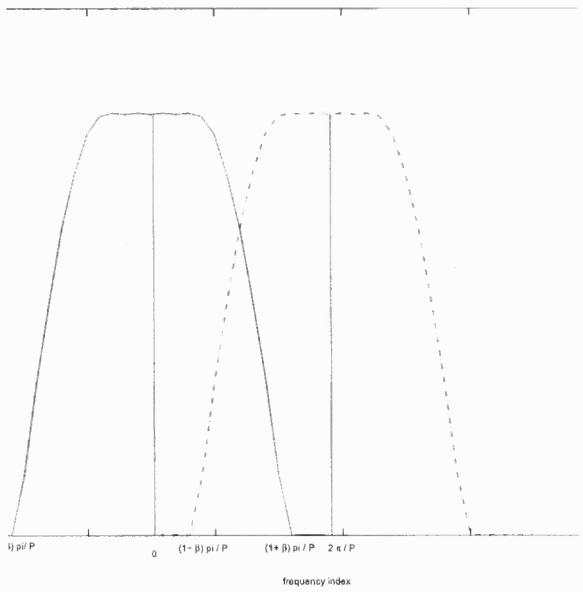

Figure 7.8 The convolution of two root raised cosine filters.

Therefore, the cyclo-spectrum $C_{ps}(k,\tau)$, whose time domain sequence is $g_{seq}(n,\tau)$, can be obtained by down-sampling the Fourier transform of $g_{corr}(n,\tau)$. This result is similar to equation (6) in [30].

Since the cyclo-spectrum is only under-sampled Frequency representation of the time domain sequence $g_{corr}(n,\tau)$, it is reasonable to say the cyclo-spectrum itself can not recover the full information of $g_{corr}(n,\tau)$, which include the delay factor of the raised cosine pulse shaping filter.

Also, as mentioned in the previous section, the delay factor estimation will not affect the estimation of the timing and frequency offset we proposed in Chapter 7. These synchronization parameters are estimated through the cyclic frequencies, which are samples of the Fourier transform of sequence $g_{corr}(n,\tau)$. Since $g_{corr}(n,\tau)$ is already fixed in the transmitter, the estimation of the delay factor in the receiver will not change its spectrum, and hence will not change the timing frequency estimation.

Now recall the Fourier transform of the product of two time domain signals, $g_{corr}(n,\tau)$, equals the frequency domain convolution of individual Fourier transform. Hence, for the

delay "0" cyclostationary sequence, as shown in Fig. 7.8, we calculate the convolution of the two root raised cosine filter and obtain

$$\begin{aligned} C_{ps}(1,0) &= \int_{\frac{1-\beta}{2P}}^{\frac{1+\beta}{2P}} \sqrt{P}\cos\left(\frac{\pi P}{2\beta}\left[|f|-\frac{1-\beta}{2P}\right]\right) \\ &\quad \cdot\sqrt{P}\cos\left(\frac{\pi P}{2\beta}\left[|f-f_0|-\frac{1-\beta}{2P}\right]\right)df \\ &= P\int_{\frac{1-\beta}{2P}}^{\frac{1+\beta}{2P}} \cos\left(\frac{\pi P}{2\beta}\left[f-\frac{1-\beta}{2P}\right]\right)\cdot\cos\left(\frac{\pi P}{2\beta}\left[f-\frac{1+\beta}{2P}\right]\right)df \\ &= \frac{\beta}{\pi} \end{aligned} \tag{7.8}$$

Note that $f_0 = P/2\pi$.

As shown in (7.8), $C_{ps}(1,0)$ is a linear function of the roll-off factor β. $C_{ps}(0,0)$ is "1" since that in practice, the raised cosine filter has the overall power of "1". Hence, $C_{ps}(1,0)/C_{ps}(0,0)$ equals to $C_{ps}(1,0)$. Also, note the above values are all real. The simulated cyclo statistics $C_{ps}(1,0)$ is plotted versus the linear function $\frac{\beta}{\pi}$ in Fig. 7.9. As shown, for delay of 100 taps, the theoretical value of $C_{ps}(1,0)$ matches the simulated value perfectly. For other delay factors larger than 4, there is still a good match except for roll-off factor $\beta = 0$. The reason is that for perfectly rectangular window shaped spectrum, which corresponds to $\beta = 0$, the delay factor must be very large to approximate the infinite sinc sequence in time domain.

The case of delay "1" cyclostationary sequence, is more complicated. Recall that the Fourier transform of a delayed timing sequence can be transformed into a frequency rotation. $C_{ps}(1,1)$ is given by

$$\begin{aligned} C_{ps}(1,1) &= \int_{\frac{1-\beta}{2P}}^{\frac{1+\beta}{2P}} \sqrt{P}\cos\left(\frac{\pi P}{2\beta}\left[|f|-\frac{1-\beta}{2P}\right]\right) \\ &\quad \cdot\sqrt{P}\cos\left(\frac{\pi P}{2\beta}\left[|f-f_0|-\frac{1-\beta}{2P}\right]\right)e^{-jf}df \\ &= \frac{1}{2}\int_{\frac{1-\beta}{2P}}^{\frac{1+\beta}{2P}} \cos\left(\frac{\pi P}{2\beta}\left[2f-\frac{1}{P}\right]\right)e^{-jf}df \end{aligned} \tag{7.9}$$

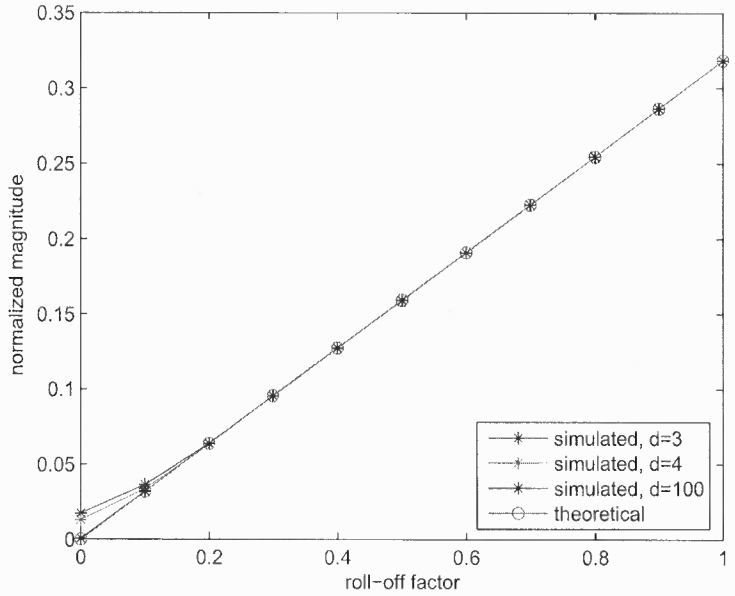

Figure 7.9 The theoretical value vs. the simulated value of $C_{ps}(1,0)$ for delay taps $d = 100$, $P = 4$.

$$= \cos\left(\frac{\pi\beta}{P}\right) e^{-j\frac{\pi}{P}} \left[\frac{\frac{\pi}{\beta}}{\left(\frac{\pi}{\beta}\right)^2 - \left(\frac{2\pi}{P}\right)^2}\right]$$

From (7.9), we can see that $C_{ps}(1,1)$ is not a linear function of roll-off factor β. However, when the sampling rate P is large, $(\frac{1}{P})^2$ goes to zero. The term $\left[\frac{\frac{\pi}{\beta}}{\left(\frac{\pi}{\beta}\right)^2 - \left(\frac{2\pi}{P}\right)^2}\right]$ approaches β/π, $\cos\left(\frac{\pi\beta}{P}\right)$ can be approximated as "1". Hence, the value of $C_{ps}(1,1)$ approaches to the value of $C_{ps}(1,0)$ when P is large.

An interesting point to note is the phase of $C_{ps}(1,1)$, obtained from (7.9), is exactly

$$\arg C_{ps}(1,1) = \frac{\pi}{P} \tag{7.10}$$

Therefore, the phase of $C_{ps}(1,1)$ is not depended on the roll-off factor β. Actually this will negate the effort to estimate the roll-off factor for the purpose of blind estimation of the timing frequency offset using $C_{ps}(1,1)$ in Chapter 7.

For the delay "1" cyclostationary sequence, note that $C_{ps}(0,1)$ is not "1". The value of $C_{ps}(0,1)$ can be calculated as

$$\begin{aligned} C_{ps}(0,1) &= \int_{-\frac{1+\beta}{2P}}^{-\frac{1-\beta}{2P}} \cos^2\left(\frac{\pi P}{2\beta}\left[|f| - \frac{1-\beta}{2P}\right]\right) e^{-j2\pi f} df \\ &\quad + \int_{\frac{1-\beta}{2P}}^{\frac{1+\beta}{2P}} \cos^2\left(\frac{\pi P}{2\beta}\left[|f| - \frac{1-\beta}{2P}\right]\right) e^{-j2\pi f} df \\ &\quad + \int_{-\frac{1-\beta}{2P}}^{\frac{1-\beta}{2P}} 1 \cdot e^{-j2\pi f} df \\ &= \left[\sin\left(\frac{\pi}{P}(1-\beta)\right) + \sin\left(\frac{\pi}{P}(1+\beta)\right)\right] \\ &\quad \cdot \left[\frac{P}{2\pi} + \frac{\frac{2\pi}{P}}{\left(\frac{\pi}{\beta}\right)^2 - \left(\frac{2\pi}{P}\right)^2}\right] \end{aligned} \tag{7.11}$$

Fig. 7.10 compares the theoretical value of $C_{ps}(1,1)/C_{ps}(0,1)$ and the simulated value. As shown in the figure, the theoretical derivation fit the simulated value perfectly. Similar to Fig. 7.9, we note that for delay taps larger than 4, there is still a good match except for roll-off factor $\beta = 0$. When $\beta = 0$, the delay taps must be very large to approximate the infinite sinc sequence.

According to (7.8) and (7.9), the mean value of delay "0" cyclo-statistics is a linear function of roll-off factor β, while that of delay "1" cyclo-statistics is not. Therefore, in the following section, we propose to use the delay "0" cyclostatistics, $C(1,0)$ for the roll-off factor estimation.

7.4.2 Roll-off factor estimation

In Chapter 7, we show that the cyclic-statistics $C(k,\tau)$ is given in (6.3). Specifically, $C(1,0)$ is given by

$$C(1,0) = \frac{\sigma_s^2}{P} R_h(0) exp^{-j2\pi\nu/P} \sum_n g_{seq}(n,0) \cdot e^{-j2\pi n/P} = \frac{\sigma_s^2}{P} R_h(0) exp^{-j2\pi\nu/P} C_{ps}(1,0) \tag{7.12}$$

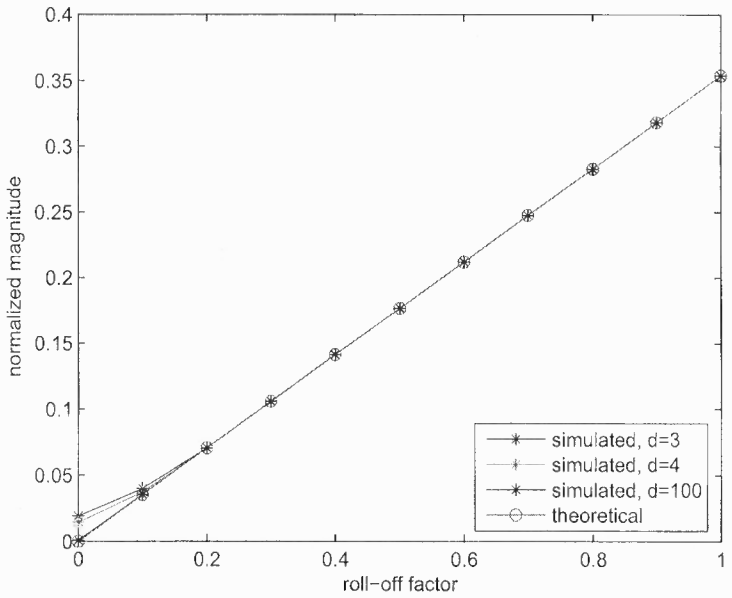

Figure 7.10 The theoretical value vs. the simulated value of $C_{ps}(1,1)/C_{ps}(0,1)$ for delay taps $d = 100$, $P = 4$.

Note that $R_h(0)$ is the overall power of the channel profile, w.l.g, it can be assumed as "1". Even if it is not, it can be combined into the estimate of the received signal power σ_s^2.

It is shown in [19] that the estimate of the cyclic-statistics, $\hat{C}(k,\tau)$ can be approximated as complex Gaussian distributed, where $\hat{C}(k,\tau)$ is the estimate of $C(k,\tau)$, in practice, it is given by

$$\hat{C}(k,\tau) = \frac{1}{M}\sum_{n=0}^{M-1} R(n,\tau)\exp(-jkn/M) \tag{7.13}$$

According to (7.8) and (7.12), the value of delay "0" cyclic-statistics $C(1,0)$ is a linear function of roll-off factor β. Hence, a direct estimator of the roll-off factor β is given by

$$\hat{\beta} = \frac{P\pi|\hat{C}(1,0)|}{\sigma_{sh}^2\hat{C}(0,0)} \tag{7.14}$$

where $\sigma_{sh}^2 = \sigma_s^2 R_h(0)$. Note that to negate the efforts to estimate the signal power σ_s^2 and the channel parameter $R_h(0)$, the normalized cyclic statistics $\frac{\hat{C}(1,0)}{\hat{C}(0,0)}$ is used.

Due to the fact that

$$C(0,0) = \frac{\sigma_s^2 R_h(0)}{P} \tag{7.15}$$

the roll-off factor estimator can also be given by

$$\hat{\beta} = \frac{P\pi|\hat{C}(1,0)|}{\sigma_{sh}^2} \tag{7.16}$$

In the next section, we are going to prove that the above estimator (7.16) is a MLE of the roll-off factor.

7.4.3 Maximum Likelihood Estimator for the roll-off factor

In this section, we are going to derive the MLE of the roll-off factor based on the delay "0" second order cyclostationarity. As we known, the cyclic-statistics $\hat{C}(1,0)$ can be approximated as Gaussian distributed. To simplify the case, we use C instead of $\hat{C}(1,0)$ in the following derivation. The likelihood function of the cyclic-statistics $C(1,0)$ can be given by

$$p\left(C_r, C_i|\beta,\theta\right) = \frac{\exp\left[-\frac{\left(\frac{C_r - a\beta\cos\theta}{\sigma_r}\right)^2 - 2\rho\frac{C_r - a\beta\cos\theta}{\sigma_r}\frac{C_i - a\beta\sin\theta}{\sigma_i} + \left(\frac{C_i - a\beta\sin\theta}{\sigma_i}\right)^2}{2(1-\rho^2)}\right]}{2\pi\sigma_r\sigma_i\sqrt{1-\rho^2}} \tag{7.17}$$

where C_r and C_i are the real and imaginary part of the cyclic-statistics $\hat{C}(1,0)$, σ_r^2 and σ_i^2 are the variance of the real and imaginary part of the non-cyclic noise of $\hat{C}(1,0)$. ρ is the correlation coefficient of the real and imaginary noise part. a is the linear function coefficient which is given by as $\frac{\sigma_{sh}^2}{\pi P}$ as in (7.16). θ is the angle corresponding to the timing offset.

After mathematical manipulations, the MLE of the roll-off factor $\hat{\beta}_{MLE}$ can be given as a function of σ_r, σ_i, ρ and θ.

$$\hat{\beta}_{MLE} = \frac{\left(\frac{C_r \cos\theta}{\sigma_r^2} + \frac{C_i \sin\theta}{\sigma_i^2} - \frac{\rho C_i \cos\theta + \rho C_r \sin\theta}{\sigma_r \sigma_i}\right)}{a\left(\frac{\cos^2\theta}{\sigma_r^2} + \frac{\sin^2\theta}{\sigma_i^2} - \frac{2\rho \sin\theta\cos\theta}{\sigma_r\sigma_i}\right)} \tag{7.18}$$

The value of θ can be obtained by using the method proposed in Chapter 7. As in Chapter 7, the timing offset is given by

$$\hat{\nu} = -P \arg\left\{C(k,\tau)/(C(-k,\tau)G_{seq}^2(k,\tau))\right\}/(4\pi k)$$

Note that the phase from the raised cosine filter $\arg\left\{G_{seq}^2(k,\tau)\right\} = 0$ for delay "0" cyclic-statistics $C(1,0)$ according to (7.8). The value of $\hat{C}(1,0)$ and $\hat{C}(-1,0)$ are conjugate to each other due to the symmetry of Fourier transform caused by the real timing sequence. Hence, the angle corresponding to the timing offset, θ is given by

$$\hat{\theta} = \arg\left\{\hat{C}(1,0)\right\} \tag{7.19}$$

Applying (7.19) into (7.18), we can show that the above MLE can be rewritten as

$$\hat{\beta}_{AMLE} = \frac{|\hat{C}(1,0)|}{a} \tag{7.20}$$

We denote the above estimator as Approximate MLE (AMLE). Note that the above AMLE is exactly the same as the estimator given by (7.16).

7.4.4 Performance analysis

According to the previous chapter, the MLE of the roll-off factor is given by in (7.18). As we known, the variance of an unbiased estimator is bounded by the inverse of the Fisher information. The Fisher information of the roll-off factor, $I(\beta)$ is defined by

$$I(\beta) = E\left[\frac{\partial^2 \ln p(C;\beta)}{\partial\beta^2}\right] = \frac{-a^2}{(1-\rho^2)}\left(\frac{\cos^2\theta}{\sigma_r^2} - \frac{2\rho\sin\theta\cos\theta\sigma_r\sigma_i}{\sigma_r\sigma_i} + \frac{\sin^2\theta}{\sigma_r^2}\right) \tag{7.21}$$

The Cramer-Rao lower bound (CRLB) of the estimator can be obtained by

$$var\left(\hat{\beta}\right) \geq \frac{1}{-I\left(\beta\right)} = \frac{\left(1-\rho^2\right)\sigma_r^2\sigma_i^2}{a^2\left(\sigma_i^2\cos^2\theta - 2\rho\sin\theta\cos\theta\sigma_r\sigma_i + \sigma_r^2\sin^2\theta\right)} \tag{7.22}$$

The CRLB depends on the value of the σ_r^2, σ_i^2 and ρ. These values, however, depend on the information of the specific raised cosine filter, such as the upsampling rate P, the roll-off factor β, and the delay d. As in chapter 6, the exact derivation of the value of σ_r^2, σ_i^2 and ρ are complicated and will not be shown here.

7.5 Simulation

Monte Carlo simulations are conducted to test the performance of the above estimators (5000 trails for each point). The number of the received symbols for cyclostationarity test was $M = P * 300 = 1200$. The raised cosine filters with roll-off factor $\beta = 0.25$, $\beta = 0.5$, $\beta = 0.75$, upsampling factor $P = 4$, and delay $d = 7$ are used. Single carrier QPSK symbols are assumed. Time-selective Rayleigh fading channel is assumed, with Doppler spread of $B_hT = 0.01$, where B_h is the bandwidth of $h(n)$. Same as in [43], the channel filter $h(n)$ is obtained by bilinearly transforming a third-order continuous-time all-pole filter, whose poles are the roots of the equation $(s^2 + 0.35\omega_0 s + \omega_0^2)(s + \omega_0) = 0$, where $\omega_0 = 2\pi B_h/1.2$. The time offset $\nu = 3$ and frequency offset $\varepsilon = 0.1$, are implemented. The normalized mean square error (NMSE) are plotted in Fig.7.11. The performance of two estimators are compared (equation 7.14 and equation 7.16). As shown in Fig. 7.11, the larger the roll-off factor, the smaller the NMSE. This is because a larger roll-off factor will cause higher peak or larger $\hat{C}(1,0)$ and thus improve the performance.

Note that specially in low SNR scenarios, the second estimator (equation 7.16) ("est2") has better performance. The first estimator (7.14) need an estimate of the value $\hat{C}(0,0)$ and at low SNR scenarios, the estimate of the value $\hat{C}(0,0)$ which include the noise power will deteriorate the performance of the estimator.

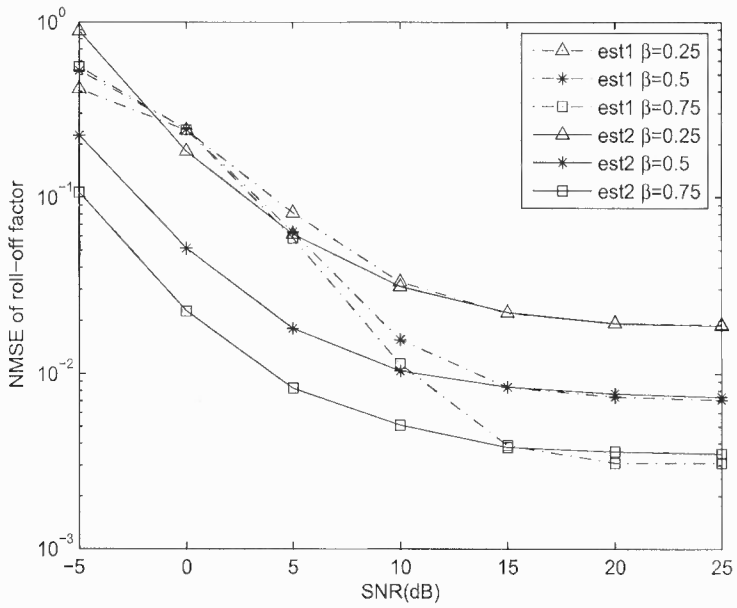

Figure 7.11 NMSE of the roll-off factor estimator for QPSK signal with $\beta = 0.25, 0.5, 0.75$, $P = 4$.

When SNR=0dB and AWGN channel is used, we plot the histogram of the estimates of these two estimators with $\beta = 0.25$. As shown in Fig.7.12, the first estimator is biased while the second is slightly biased. The first estimator is biased because the term $\hat{C}(0,0)$ in the first estimator (7.14) include power of the additive noise. The second AMLE is actually biased because the cyclo-spectrum noise is included. For performance comparison, we limit to the cased $P = 4$ and synchronized AWGN channel (without timing offset). The MLE for this case will be

$$\hat{\beta}_{MLE} = \frac{Real\{\hat{C}(1,0)\}}{a} \tag{7.23}$$

where $Real\{\cdot\}$ is calculating the real part. We compare the above MLE with the previous proposed estimators to the CRLB in Fig. 7.13. As it is shown, the AMLE has almost the same performance as the MLE in high SNR scenarios. When the SNR is very low, the estimator 1 (7.14) even outperform the CRLB. That is because the CRLB is only a local bound. The implied condition that $|\hat{C}(1,0)| < |\hat{C}(0,0)|$ make the MSE of the estimator 1

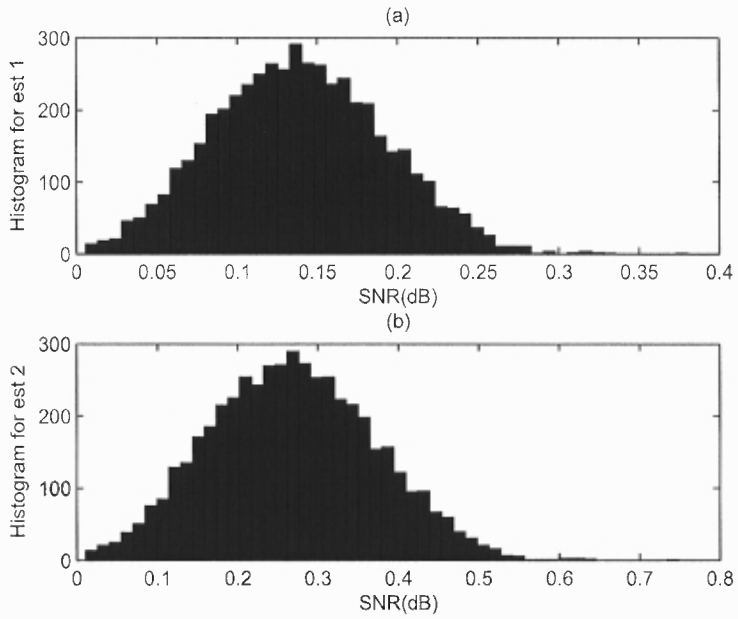

Figure 7.12 Histogram of the roll-off factor estimate for estimator 1 and 2.

(7.14) is even smaller than the bound. The performance of the estimator can be improved when there is more observed symbols. Similar to the above simulation set up, we show in Fig.7.14 the performance of the ML estimator (equation 7.16) for different M. It is obvious that the larger the size M, the better the performance.

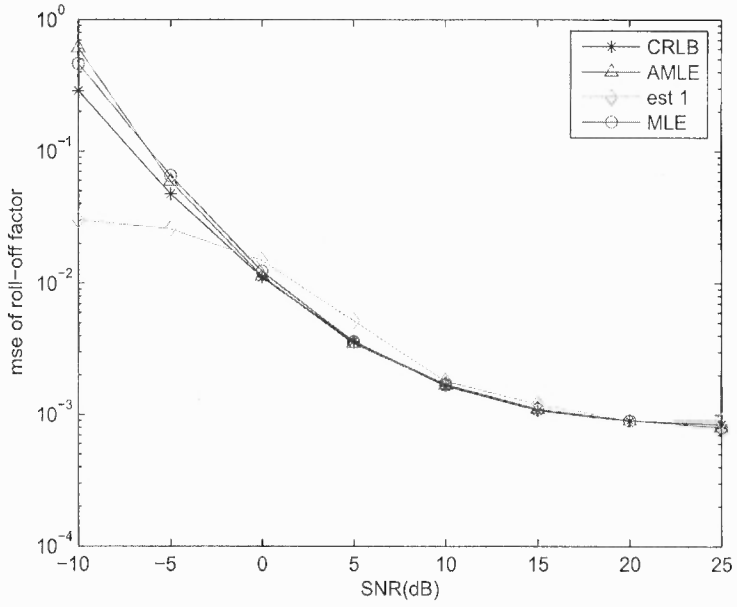

Figure 7.13 Performance comparison of different estimators with CRLB, P=4, $\beta = 0.25$.

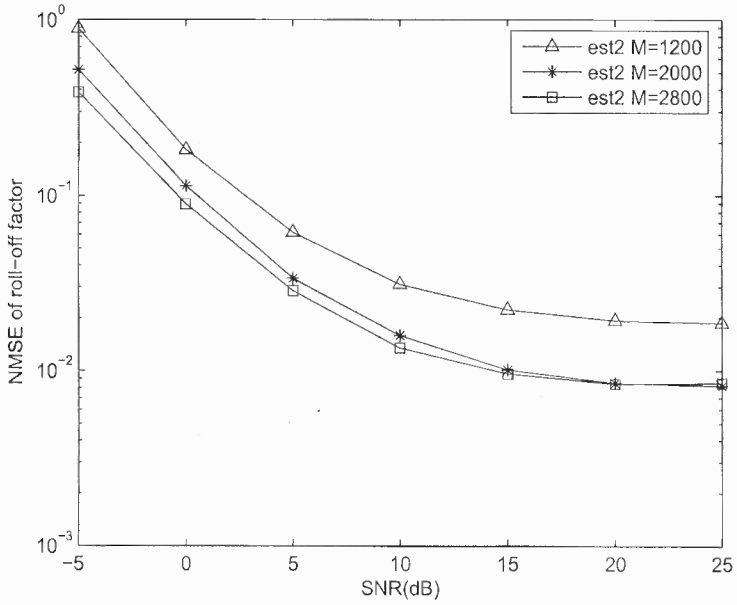

Figure 7.14 NMSE of the roll-off factor estimator for QPSK signal with $\beta = 0.25$, $P = 4$, and M=1200, 2000, 2800.

Part III

MIMO CLASSIFICATION

CHAPTER 8

STC AND BLAST MIMO MODULATION RECOGNITION

8.1 Introduction

The great potential provided by the use of multiple input multiple output (MIMO) encouraged intensive research efforts in the field of communications in recent years. This effort led to the design and implementation of MIMO systems in commercial and military communication systems. The new scenario introduces many new challenges for both cognitive radios and surveillance systems.

One form of exploring transmit diversity in MIMO is to apply STC. Alamouti's STC is one of the first which studied the case of two transmitted antennas [44]. Tarokh extended the results to the case of more transmitting antennas [45]. It was shown that for different transmission rate, coding schemes are different. The STC schemes introduce redundant information and explore the spatial diversity for better system performance.

Different from the STC schemes, Bell Labs Layered Space-Time Architecture (BLAST) exploits spatial diversity to transmit more information [46]. Both schemes use multiple transmit antennas and their decoding schemes are different depending on their coding schemes.

The goal of this chapter is to blindly recognize the spatial coding schemes, or, more specifically, to distinguish STC from BLAST schemes. We only consider the linear space time block coding (STBC), proposed in [44] and [45]. Due to the redundant information introduced in the STC schemes, the received signals will have temporal and spatial correlations; while in the BLAST schemes, this is not the case. Since the time correlation introduced in STC is in a block mode, we apply the cyclostationarity test to explore it. The cyclostationarity test does not only distinguish STC schemes from BLAST scheme, but also can find out the specific coding schemes used, whether it is full rate, half rate or other. Furthermore such approach can help extract the timing and frequency synchronization parameters.

8.2 System model and detection problem

Consider a MIMO environment with L transmit antennas and M receive antennas. The kth received data vector $\mathbf{r}(k)$ is of size $(M \times 1)$ which is given by

$$\mathbf{r}(k) = \mathbf{H}(k)\,\mathbf{s}(k) + \mathbf{w}(k) \tag{8.1}$$

where $\mathbf{H}(k)$ is the Raleigh distributed channel transfer matrix of $(M \times L)$. Assume that the channel is slow time varying, to simplify the derivation, we will use block fading channel where the channel is assumed to be the same during the detection period. $\mathbf{w}(k)$ is an additive white Gaussian noise (AWGN) with variance σ_w^2, which is independent of the signal. $\mathbf{s}(k)$ is the $(k \bmod T)$th column vector of the $(L \times T)$ transmission matrix (where T is the block size), whose entries are linear combinations of the random m-PSK ($m > 2$) or m-QAM signal and their conjugates.

For example, in Alamouti's scheme, when synchronized, $\mathbf{s}(k)$ and $\mathbf{s}(k+1)$ are given by

$$\begin{bmatrix} \mathbf{s}(k) & \mathbf{s}(k+1) \end{bmatrix} = \begin{bmatrix} x_1 & -x_2^* \\ x_2 & x_1^* \end{bmatrix} \tag{8.2}$$

where x_1, x_2 are all random m-PSK signal with variance σ_s^2. Note that we ignore the timing index for x_1, x_2 for simplification. On the other hand, in BLAST scheme, $\mathbf{s}(k)$ is composed of independent random m-PSK signals.

Suppose $M = 2$, for Alamouti's scheme, the synchronized received signal at antenna i with length $T = 2$ can be rewritten as

$$\begin{bmatrix} r_i(k) \\ r_i(k+1) \end{bmatrix} = \begin{bmatrix} h_{i1}x_1 + h_{i2}x_2 + w_i(k) \\ -h_{i1}x_2^* + h_{i2}x_1^* + w_i(k+1) \end{bmatrix} \tag{8.3}$$

where $r_i(k)$ is the kth synchronized received signal at antenna i. h_{ij} represents the channel from the jth transmit antenna to the ith receive antenna. Since the channel is block fading,

the time index k in the channel parameter is ignored for simplification. As it is shown, $r_i(k)$ and $r_i(k+1)$ are composed of correlated signals.

As for the BLAST scheme, the received signal at antenna i with length $T = 2$ can be rewritten as

$$\begin{bmatrix} r_i(k) \\ r_i(k+1) \end{bmatrix} = \begin{bmatrix} h_{i,1}x_1 + h_{i,2}x_2 + w_i(k) \\ h_{i,1}x_3 + h_{i,2}x_4 + w_i(k+1) \end{bmatrix} \tag{8.4}$$

Note that the transmitted signals x_i, $i = 1, 2, 3, 4$, is independent from each other. Thus, the received signal $r_i(k)$ and $r_i(k+1)$ are independent from each other.

If we restrict our attention to only linear processing, the detection problem can be given as

$$\begin{aligned} &\mathcal{H}_1: \ g[r_i(k), r_j(k+1)] \text{ is statistically cyclic} \\ &\Longrightarrow \text{STC scheme;} \\ &\mathcal{H}_0: \ g[r_i(k), r_j(k+1)] \text{ is not statistically cyclic} \\ &\Longrightarrow \text{BLAST scheme;} \end{aligned} \tag{8.5}$$

where $g[\bullet]$ is a linear correlator function defined as

$$g[\bullet] = r_i(k)\, r_j(k+1) \text{ or } r_i(k)\, r_j^*(k+1) \tag{8.6}$$

where $0 \leq i, j \in I < M$. One can choose different correlators $g[\bullet]$ as long as the resulted sequence for the STC schemes is statistically cyclic.

The above detector for distinguishing Alamouti's STC scheme from BLAST can be generalized to the case where the number of transmit antenna L is larger than 2. Since the STC schemes is block coding, the correlation of the transmitted signals is within one block, and the detection problem can be rewritten as

$$\begin{aligned} &\mathcal{H}_1: \ g[r_i(k), r_j(k+u)] \text{ is statistically cyclic} \\ &\Longrightarrow \text{STC scheme;} \end{aligned} \tag{8.7}$$

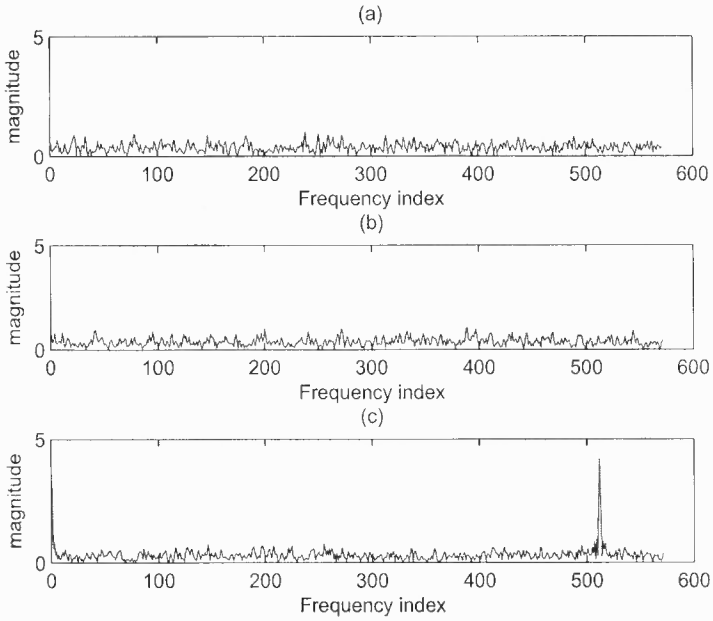

Figure 8.1 The cyclo-spectrum of the statistically cyclic sequence (a) $r_i(k)\, r_j^*(k+1)$, $i \neq j$ (b) $r_i(k)\, r_i(k+1)$ (c) $r_i(k)\, r_j(k+1)$, $i \neq j$

$$\mathcal{H}_0\colon\ g\left[r_i(k), r_j(k+u)\right] \text{ is not statistically cyclic}$$

$$\Longrightarrow \text{BLAST scheme;}$$

where u is an integer less than the block length T.

8.3 Criteria for choosing the correlator

As it is shown in the previous section, we have not yet specified $g[\bullet]$. There is no unique correlator for our detection problem. That is, we have the degree of freedom to choose them. In fact, it is possible to show that, even though the received signals in STC scheme contains correlated signals, not all the correlators can generate a statistically cyclic sequence.

For example, as shown in Fig.8.1, to detect an Alamouti's scheme, auto correlators $r_i(k)\, r_i(k+1), 0 \leq i \in I < M$, cross conjugate correlators $r_i(k)\, r_j^*(k+1), i \neq j \in I <$

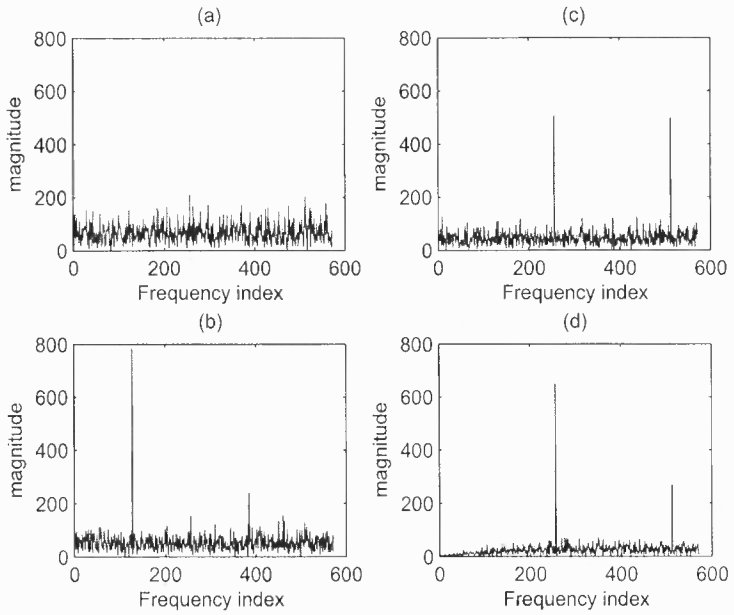

Figure 8.2 The cyclo-spectrum of the statistically cyclic sequence (a) $L = 3$, $T = 8$, half rate, $r_i(k)\, r_j(k+1)$, $i \neq j$ (b) $L = 3$, $T = 8$, half rate, $r_i(k)\, r_j(k+5)$, $i \neq j$ (c) $L = 3$, $T = 4$, rate 3/4, $r_i(k)\, r_j(k+1)$, $i \neq j$ (d) $L = 3$, $T = 4$, rate 3/4, $|r_i(k)|^2$.

M, are not statistically cyclic, while cross correlators $r_i(k)\, r_j(k+1)$, $i \neq j$, is statistically cyclic.

From (8.5) and (8.7), the criteria to choose a correlator is to make the resulted sequence statistically cyclic or

$$E\{g[r_i(k), r_j(k+u)]\} \text{ or } E\{g[r_i(k), r_j^*(k+u)]\} \tag{8.8}$$
$$= f(k) = f(k+lp), l \text{ is integer}$$

where $f(k)$ is a periodic function with period p.

We can verify (8.8) with the previous example of Alamouti's scheme. Extending this result to more transmit antennas, one finds that the choice of correlator depends on the specific STC scheme applied.

As shown in Fig.8.2, when the number of transmit antenna $L = 3$, $T = 4$, which corresponds to the rate $3/4$ STBC, we found by experiment that one can choose correlators

given by $r_i(k) r_j^*(k+u), r_i(k) r_j(k+u), r_i(k) r_i^*(k+u), i \neq j, 0 \leq i, j \in I < M, u \in I < 4$, or the energy detector $|r_m(k)|^2$. If $L = 3, T = 8$, which corresponds to the half rate STBC, we found by experiment that one can choose correlator given by $r_i(k) r_i^*(k+u)$, $0 < u \in I < 4, r_i(k) r_j^*(k+b), r_i(k) r_j(k+b), i \neq j, 0 \leq i, j \in I < M, 0 < b \in I < 8$.

For all these correlators, the BLAST scheme can not give us a statistically cyclic sequence.

According to (8.8), we have only listed the possible correlators for Alamouti's and Tarokh's (half rate and 3/4 rate) scheme. For the general cases, a simple method can be employed by using the transmission matrix of the STC scheme to get the possible correlators satisfying (8.8). Essentially, we can get the following statements (see Appendix for proof).

Theorem 1: *The cross (conjugate) correlation between sequences from any two receiving antenna or auto conjugate correlation of a sequence at any receiving antenna, are statistically cyclic, if for any given* $0 \leq u < T$, *the matrices* $E\left\{s(k)\, s(k+u)^T\right\}$ *or* $E\left\{s(k)\, s(k+u)^H\right\}$ *are not the same;*

Theorem 2: *The auto correlation of a sequence at any of the receiving antenna is statistically cyclic, if for any given* $0 \leq u < T$, *the matrices* $E\left\{s(k)\, s(k+u)^T\right\}$ *is not skew-symmetric with the same diagonals. That is when the matrices' diagonals are not the same, the auto correlation sequence at any receiving antenna is statistically cyclic.*

We can evaluate a table composed of matrices for straightforward view. For example, when the number of transmit antenna $L = 3, T = 4$, which corresponds to the rate $3/4$ STBC, the table is given by

$\mathrm{s}(0)\,\mathrm{s}(0)^H$	$\mathrm{s}(0)\,\mathrm{s}(1)^T$	$\mathrm{s}(0)\,\mathrm{s}(2)^T$	$\mathrm{s}(0)\,\mathrm{s}(3)^T$
$\mathrm{s}(1)\,\mathrm{s}(0)^H$	$\mathrm{s}(1)\,\mathrm{s}(1)^H$	$\mathrm{s}(1)\,\mathrm{s}(2)^T$	$\mathrm{s}(1)\,\mathrm{s}(3)^T$
$\mathrm{s}(2)\,\mathrm{s}(0)^H$	$\mathrm{s}(2)\,\mathrm{s}(1)^H$	$\mathrm{s}(2)\,\mathrm{s}(2)^H$	$\mathrm{s}(2)\,\mathrm{s}(3)^T$
$\mathrm{s}(3)\,\mathrm{s}(0)^H$	$\mathrm{s}(3)\,\mathrm{s}(1)^H$	$\mathrm{s}(3)\,\mathrm{s}(2)^H$	$\mathrm{s}(3)\,\mathrm{s}(3)^H$

(8.9)

where $\mathbf{s}(i)$, $i = 0, 1, 2, 3$ are actually $\mathbf{s}(k|k \bmod T = i)$, which are the four column vectors of the transmission matrix [45]. It is given by

$$\begin{aligned}
\mathbf{s}(0) &= \left[\begin{array}{ccc} x_1, & x_2, & x_3/\sqrt{2} \end{array} \right]^T \\
\mathbf{s}(1) &= \left[\begin{array}{ccc} -x_2^*, & x_1^*, & x_3/\sqrt{2} \end{array} \right]^T \\
\mathbf{s}(2) &= \left[\begin{array}{ccc} x_3^*/\sqrt{2}, & x_3^*/\sqrt{2}, & \left(-x_1 - x_1^* + x_2 - x_2^*\right)/2 \end{array} \right]^T \\
\mathbf{s}(3) &= \left[\begin{array}{ccc} x_3^*/\sqrt{2}, & -x_3^*/\sqrt{2}, & \left(x_1 - x_1^* + x_2 + x_2^*\right)/2 \end{array} \right]^T
\end{aligned} \tag{8.10}$$

The correlation matrices of size 3×3 are above the diagonal of the table given by (8.9); while the conjugate correlation matrices are below the diagonal of the table.

To check whether we can use the energy detector, we simply check the matrices along the principal diagonal, which corresponds to $E\left[\mathbf{s}(k)\,\mathbf{s}(k)^H\right]$. These matrices are given by **A**, **A**, **B**, **B**, where

$$\mathbf{A} = \begin{bmatrix} \sigma_s^2 & 0 & 0 \\ 0 & \sigma_s^2 & 0 \\ 0 & 0 & \frac{\sigma_s^2}{2} \end{bmatrix} \tag{8.11}$$

and

$$\mathbf{B} = \begin{bmatrix} \sigma_s^2 & 0 & 0 \\ 0 & \sigma_s^2 & 0 \\ 0 & 0 & 0 \end{bmatrix} \tag{8.12}$$

Apparently, their diagonals are not all the same. Thus following Theorem 2, energy detector will work for the detection problem.

To check whether the auto correlator $r_i(k)\, r_i(k+1)$ is statistically cyclic, we can simply check the matrices along the first sub-diagonal of the table (8.9) on the top. The fourth matrix along the sub-diagonal is zero matrix because the transmitted signal out of one STC block is independent of the other STC block. The four matrices are given by **C**,

D, 0, 0, where

$$\mathbf{C} = \begin{bmatrix} 0 & \sigma_s^2 & 0 \\ -\sigma_s^2 & 0 & 0 \\ 0 & 0 & 0 \end{bmatrix} \tag{8.13}$$

and

$$\mathbf{D} = \begin{bmatrix} 0 & 0 & \frac{-\sigma_s^2}{2} \\ 0 & 0 & \frac{-\sigma_s^2}{2} \\ \frac{\sigma_s^2}{2} & \frac{\sigma_s^2}{2} & 0 \end{bmatrix} \tag{8.14}$$

Since the matrices are all skew symmetric (with same diagonals), we can conclude that the auto correlator $r_i(k)\, r_i(k+1)$ will not work. However, according to Theorem 1, the cross correlator $r_i(k)\, r_j(k+1)$ will work since these matrices given by C, D, 0, 0, are not all the same.

According to the above rules, one can conclude *that a common correlator which is suitable for all STC schemes in [44] and [45] is* $r_i(k)\, r_j(k+1)$, $i \neq j$. However, this common correlator does not promise a good detection performance. For example, as shown in Fig.8.2(a) , when $L = 3$, $T = 8$, the peak at frequency index 256 is only slightly higher than others. Consequently, the performance of the detector with such correlator is quite poor compared to others. Therefore, in the next section, we are going to find some combining process for the correlators to improve the detection performance.

8.4 Detection with prior knowledge

8.4.1 The block length T is known

When the block length T is known, we can get the cyclic frequencies α is a multiple of $\frac{2\pi}{T}$. According to previous section, all the correlators satisfy the criteria (8.8) are statistically cyclic. The question is then arise; how to combine these common correlators together to improve the performance of the detector?

We recall that in [19], to combine the cyclic statistics of the correlator with different delays $r(k)\,r(k+\tau_i)$, $i = 1, \cdots, q$, Dandawaté and Giannakis treat the cyclostationarity test problem as detecting nonzeroness of the unknown mean of a multivariate normal random variables. The test statistic was given by

$$\kappa = \mathbf{R}_{rr}(\alpha)\,\mathbf{Y}_{rr}^{-1}\mathbf{R}_{rr}(\alpha)^{T} \tag{8.15}$$

where $\mathbf{R}_{rr}(\alpha)$ is the $1 \times 2q$ row vectors cyclic spectrum at cyclic frequency α with delays $(\tau_1, \cdots, \tau_q)$

$$\mathbf{R}_{rr}(\alpha) = \begin{bmatrix} \mathrm{Re}\left(R(\alpha,\tau_1)\right), \cdots, \mathrm{Re}\left(R(\alpha,\tau_q)\right), \\ \mathrm{Im}\left(R(\alpha,\tau_1)\right), \cdots, \mathrm{Im}\left(R(\alpha,\tau_q)\right) \end{bmatrix} \tag{8.16}$$

in which $R(\alpha,\tau_i)$ is the estimate of the cyclic spectrum at cycle frequency α for delay τ_i, which is given by

$$R(\alpha,\tau_i) = \frac{1}{N}\sum_{k=0}^{N} r(k)\,r(k+\tau_i)\exp(-jk\alpha) \tag{8.17}$$

$\mathbf{Y}_{rr}$ is the asymptotic covariance matrix of the estimator $\mathbf{R}_{rr}(\alpha)$, which is a $2q \times 2q$ matrix computed using the cyclic-spectrum given in [19].

The performance of the detector given by (8.15) is better than a single correlator detector at only one τ. One can show that, in the test statistic given by (8.15), a prewhitening filter is applied to the different cyclic spectrums before summing them together.

Similar to [19], we suggest to combine different common correlators by applying a prewhitening filter before summing them together. In such a case, the test statistic is the same form as (8.15).

Therefore, for this combining process, the detection algorithm can be implemented using the following steps:

Step 1: Get P common correlators according to the criteria (8.8) with the prior knowledge;

Step 2: Computing the test statistic, κ, given by (8.15) at cyclic frequency $\alpha = \frac{2\pi}{T}$;

Step 3: For a given probability of false alarms, P_F, using the central χ^2 tables for $2P$ degrees of freedom, find a threshold γ so that $P_F = \Pr\{\chi^2 > \gamma\}$;

Step 4: Declare it is STC if $\kappa \geq \gamma$; otherwise, decide it is BLAST.

8.4.2 Both the channel parameters and the specific STC are known

In the cyclostationarity test derived above, we assume the mean of the cyclic-correlations, $E\{R_m(\alpha)\}$ is unknown. Similar to (8.17), the cyclic spectrum, $E\{R_m(\alpha)\}$, is the expectation of the Fourier transform of the mth correlator. Note that $E\{R_m(\alpha)\}$ can be determined by the expectation of the correlator, which is dependent on the specific STC schemes and the channel parameters. That is, the expectation of the correlator will affect $E\{R_m(\alpha)\}$.

For example, when the number of transmit antenna $L = 3$, $T = 4$, the expectation of the correlator $r_i(k) r_j(k+1)$ is given by

$$\begin{aligned} & E\{r_i(k) r_j(k+1)\} \\ &= \left(\frac{h_{j1}h_{i3} + h_{j2}h_{i3} - h_{j3}h_{i1} - h_{j3}h_{i2}}{2}\right) \delta[(k+1) \bmod 4] \\ &+ (h_{i1}h_{j2} - h_{j1}h_{i2})\, \delta[k \bmod 4] \end{aligned} \tag{8.18}$$

where $\delta[k]$ is the delta function. While the expectation of the correlator $r_i(k) r_j(k+2)$ is given by

$$\begin{aligned} & E\{r_i(k) r_j(k+2)\} \\ &= \left(\frac{h_{j1}h_{i3} - h_{j2}h_{i3} - h_{j3}h_{i1} + h_{j3}h_{i2}}{2}\right) \delta[(k+1) \bmod 4] \\ &+ \left(\frac{h_{j1}h_{i3} + h_{j2}h_{i3} - h_{j3}h_{i1} - h_{j3}h_{i2}}{2}\right) \delta[k \bmod 4] \end{aligned} \tag{8.19}$$

Similarly, we can get the expectation for $r_i(k) r_j(k+3)$. Obviously, these cyclic sequences generated by the correlators with different delays has different spectral shaping. Consequently, the expectations of the cyclic spectrums at the cyclic frequency α will have different phases. Assume the observed sequence is long enough, the phase of the first peak

of the statistically cyclic sequence ($\alpha = \frac{2\pi}{T}$) can be given by

$$\phi = angle \left\{ \begin{array}{c} \frac{1}{T}\sum_{k=0}^{T-1} E\left\{g\left[r_i\left(k\right), r_i\left(k+u\right)\right]\right\} \\ \cdot \exp\left[-\frac{j2\pi(k \bmod T)}{T}\right] \end{array} \right\} \tag{8.20}$$

where $angle\left\{\bullet\right\}$ represents the unwrapped phase operator. The term inside the expectation is the correlator satisfying (8.8). Obviously, combining (8.18), (8.19) and (8.20), we can find that the phases depends on the channel parameters as well as the specific STC schemes. For example, in Alamouti's scheme, suppose the correlator we use is $r_i\left(k\right) r_j\left(k+1\right)$, $i \neq j$, the phase can be calculated using (8.20) as

$$\phi = angle\left\{h_{11}h_{22} - h_{12}h_{21}\right\} \tag{8.21}$$

When we have the prior knowledge of the channel as well as the possible STC scheme, which consequently give us the approximate phase ϕ_m, $m = 1, ...P$, corresponding to the mean of P cyclic sequences, a simple non-ML suboptimal test statistic can be given by

$$\kappa = \left| \sum_{m=0}^{P-1} \exp\left(-j\phi_m\right) R_m\left(\alpha\right) \right|^2 \tag{8.22}$$

where P is the number of correlators satisfying (8.8).

Therefore, for this combining process, the detection algorithm can be implemented using the following steps:

Step 1: Get P common correlators according to the criteria (8.8) with the prior knowledge;

Step 2: Compute the phase for these correlators at cyclic frequency $\alpha = \frac{2\pi}{T}$;

Step 3: Computing the test statistic, κ, given by (8.22) at cyclic frequency $\alpha = \frac{2\pi}{T}$;

Step 4: For a given probability of false alarms, P_F, using the central χ^2 tables for 2 degrees of freedom, find a threshold γ so that $P_F = \Pr\left\{\chi^2 > \gamma\right\}$;

Step 5: Declare it is STC if $\kappa \geq \gamma$; otherwise, decide it is BLAST.

8.4.3 Performance analysis of the two combining algorithms

In the previous subsections, to improve the performance of the detector, two algorithms to combine the correlators have been proposed. The first algorithm requires computing the inverse of the asymptotic covariance matrix of size $2q \times 2q$ each run of Monte Carlo experiment, resulting in a heavy computational burden. The second suboptimal algorithm is much simpler than the first one. However, it requires the prior knowledge of the channel parameters and the specific STC scheme we are going to detect.

Essentially, the first algorithm prewhitens the noise before combining several complex signals with unknown means. With the prior knowledge of the phase of the mean value of the complex signals, the second suboptimal algorithm corrects the phase of the means and sum them together without prewhitening noise. Of course, the optimal but much complicated algorithm can be the combination of these two algorithms. Actually, even though suboptimal, the second algorithm outperforms the first algorithm when the phase of the two unknown means has a large difference.

8.5 Simulation

Monte Carlo simulations are conducted to test the performance of the above detectors for Rayleigh block i.i.d channels (5000 experiments for each point). In the first scenario, Alamouti's STC scheme and the MIMO BLAST scheme are used. QPSK modulation is used for both transmit antennas. The number of receiver antenna is 2. The number of the received symbols for each detection block is 500. The probability of false alarm is 0.95. The cyclic frequency for testing is set as $\alpha = \frac{2\pi}{T}$. As it is shown in Fig.8.3, three different detectors: single correlator $r_1(k)\, r_2(k+1)$ (single), the combined correlators for correlators $r_1(k)\, r_2(k+1)$ and $r_2(k)\, r_1(k+1)$ using test statistic given by (8.15) (combined 1) and (8.22) (combined 2) are applied, respectively. As it is shown from Fig.8.3, both of the algorithms which combine the linear correlators outperform the detector

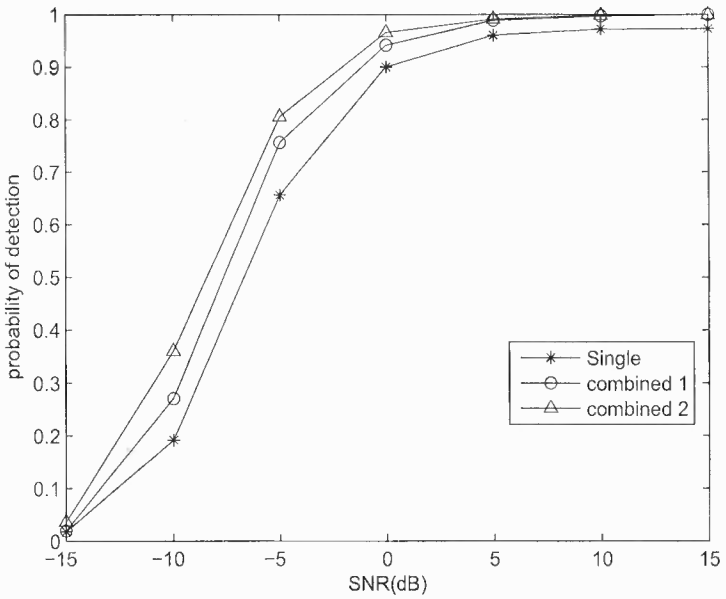

Figure 8.3 Probability of detection for Alamouti's scheme.

with only one linear correlator. The second algorithm (combined 2) outperforms the first one (combined 1) because the phase difference for the two correlators is approximately π.

Secondly, 3/4 rate STC scheme with $L = 3$, and the MIMO BLAST scheme are used. Similar simulation settings are applied as the first scenario. As it is shown in Fig.8.4, three different detectors: single correlator $r_1(k)\, r_2(k+1)$ (single), the combined correlators for correlators $r_1(k)\, r_2(k+1)$, $r_1^*(k)\, r_2(k+1)$ and $|r_i(k)|^2$ using test statistic given by (8.15) (combined 1) and (8.22) (combined 2) are applied, respectively. These correlators were chosen randomly from those which are cyclostationary. Again, both of the algorithms which combine the linear correlators outperform the detector with only one linear correlator. A larger gap between the combined (1&2) algorithms and the single correlator can be observed due to more degrees of freedom (three correlators).

Still, the second algorithm (combined 2) outperforms the first combined algorithm (combined 1). The phase difference of the mean value of the cyclic statistics at cyclic frequency $\alpha = \frac{2\pi}{T}$ is more than $\pi/2$ for any two correlators.

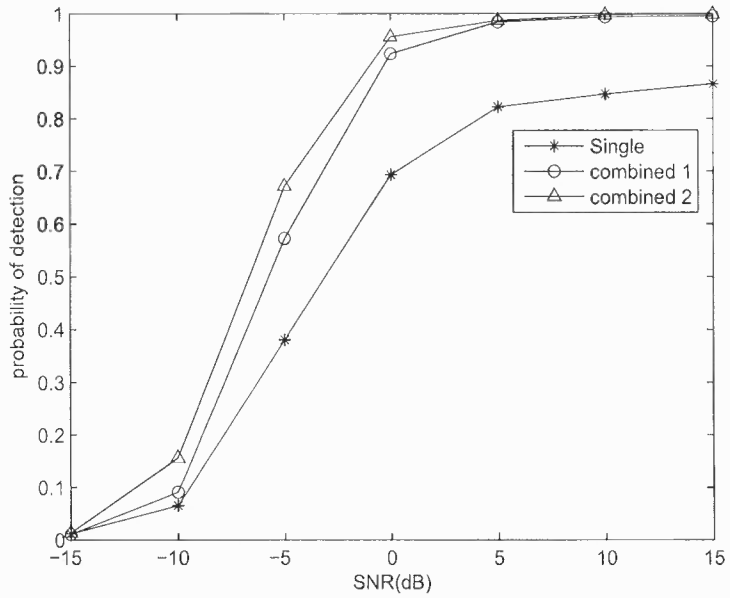

Figure 8.4 Probability of detection for STC 3/4 rate scheme.

8.6 Proof for Theorem 1 & 2

Proof for Theorem 1:

For the cross correlator or cross conjugate correlator or auto conjugate correlator, the expectation is given by

$$E\left\{r_i\left(k\right)r_j\left(k+u\right)\right\} = \mathbf{h}_i E\left\{\mathrm{s}\left(k\right)\mathrm{s}\left(k+u\right)^T\right\}\mathbf{h}_j^T \tag{8.23}$$

$$\text{or } E\left\{r_i\left(k\right)r_j^*\left(k+u\right)\right\} = \mathbf{h}_i E\left\{\mathrm{s}\left(k\right)\mathrm{s}\left(k+u\right)^H\right\}\mathbf{h}_j^H$$

$$\text{or } E\left\{r_i\left(k\right)r_i^*\left(k+u\right)\right\} = \mathbf{h}_i E\left\{\mathrm{s}\left(k\right)\mathrm{s}\left(k+u\right)^H\right\}\mathbf{h}_i^H$$

where $\mathbf{h}_i$, $\mathbf{h}_j$, are the ith and jth row vector of the channel matrix $\mathbf{H}$ respectively.

Since the channel parameter is randomly chosen, the term of the right hand side (RHS) of the equation is the same only when $E\left\{\mathrm{s}\left(k\right)\mathrm{s}\left(k+u\right)^T\right\}$ or $E\left\{\mathrm{s}\left(k\right)\mathrm{s}\left(k+u\right)^H\right\}$ is the same. Only when the terms of $E\left\{\mathrm{s}\left(k\right)\mathrm{s}\left(k+u\right)^T\right\}$ or $E\left\{\mathrm{s}\left(k\right)\mathrm{s}\left(k+u\right)^H\right\}$ is not the same, the resulted correlator is periodic with a period larger than zero. Or we can say, the correlator is statistically cyclic. Thus, we complete the proof for Theorem 1.

Proof for Theorem 2:

For the auto correlator, the expectation is given by

$$E\left\{r_i\left(k\right)r_i\left(k+u\right)\right\} = \mathbf{h}_i E\left\{\mathbf{s}\left(k\right)\mathbf{s}\left(k+u\right)^T\right\}\mathbf{h}_i^T \tag{8.24}$$

For the auto correlator, the term of the RHS of the equation can be rewritten as

$$\begin{aligned}&\mathbf{h}_i E\left\{\mathbf{s}\left(k\right)\mathbf{s}\left(k+u\right)^T\right\}\mathbf{h}_i^T \\ &= \sum_{k=0}^{T-1} h_{ik}^2 \mathbf{S}_{kk} + \sum_{k=0}^{T-1}\sum_{l=0,l\neq k}^{T-1}\left(h_{ik}h_{il}\mathbf{S}_{lk} + h_{ik}h_{il}\mathbf{S}_{kl}\right)\end{aligned} \tag{8.25}$$

where $\mathbf{S}_{kk}$ represents the diagonal element of matrix $E\left\{\mathbf{s}\left(k\right)\mathbf{s}\left(k+u\right)^T\right\}$ and $\mathbf{S}_{lk}$, $\mathbf{S}_{kl}$ are the (l,k)th and (k,l)th elements of the matrix.

When the diagonal elements are not the same, the term $\mathbf{h}_i E\left\{\mathbf{s}\left(k\right)\mathbf{s}\left(k+u\right)^T\right\}\mathbf{h}_i^T$ will not be the same due to the randomness of the channel parameters. When the diagonals are the same, and if $\mathbf{S}_{lk} = -\mathbf{S}_{kl}$, we can get that the second sum term in (8.25) is zero and consequently, the LHS of (8.25) will be the same. Since the correlator is statistically cyclic if the LHS of (8.25) are not the same. We complete the proof for Theorem 2.

REFERENCES

[1] Bolcskei, H.; "Blind estimation of symbol timing and carrier frequency offset in wireless OFDM systems", Communications, IEEE Transactions on, Vol. 49, Issue 6, June 2001 Page(s):988 - 999.

[2] A. Punchihewa, O. A. Dobre, S. Rajan, and R. Inkol, "Cyclostationarity-based algorithm for blind recognition of OFDM and single carrier linear digital modulations," in Proc. IEEE PIMRC 2007, Athens, Greece, Page(s): 1-5.

[3] T. Yücek and H. Arslan, "OFDM Signal Identification and Transmission Parameter Estimation for Cognitive Radio Applications", IEEE Global Communications Conference (Globecom), November 2007, Page(s):4056-4060.

[4] Li H., Bar-Ness Y., Abdi A., Somekh O. And Su W., "OFDM Modulation Classification and Parameters Extraction," Int. Conference on Cognitive Radio Oriented Wireless Networks and Commun. (Crowncom), Mykonis, Greece, June 2006, Page(s):1-6.

[5] Li H., "Advanced Methods in Automatic Modulation Classification for Emerging Technologies," PhD. thesis, Electrical and Computer Engineering, New Jersey Institute of Technology, Newark, NJ, May 2006.

[6] Akmouche, W., "Detection of multicarrier modulations using 4th-order cumulants", IEEE MILCOM 1999, Vol. 1, Page(s):432-436.

[7] Annathram Swami, Brian M. Sadler, "Hierarchical Digital Modulation Classification Using Cumulants", IEEE Trans. On Communications, Vol. 48, No. 3, March 2000, Page(s):416-429.

[8] IEEE Std 802.11a-1999, "Supplement to IEEE standard for information technology - telecommunications and information exchange between systems - local and metroplitan area networks - specific requirements. Part 11: wireless LAN medium access control (MAC) and physical layer (PHY) specifications: high-speed physcial layer in the 5GHz band". http://www.ieee.org, Dec. 1999.

[9] IEEE Std 802.16-2004, May 2004.

[10] ETSI TS 101 475 V1.3.1 (2001-12), "Broadband radio access networks (BRAN); HIPERLAN type 2; physical (PHY) layer". http://www.etsi.org, Dec. 2001.

[11] 3GPP TR 25.814 V1.4.0 (2006-05), "Physical Layer Aspects for Evolved UTRA".

[12] Miao Shi, Bar-Ness, Y., Wei Su, "Blind OFDM Systems Parameters Estimation for Software Defined Radio", IEEE DySpan, April 2007, Page(s): 119-122.

[13] G.B. Giannakis, M.K. Tsatsanis, "Time-domain tests for Gaussianity and time-reversibility", IEEE Transactions on Signal Processing, Vol.42, no.12, Dec 1994, Page(s): 3460-3472.

[14] Ishii, H.; Wornell, G.W.; "OFDM Blind Parameter Identification in Cognitive Radios", IEEE PIMRC 2005, Vol. 1, 11-14 Sept. 2005 Page(s):700-705.

[15] Byungjoon Park; Hyunsoo Cheon; Eunseok Ko; Changeon Kang; Daesik Hong; "A blind OFDM synchronization algorithm based on cyclic correlation", Signal Processing Letters, IEEE, Vol. 11, Issue 2, Part 1, Feb. 2004 Page(s):83-85

[16] Akmouche, W.; Kerherve, E.; Quinquis, A.; "OFDM spectral characterization: estimation of the bandwidth and the number of sub-carriers", Statistical Signal and Array Processing, 2000. Proceedings of the Tenth IEEE Workshop on, 14-16 Aug. 2000 Page(s):48-52.

[17] Oner, M.; Jondral, F.; "Cyclostationarity based air interface recognition for software radio systems", Radio and Wireless Conference, 2004 IEEE, 19-22 Sept. 2004 Page(s):263-266.

[18] Peng Liu; Bing-bing Li; Zhao-yang Lu; Feng-kui Gong; "A Blind Time-parameters Estimation Scheme for OFDM in Multi-path Channel", Wireless Communications, Networking and Mobile Computing, 2005. Proceedings. 2005, Vol. 1, 23-26, Sept. 2005 Page(s):242-247.

[19] Dandawaté, A.V.; Giannakis, G.B.; "Statistical tests for presence of cyclostationarity", IEEE Trans. on Signal Processing, Vol. 42, Issue 9, Sept. 1994 Page(s):2355-2369.

[20] Miao Shi, Bar-Ness, Y., Wei Su, "Fourth order cumulants in Distinguishing Single Carrier from OFDM signals", IEEE MILCOM, Nov. 2008.

[21] Jan-Jaap van de Beek, Magnus Sandell, and Per Ola Börjesson, "ML Estimation of Time and Frequency Offset in OFDM Systems", IEEE Trans. on Signal Processing, VOL. 45, No. 7, JULY 1997, Nov. 2008, Page(s):1800-1805.

[22] Miao Shi, Bar-Ness, Y.,"Revisiting the Timing and Frequency Offset Estimation Based on Cyclostationarity", submitted to IEEE Commu. Letter.

[24] Bo Ai; Zhi-xing Yang; Chang-yong Pan; Jian-hua Ge; Yong Wang; Zhen Lu; "On the synchronization techniques for wireless OFDM systems" ,Broadcasting, IEEE Transactions on, Volume 52, Issue 2, June 2006 Page(s):236-244.

[25] T.M.Schmidl and D.C.Cox, "Robust frequency and timing. synchronization. for. OFDM," IEEE. Trans .on. Comms.Vol.45,No.12,Dec 1997,Page(s): 1613-1621.

[26] W.R. Bennett, Statistics of regenerative digital transmission, Bell System Technical Journal 37 (November 1958), Page(s):1501-1542.

[27] W.A. Gardner, Cyclostationarity in Communications and Signal Processing, IEEE Press, New York, NY, 1994.

[28] W.A. Gardner, Antonio Napolitano, and Luigi Paura "Cyclostationarity: Half a century of research", Signal Processing, Vol. 86, Issue 4, April 2006, Page(s): 639-697.

[29] W.A. Gardner, "Cyclic Wiener filtering: theory and method", IEEE Trans. on Communications, Vol. 41, Issue 1, Jan. 1993, Page(s): 151-163.

[30] Gini, F., Giannakis, G.B. , "Frequency offset and symbol timing recovery in flat-fadingchannels: a cyclostationary approach," IEEE Trans. on Communications, Vol. 46, Issue 3, Mar. 1998 Page(s):400-411.

[31] L. Tong, X. Guanghan, T. Kailath, "Blind identification and equalization based on second-order statistics: a time domain approach", IEEE Trans. on Information Theory, Vol. 40 Issue 2, March 1994, Page(s): 340-349.

[32] L. Mazet, Ph. Loubaton, "Cyclic correlation based symbol rate estimation", Signals, Systems, and Computers, 1999. Conference Record of the Thirty-Third Asilomar Conference on , Vol. 2, Oct. 1999, Page(s):1008-1012.

[33] Carlos Mosquera, Sandro Scalise, and Roberto Lpez-Valcarce, "Non-Data-Aided Symbol Rate Estimation of Linearly Modulated Signals", IEEE Trans. on Signal Processing, Vol. 56, No. 2, Feb. 2008, Page(s):664-674.

[34] Miao Shi, Bar-Ness, Y., Wei Su, "STC and BLAST MIMO modulation recognition", IEEE GLOBECOM, Nov. 2007, Page(s):3034-3039.

[35] Kyouwoong Kim, Akbar, I.A., Bae, K.K., Jung-sun Urn, Spooner C.M., Reed J.H., "Cyclostationary Approaches to Signal Detection and Classification in Cognitive Radio", Signal Processing, Vol. 85, Issue 12, Dec. 2005, Page(s): 2233-2303.

[36] Sutton P.D., Nolan K.E., Doyle, L.E., "Cyclostationary Signatures in Practical Cognitive Radio Applications", Selected Areas in Communications, IEEE Journal on, Jan. 2008 Vol. 26, Issue: 1, Page(s): 13-24.

[37] Lunden Jarmo, Koivunen Visa, Huttunen Anu, Poor H. Vincent, "Spectrum Sensing in Cognitive Radios Based on Multiple Cyclic Frequencies", IEEE CrownCom, Aug. 2007, Page(s): 37-43.

[38] Erchin Serpedin, Flaviu Panduru, Ilkay Sari, and Georgios B. Giannakis, "Bibliography on cyclostationarity", Signal Processing, Vol. 85, Issue 12, Dec. 2005, Page(s): 2233-2303.

[39] Miao Shi, Bar-Ness, Y., Wei Su, "A simple method to enhance the detection of the second order cyclostationarity", IEEE GLOBECOM 2008, Nov. 30, 2008, Page(s): 1-6.

[40] M. Ghogho, A. Swami, T. Durrani, "On blind carrier recovery in time-selective fading channels," 33rd Asilomar Conference on Signals, Systems and Computers, vol. 1, 24-27 Oct. 1999, Page(s): 243-247.

[41] M. Oerder and H. Meyr, "Digital filter and square timing recovery," IEEE Trans. Commun., vol. 36, May 1988, Page(s): 605C612.

[42] K.E. Scott and E.B. Olasz, "Simultaneous clock phase and frequency offset estimation", IEEE Trans. on Commu. 43, July 1995, Page(s): 2263-2270.

[43] Yan Wang, Philippe Ciblat, Erchin Serpedin, and Philippe Loubaton, "Performance Analysis of a Class of Nondata-aided Frequency Offset and Symbol Timing Estimators for Flat-Fading Channels", IEEE Trans. on Signal Processing, Vol. 50, No. 9, Sept. 2002, Page(s): 2295-2305.

[44] Alamouti, S.M.; "A simple transmit diversity technique for wireless communications," Selected Areas in Communications, IEEE Journal on, Volume 16, Issue 8, Oct. 1998, Page(s):1451 - 1458.

[45] Tarokh, V.; Jafarkhani, H.; Calderbank, A.R.; "Space-time block coding for wireless communications: performance results", Selected Areas in Communications, IEEE Journal on, Volume 17, Issue 3, March 1999, Page(s):451 - 460.

[46] BLAST: Bell Labs Layered Space-Time, "http://www1.bell-labs.com/project/blast/".

[47] Steven M. Kay; "Fundamentals of statistical signal processing", Prentice Hall PTR.

[48] Perros-Meilhac L., Moulines E., Chevalier P., "On the pulse shape filter estimation in a multipath context", Signals, Systems and Computers, Conference Record of the Thirty-Fourth Asilomar Conference, Vol.1, Oct. 29, 2000, Page(s): 600-604.

[49] Haiyuan Xu, Yiyu Zhou, Zhitao Huang, "Blind Roll-Off Factor and Symbol Rate Estimation Using IFFT and Least Squares Estimator", Wireless Communications, Networking and Mobile Computing, 2007. WiCom 2007. International Conference, Sept. 2007, Page(s): 1052-1055.

[50] Wiki: Raised cosine filter, "http://en.wikipedia.org/wiki/".

[51] W.A. Gardner, C.-K. Chen,"Signal-selective time-difference-of-arrival estimation for passivelocation of man-made signal sources in highly corruptive environments.I. Theory and method", IEEE Trans. Signal Processing, vol. 40, No.5, May 1992, Page(s): 1168-1184.